INJECTABLE MACROPOROUS HYDROGEL FOR WOUND HEALING AND TISSUE ENGINEERING

BY

SHUJIE HOU

BS in Chemical Engineering, University of New Hampshire, 2015

DISSERTATION

Submitted to the University of New Hampshire

in Partial Fulfillment of

the Requirements for the Degree of

Doctor of Philosophy in Chemical Engineering

September, 2019

This thesis/dissertation was examined and approved in partial fulfillment of the requirements for the degree of

Ph.D. in Chemical Engineering by:

Thesis/Dissertation Director, Kyung Jae Jeong, Assistant professor of Chemical Engineering

Russell Carr, Professor and chair of Chemical Engineering

Kang Wu, Assistant professor of Chemical Engineering

Young Jo Kim, Assistant professor of Chemical Engineering

Don Wojchowski, Professor of Molecular, Cellular, and Biomedical Sciences

On [May 28th 2019]

Approval signatures are on file with the University of New Hampshire Graduate School.

ACKNOWLEDGEMENTS

First and foremost, I must acknowledge my advisor, Dr. Kyung Jae Jeong who taught me everything I know about biomaterials. He was an invaluable source of knowledge in this field of research and an inspirational source of creative research projects. Dr. Jeong, thank you for all of your support and your guidance leading me in the world of research.

I would also like to acknowledge my other committee members, Dr. Carr, Dr. Wu, Dr. Kim, and Dr. Wojchowski. Thank you to Dr. Brian Zukas and Dr. Nivedita Gupta for teaching me everything I know about rheology. And thank you to Dr. Carr for always being willing to help with degree related questions. Also, I want to thank Nancy Cherim and Dr. Mark Townley from the University Instrument Center (UIC) at UNH for answering my technical questions. I would also thank NIH COBRE Center of Integrated Biomedical and Bioengineering Research (CIBBR, P20GM113131) for supporting the research.

I would also like to acknowledge the past and present students of the Jeong lab group; Alison Deyett, Rachel Lake, Chante Jones, Thanh Dinh, Benjamin Shalek, Dr. Shiwha Park, Seth Edward, Ryann Boudreau, Rachel Yee, Jason Brown, Lara Weed, Roisin Williams, Vinjai Vale, Avery Normandin, Kenan Mazic, Caroline Houston, Alex Nguyen, Salimah Hussien, Roopa Bhat, Juhi Gupta, and Connor Joyce. I enjoyed my time with all my labmates and I wish them the best of luck in their endeavors. Finally, I would like to acknowledge my parents, Chao Hou and Youlai Guo, for loving me and encouraging me to study in United States for my degree.

TABLE OF CONTENTS

FIGURE CONTENT

Chapter 5

APPENDICES

ABSTRACT

INJECTABLE MACROPOROUS HYDROGEL FOR WOUND HEALING AND TISSUE ENGINEERING

BY

SHUJIE HOU

University of New Hampshire, May, 2019

Injectable hydrogels can be useful for facilitating wound healing and tissue engineering since they can serve as a temporary matrix during wound healing or tissue engineering processes. However, lack of pore structures in most injectable hydrogels limits cell infiltration and spreading. Here, an injectable macroporous hydrogel system was developed by crosslinking preformed microgels. By this approach, pores were created in the interstitial spaces between microgels, allowing cell infiltration and spreading.

Gelatin macroporous hydrogel was first tested for wound healing. The average size of the gelatin microgel was 250 μm in diameter. When mixed with microbial transglutaminase (mTG), the microgels adhered to each other forming macroporous hydrogel. The viscoelastic properties of the porous hydrogel were similar to those of nonporous gelatin hydrogel made by adding mTG to a homogeneous gelatin solution. The porous hydrogel supported higher cellular proliferation of human dermal fibroblasts (hDFs) than the nonporous hydrogel over two weeks, and allowed the migration of hDFs into the pores. In contrast, hDFs were unable to permeate the surface of the nonporous hydrogel. Next, to demonstrate potential use in wound healing, gelatin microgels were injected with mTG into a cut out section of an excised porcine cornea. Due to the action of mTG, the porous hydrogel stably adhered to the corneal tissue for two weeks. Confocal microscope images showed that a large number of cells from the corneal tissue migrated into the

interstitial space of the porous hydrogel. The porous hydrogel was also used for the controlled release of platelet-derived growth factor (PDGF), increasing the proliferation of hDFs compared to the nonporous hydrogel. Thus, this gelatin macroporous hydrogel has much potential as a useful tool in wound healing applications.

The gelatin macroporous hydrogel system was also tested for use in tissue engineering applications. Multiple cell types were encapsulated and tested for viability in this hydrogel system including hDFs, adipose-derived stem cells (ADSCs), human umbilical vein endothelial cells (HUVECs), and HL-1 cardiac muscle cell line (HL-1). In all cases, encapsulated cells were shown to be viable. With ADSCs, the macroporous hydrogel was shown to enhance osteogenic differentiation; with HUVECs, the macroporous hydrogel promoted cell connections important for neovascular formation; and with HL-1, macroporous hydrogel enhanced gap junction formation, important for proper heart muscle function. Considerable potential, therefore, also exists for this gelatin macroporous hydrogel system to be applied in tissue engineering applications.

However, gelatin macroporous hydrogel has a disadvantage of slow curing which would tend to make it unsuitable in clinical applications. To obviate this problem, the system was optimized by inducing photocrosslinking of gelatin methacryloyl (GelMA) in conjunction with the enzymatic crosslinking of gelatin by mTG. The gelatin and GelMA composite (Gelatin/GelMa) microgels with mTG, photoinitiator, and hDFs, can be crosslinked in 2.5 mins with ultraviolet (UV) irradiation. The photoinitiator concentration was also optimized to maintain rapid curing while minimizing cytotoxicity. In conclusion, this injectable biodegradable Gelatin/GelMA macroporous hydrogel system exhibited rapid gelation, maximal bioactivity for

encapsulated cells, and capability for tissue adhesion, making it appropriate for use in tissue engineering applications.

Chapter 1:

Introduction

Hydrogel is a highly versatile material which has found numerous applications in medicine and biotechnology. Hydrogels can be made of many different materials and formed by different crosslinking mechanisms depending on the application. The scope of hydrogel-based research is vast and is still expanding. The main focus of this thesis is injectable macroporous hydrogels and their potential applications in wound healing and tissue engineering.

Here is an overview of this thesis.

In Chapter 2, a literature review on the latest advancements in hydrogel research is provided. I start with a general discussion of the materials and crosslinking mechanisms of hydrogels. The focus is then narrowed to injectable hydrogels, and the major limitations of the current injectable hydrogels for medical and biotechnological applications are discussed. As a conclusion to the chapter, the motivation of my research is provided.

In Chapter 3, a novel injectable macroporous hydrogel for wound healing is introduced. A highly porous bulk hydrogel was formed by assembling and curing spherical microscale gelatin hydrogels, called gelatin microgels. The curing process was achieved by enzymatic actions by microbial transglutaminase (mTG). Macropores were formed from the interstitial space between microgels. I demonstrate that this simple and cost-effective method can significantly enhance the interactions between human cells and the hydrogel. A potential application of this formulation for wound healing is demonstrated using an ex vivo model.

In Chapter 4, I demonstrate that this novel injectable hydrogel can be used to encapsulate various mammalian cells for tissue engineering and cell delivery applications. Examples include the encapsulation of human dermal fibroblasts (hDFs), human adipose-derived stem cells (ADSCs), and a mouse cardiomyocyte cell line (HL-1). Differences in cellular responses between culture in

the macroporous hydrogel and that in traditional nonporous hydrogels are highlighted in the context of tissue engineering applications.

In Chapter 5, composite microgels made of gelatin and gelatin methacryloyl (GelMA) are introduced. These microgels were developed to overcome the slow curing speed (~1 hour) of the gelatin-based microgels. By employing a dual crosslinking mechanism – UV photopolymerization of GelMA and mTG crosslinking of gelatin – rapid curing (~ minutes) of the microgels and tissue adhesion to the resulting hydrogel are demonstrated. I demonstrate that this composite formulation increases the clinical relevance of the microgel-based hydrogel.

Future work is presented in Chapter 6.

Chapter 2:

Literature Review

2.1 Materials for Hydrogel

Hydrogel is a crosslinked network of hydrophilic polymers [1]. Hydrogels have found numerous applications in medicine and biotechnology as materials to interface with human cells and tissues due to its high water content, matching the physiological conditions of human tissues [2]. Both natural and synthetic polymers can be used to make hydrogels. Natural materials that can be made into hydrogels include (i) proteins such as collagen, gelatin, elastin, and silk fibroin, and (ii) polysaccharides such as alginate, chitosan, and hyaluronic acid (HA). Natural polymers in general have the advantage of possessing the inherent biological signals and functions that favor interactions with cells. However, it is often not easy to control the mechanical and chemical properties of hydrogels made from natural polymers due to batch-to-batch chemical variance of natural polymers [3]. Synthetic polymers, on the other hand, allow more precise control of the material properties of the hydrogel. Examples include polyethylene glycol (PEG), poly(vinyl alcohol) (PVA), poly(N-isopropylacrylamide) (PNIPAAm), and poly(2-hydroxyethylmethacrylate) (pHEMA). Copolymers of different polymers can result in improved mechanical properties or stimuli-responsiveness. However, most synthetic materials do not exhibit bioactivities and require further modifications with peptides or proteins.

2.1.1. Natural polymers

Collagen is the main component of extracellular matrix (ECM), which is the basic scaffolding for cellular growth in tissues [4]. The structure of collagen consists of three polypeptide chains twisted together to form a triple-helical structure [4]. As a main component of ECM of most tissues, collagen contains amino acid sequences, such as arginine-glycine-aspartic acid (RGD), that promote cell adhesion and proliferation [5]. It is also degradable via proteinases, specifically

collagenase; therefore, hydrogels made of collagen naturally degrade in the body by the action of collagenases secreted by cells [6]. Collagen can be covalently crosslinked by UV, without any chemical modifications, in the presence of riboflavin (vitamin B12), which acts as a photoinitiator [7]. This method was used to encapsulate fibrochondrocytes for the regeneration of meniscus tissue. One disadvantage of collagen-based hydrogels is low mechanical strength due to low collagen solubility in water [8]. In addition, there is a potential risk of immunogenicity when used *in vivo* [9].

Gelatin, which is obtained by partial hydrolysis of collagen, is less immunogenic than collagen while retaining important biological functions of collagen, such as promoting cell adhesion through the RGD sequence [10], which has been utilized for coating substrates for *in vitro* cell cultures [11]. Gelatin has a much higher solubility in water than collagen, which makes it much easier to handle [12]. In addition, high polymer concentration of gelatin can result in a mechanically more stable hydrogel than collagen. Gelatin contains high occurrences of amino acids with useful chemical functional groups (e.g. primary amines, carboxyls) for facile chemical modifications. Substituting the primary amines of lysine residues with methacryloyl groups results in gelatin methacryloyl (GelMA), which is widely used in tissue engineering and regenerative medicine due to its rapid gelation by UV irradiation [13-16]. Similar to collagen, gelatin hydrogels can be degraded by collagenases [17].

Silk fibroin is a protein isolated from silk cocoons by removing sericin. [18]. An aqueous solution of silk fibroin is readily crosslinked to form a hydrogel by the formation of β-sheets using various external stimuli including heat [19], solvent exchange [20], and shear stress [21]. Silk fibroin has been widely used as a biomaterial due to its excellent mechanical properties, biocompatibility, and bioinertness. Sun *et al*. modified silk fibroin hydrogel with a cell adhesive peptide

(isoleucine–lysine–valine–alanine– valine (IKVAV)), a sequence derived from laminin, and demonstrated that it improved the survival of encapsulated neural stem cells (NSCs) and their neuronal differentiation [22].

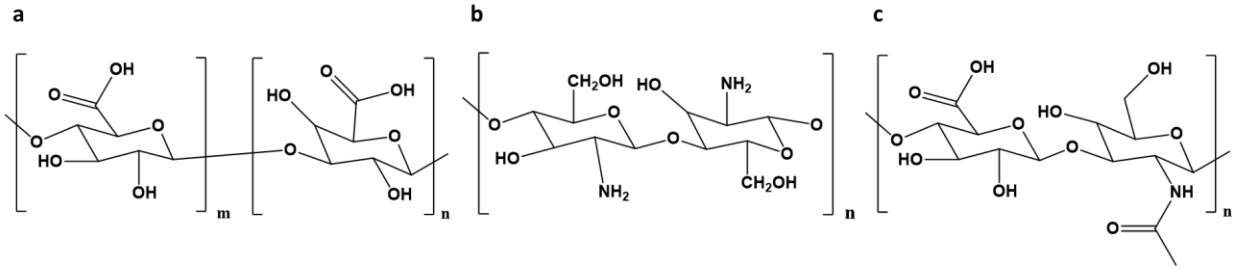

Figure 2.1: Chemical structures of the natural materials a) alginate, b) chitosan, and c) hyaluronic acid (HA).

Alginate (Fig. 2.1a) is a naturally derived polysaccharide from algae, which contains units of (1-4)-linked β-D-mannuronic acid and α-L-guluronic acid [23]. It is a widely used material due to its excellent biocompatibility, biodegradability, and low toxicity [24]. The carboxyl groups on the backbone of alginate allow facile chemical modifications with biofunctional moieties, such as cell adhesive ligands. In addition, the carboxyl groups enable the rapid formation of an ionically crosslinked hydrogel upon addition of multi-valent cations, such as Ca^{2+} or Mg^{2+} [25]. Utilizing this simple mechanism, Tabriz *et al*. reported that an alginate solution could be 3D-printed along with human cells, thus demonstrating the potential for 3D printing-based tissue engineering [26]. Alginate can be chemically modified to make mechanically more stable hydrogels. García-Astrain and Avérous utilized furan-modified alginate, crosslinked by a Diels-Alder reaction that had no side reactions and created no toxic conditions. This covalently crosslinked alginate hydrogel was used for a controlled release of vanillin, a small molecule drug [24].

Chitosan (Fig. 2.1b) is a linear polysaccharide which is produced by deacetylation of chitin, a polymer derived from glucose [27]. Chitosan has been shown to support cell adhesion and

proliferation [28], and is also biodegradable by human enzymes such as lysozyme [29]. Kim *et al*. produced a degradable hydrogel based on a chitosan-lysozyme pairing. Methacrylated glycol chitosan and methacrylated lysozyme were photocrosslinked and bone marrow stromal cells (BMSCs) were encapsulated. This hydrogel could be degraded in a cell-independent manner via lysozyme degradation of chitosan. The viability of the cells was well maintained and cell osteogenic differentiation was enhanced by the presence of lysozyme [30]. Chitosan-based hydrogels can also be made pH-responsive by modifications that convert chitosan to a polyampholyte, a polymer carrying oppositely charged groups on its chain. In this form, a pH higher than the isoelectric point induces the polymer's self-assembly by electrostatic complexation[31-32]. Due to the primary amines in the chitosan structure, which is cause it to be crosslinked with ironic interaction, chitosan can be crosslinked by the addition of multi-valent anions such as tripolyphosphate (TPP) [33] or alginate [34].

HA (Fig. 2.1c) is a natural glycosaminoglycan (GAG) which occurs in the ECM of connective tissues [35]. It is biocompatible and allows cell adhesion, cell migration, proliferation, differentiation, and angiogenesis [36]. Luo *et al*. developed a fast curing HA hydrogel based on a reaction between azide and aldehyde and used this hydrogel for the enzyme-triggered release of various small molecule drugs including hydrocortisone, prednisolone, cortisone, dexamethasone, and prednisone [35]. Han *et al*. reported a HA-based *in situ* cell encapsulation system for cartilage regeneration. HA was crosslinked by click chemistry between cyclooctyne and azide in the presence of chondrocytes. The chondrocytes encapsulated in this HA hydrogel generated a cartilaginous tissue both *in vitro* and *in vivo* [37].

2.1.2 Synthetic material

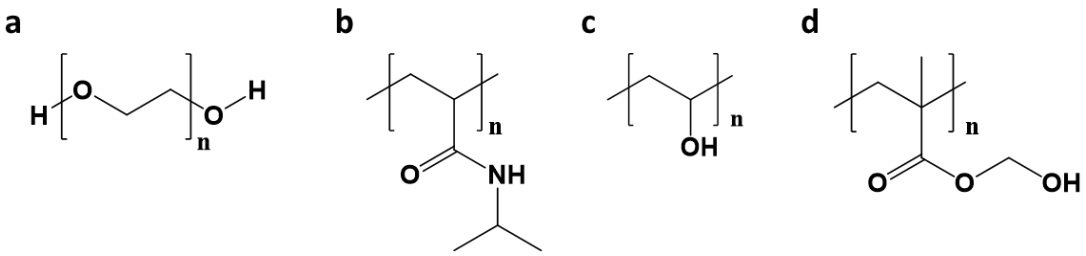

Figure 2.2: Chemical structures of the synthetic materials a) PEG, b) PNIPAAm, c) PVA, and d) pHEMA

PEG (Fig. 2.2a) is one of the most widely used synthetic polymers for hydrogels. PEG is an inert and non-degradable polymer and does not have functional groups that can be crosslinked for gelation under physiological conditions. However, the excellent biocompatibility of PEG propelled the development of several methods of chemical modifications for crosslinking [38-39], cell adhesion, and enzymatic degradation [39-40]. Henise *et al*. reported a PEG hydrogel-based drug delivery system utilizing multi-arm PEG (8-arm). Four arms of the 8-arm PEG were used to attach drug molecules through a fast-degrading linker while the other 4 arms were used to crosslink the PEG molecules through a slow-degrading linker. By adjusting the degradation rates of the linkers, the drug release rate and the hydrogel degradation rate could be controlled [40]. Sridhar *et al*. developed matrix metallopeptidase (MMP)-sensitive biodegradable PEG-based hydrogel by crosslinking 4-arm PEG amide with the thiol of a peptide linker derived from collagen, KCGPQG↓IWGQCK (where the arrow indicates cleavage site, which can be cleaved by MMP-8 and MMP-13 secreted by chondrocytes), and transforming growth factor beta 1 (TGF-β1). In this hydrogel, a mixture of mesenchymal stem cells (MSCs) and chondrocytes was encapsulated. Timely degradation of the hydrogel by the encapsulated cells yielded a cartilaginous tissue *in vitro* as shown by collagen distribution [39].

PNIPAAm (Fig. 2.2b) is a biocompatible and thermosensitive polymer, exhibiting a lower critical solution temperature (LCST), which means an aqueous solution of PNIPAAm undergoes a phase transition to a physically crosslinked hydrogel at a temperature higher than its LCST [41]. This phase transition is caused by the increased thermal energy of water molecules and enhanced hydrophobic interactions among the polymer molecules. This useful thermal property of PNIPAAm has led to the development of many stimuli responsive hydrogels for drug delivery and *in vitro* cell culture [42]. Ekerdt *et al*. synthesized a composite polymer from HA and PNIPAAm which formed a thermo-reversible hydrogel. This HA-PNIPAAm composite solution was able to encapsulate human pluripotent stem cells (hPSCs) when heated to 37 °C and the recovery of cells could be achieved simply by 'melting' the hydrogel at a low temperature [43].

PVA (Fig. 2.2c) is a biocompatible and non-toxic hydrophilic polymer [44]. It can be physically crosslinked via phase separation caused by hydrogen bond and hydrophobic interactions to form a hydrogel using freeze-thaw processes, or by chemical crosslinking with aldehydes. In some examples, PVA was made into a hydrogel by photopolymerization [45]. Chen *et al*. developed a PVA-based nanosized hydrogels (nanogels) which could be degraded at low pH (5.0) through the acetal linkages. These nanogels were used to encapsulate and release paclitaxel in the acidic cancer microenvironment [46].

pHEMA (Fig. 2.2d) is another widely used polymer for hydrogels. When crosslinked by various radical polymerization methods, pHEMA forms a soft, flexible, and optically transparent hydrogel [47]. The major application of pHEMA hydrogels has been in contact lenses. Further chemical modifications can make pHEMA hydrogels into therapeutic contact lenses for various ocular diseases [48].

2.1.3. Copolymers

Hydrogels made of copolymers of different polymers often result in enhanced mechanical or chemical properties. A popular form of copolymer used in biofunctional hydrogels is a triblock copolymer containing hydrophilic and hydrophobic polymers, such as polyethylene oxide (PEO)-polypropylene oxide (PPO)-PEO (Pluronic), poly(lactic-co-glycolic acid) (PLGA)-PEG-PLGA, PEG-poly-L-lactide (PLLA)-PEG, polycaprolactone (PCL)-PEG-PCL, poly(caprolactone-co-lactide) (PCLA)-PEG-PCLA, and PEG-PCL-PEG, which exhibit temperature-triggered gelation above LCST [49-50]. They can first assemble into micelles and bridged micelles at low temperatures, and then further gelation proceeds by the ordered packing of bridged micelles at higher temperature [38, 51].

2.2. Crosslinking Mechanisms for Hydrogels

A hydrogel is a *crosslinked* network of hydrophilic polymers. Uncrosslinked hydrophilic polymers will fully disperse in water, instead of forming a hydrogel. Crosslinking can largely be categorized into physical (non-covalent) and chemical (covalent) crosslinking. Physical crosslinking includes thermal crosslinking, ionic crosslinking, β-sheet formation, and specific biological recognitions including leucine zipper self-assembly, and DNA hybridization, while chemical crosslinking includes photopolymerization, Michael-type addition, carboxyl-to-amine crosslinking, small molecule crosslinking, and enzymatic crosslinking.

2.2.1. Physical crosslinking

Physical crosslinking methods are often used due to their reversible nature and fast curing speed. They are very useful for *in situ* gelation, which means that a polymer solution is crosslinked to form a hydrogel on site [52].

One of the common physical crosslinking mechanisms is a temperature change, which is called thermal crosslinking. The most common thermal crosslinking utilizes LCST [53] as explained earlier. Another kind of thermal crosslinking is based on the upper critical solution temperature (UCST) [54]. In this case, hydrogel is formed at lower temperatures than UCST. Gelatin, for example, is physically crosslinked at a low temperature and melts beyond the UCST.

Ionic crosslinking can be applied to polymers that have net charges; when oppositely charged molecules are present, the polymers can be crosslinked by the ionic interactions. Ionic crosslinking of alginate by divalent cations, such as calcium (Ca^{2+}) and magnesium (Mg^{2+}), has been widely used for rapid gelation [25]. On the other hand, chitosan is a positively charged polymer, and can be crosslinked by negatively charged ions, such as TPP or alginate [33-34].

β-sheet formation is produced by packing of hydrophobic groups in repeat units of the primary protein structure, which leads to both intra- and intermolecular crystallization structures [55]. Silk fibroin can be crosslinked by β-sheets, held together by hydrophobic interactions within polypeptide segments containing repeated hydrophobic residue units.

A leucine zipper is a pair of self-assembling *alpha*-helical peptides containing periodic leucine residues. The self-assembly of the hydrogel is driven by hydrophobic interactions. Leucine zippers can be incorporated into polymers and used as a crosslinking mechanism to form reversible hydrogels [56-58].

Deoxyribonucleic acid (DNA) hybridization is a reversible self-assembly between two DNA strands of complementary sequences based on guanine-cytosine (G-C) and adenine-thymidine (A-T) pairs. Hydrophilic polymers can be modified with DNA strands and crosslinked through

specific DNA hybridization. This crosslinking method has been used to create fast curing, shape-memory, and self-healing hydrogels [59].

2.2.2. Chemical crosslinking

Chemical crosslinking involves covalent bond formations between polymer chains. Covalent bonds are irreversible and usually result in more mechanically stable hydrogels.

Photopolymerization is one of the widely used crosslinking mechanisms due to its short gelation time and possibilities for *in situ* gelation. It is normally initiated by UV irradiation, resulting in free radicals being generated by photoinitiators and then propagation of radical polymerization. In general, polymers are conjugated with acrylate or methacrylate groups for photopolymerization [60-61]. This method of crosslinking has been applied to many polymers such as pHEMA [60], collagen [62], gelatin [61], PEG [63], PVA [46], and PNIPAAm [64]. However, due to the cytotoxicity of the photoinitiator and the free radicals, it can be harmful for cells, leading to low cell viability. To reduce the cytotoxicity of the photopolymerization process, anti-oxidants (e.g. ascorbic acid) can be added during polymerization [65-66].

Michael-type addition refers to electron-deficient olefins (e.g. vinyl sulfone, maleimide) reacting with electron-rich nucleophilic compounds (e.g. thiol) [67-68]. The significance of this method is that there is no side product formation during the reaction. Most of the Michael-type addition processes can occur in physiologically relevant conditions and are minimally cytotoxic [69-70]. Stewart *et al*. developed a PEG hydrogel by utilizing the Michael-type addition between vinyl sulfone and thiols as a crosslinking mechanism to encapsulate NIH 3T3 Mus musculus fibroblasts to be used as synthetic ECM [71].

Carboxyl-to-amine crosslinking is linking carboxylic acids to primary amines to form amide bonds [72-74]. This is normally achieved by activating the carboxyl group with the water-soluble 1-ethyl-3-(-3-dimethylaminopropyl) carbodiimide hydrochloride (EDC), which forms an o-acylisourea intermediate that reacts with a primary amine to form an amide bond [75]. One disadvantage of this method is cytotoxicity [76], and it cannot be used in the presence of cells [77].

Enzymatic crosslinking is widely used for hydrogels due to its biocompatibility. Transglutaminase crosslinks proteins and peptides by creating an amide bond between glutamine and lysine residues. Collagen [78] or gelatin [79] can be crosslinked to form a hydrogel by the addition of transglutaminase. Horseradish peroxidase (HRP), which catalyzes the crosslinking of polymer-phenol conjugates in the presence of hydrogen peroxide (H_2O_2) [80], has been used for crosslinking silk fibroin [81] and HA [82].

2.3. Applications for Hydrogels

Due to its high water content and general biocompatibility, hydrogel has been used for applications in medicine and biotechnologies including drug delivery, contact lens, wound healing, and tissue engineering.

2.3.1. Drug delivery

Hydrogel is a particularly appealing drug delivery system for proteins and peptides [83]. Unlike hydrophobic polymer-based drug delivery systems in which proteins can denature, proteins can retain their 3D structures in the well-hydrated hydrogel space. Small molecule drugs can also be delivered from hydrogels. Inclusion of drugs in hydrogels protects the drugs from degradation and increases their bioavailability [84]. Controlled release of drugs from hydrogels can be achieved by two types of mechanisms. (1) Drugs can be loaded in the hydrogel and only slowly released

because of increased mass transfer resistance by the polymer meshes [7]. To further delay the release and the initial burst release, ionic interactions can be utilized as well [85-86]. In these cases, drug release is achieved by passive diffusion. (2) Drug release from the hydrogels can also be achieved by environmental stimuli. Examples include the enzymatic degradation of hydrogels [40] and temperature change-induced structural changes of hydrogels [87].

2.3.2. Contact lens

Hydrogel has been a choice material for contact lenses due to its high water content, optical transparency, and good mechanical strength [88-90]. Drug delivery or other therapeutic functions can be added to hydrogel-based contact lenses to treat ocular diseases. Malakooti *et al.* developed a pHEMA hydrogel-based contact lens for the controlled release of Polymyxin B, a lipopeptide antibiotic [91].

2.3.3. Wound healing

The human body has a capacity to repair damaged tissues. A natural wound healing process usually involves blood clot formation (hemostasis), clearance of pathogens by the innate immune cells (inflammation), migration and proliferation of fibroblasts (proliferation), and restoration of the tissue (tissue remodeling) [92]. The initial blood clot serves as a temporary matrix for the tissue remodeling and contains many chemokines and growth factors to attract innate immune cells and fibroblasts for the complete healing. However, when the wound is larger than a critical size or when the patient is under special health conditions (e.g. diabetes), the natural healing can be compromised [93]. To accelerate the wound healing process for such adverse cases, use of hydrogels has been suggested due to their similarity to the natural tissue microenvironment. Biodegradable hydrogels, when applied to the wound site, can serve as a temporary scaffold

allowing cell migration and proliferation for the tissue remodeling process [94]. Various growth factors can be incorporated in the hydrogel to mimic the microenvironment of tissue repair and further enhance the healing process. Examples of growth factors, incorporated in the hydrogels for wound healing, include platelet-derived growth factor (PDGF), transforming growth factor beta (TGF-β), epidermal growth factor (EGF), and fibroblast growth factor (FGF) [95]. To conform to the irregular topography of wounds, injectable hydrogel formulations are highly desired.

2.3.4. Tissue engineering

Tissue engineering aims to build a functional tissue in the laboratory to overcome the lack of donor organs/tissues for transplantation [96]. Tissue engineering utilizes a combination of a cell population of the target tissue dispersed in a 3D space of a biodegradable scaffold as an artificial ECM. Biological signals, such as cell adhesive ligands and growth factors should be incorporated as well. Hydrogel has been a popular choice for the artificial ECM due to its hydrated microenvironment mimicking the native tissue [97].

Cells can be introduced in the 3D hydrogel space in two ways: (1) cells can be added into the 3D space of a preformed hydrogel either by direct injection into multiple locations within the hydrogel or by promoting cell migration from the exterior, and (2) cells can be encapsulated in the hydrogel by mixing the cells in a polymer solution prior to the gelation process [98]. An advantage of the first approach is there are far fewer restrictions on the crosslinking mechanisms for gelation because cells are added after the hydrogel has formed. Cytotoxic processes can still be used as long as toxic reactants and side products are removed before the addition of cells. Therefore, chemical and mechanical properties of the final hydrogel can be tuned more easily. However, achieving full dispersion of the cells in the hydrogel space is not trivial. The injection

process can also damage the hydrogel structure. There can be significant shape mismatch between the preformed hydrogel-cell construct and the target tissue. The second approach utilizes an injectable hydrogel formulation, which is initially an aqueous polymer solution and can be mixed with a cell suspension. Crosslinking of polymers in the presence of cells results in a hydrogel with cells well-dispersed in the 3D hydrogel phase. Due to the injectable nature of this approach, the incorporation of the hydrogel-cell construct may not require an incision. The crosslinking process, however, needs to be non-cytotoxic.

2.4. Limitations of Current Injectable Hydrogels

The main theme of this thesis is the creation of injectable hydrogels for wound healing and tissue engineering. One of the major limitations of most injectable hydrogels for such applications is lack of macropores. In wound healing, migration of host cells into traditional nonporous hydrogels is severely delayed, making those injectable formulations ineffective. In tissue engineering, injectable hydrogels can be used to encapsulate cells during the gelation process, achieving good dispersion of the cells within the 3D space. However, due to the lack of macropores, the encapsulated cells are trapped in the polymer mesh, preventing the cells from spreading and proliferating. These limitations have prompted the development of injectable and macroporous hydrogels.

2.5. Injectable Macroporous Hydrogel

Various efforts have been reported in the literature about injectable and macroporous hydrogels. Macropores should be larger than the dimension of human cells (> 30 μm) to be effective.

Patterson *et al.* developed an injectable hydrogel using multi-arm PEG crosslinked by matrix metalloproteinase (MMP)-sensitive peptide strands. It is initially not a macroporous hydrogel.

However, the crosslinking peptides can be cleaved by MMPs secreted by the surrounding cells, creating 'pores' for cell migration. This formulation was used to enable cell invasion into the hydrogel, suitable in angiogenesis applications [99-102]. Schultz *et al.* applied a similar strategy, using MMP-degradable hydrogels in cell-mediated scaffold remodeling to enhance cell spreading and migration [101]. However, as cell migration and hydrogel degradation proceed, mechanical integrity of the hydrogel is compromised.

Koshy *et al.* made an injectable and macroporous hydrogel by crosslinking polymers at a low temperature, inducing a phase separation between polymers and ice crystals. Pores were created by melting the ice crystals. The resulting hydrogel was highly porous and injectable, and yet elastic enough to regain its original shape after injection. Injectable macroporous hydrogels of alginate and gelatin were produced using this method for the purpose of delivering proteins (granulocyte-macrophage colony-stimulating factor and interleukin 2) in the hydrogel to represent for the application of immunotherapy. Meanwhile, porosity has been a new important factor of the injectable hydrogel. The normal hydrogel holds a nanoporous network structure. However, when the interconnected pores are larger than the cell size (~10 micron), the hydrogel will allow better cell infiltration and development [99, 103-105]. One disadvantage of this approach is that the shape of the hydrogel is pre-determined. Tissue adhesion of this hydrogel is another challenge for wound healing and tissue engineering applications.

Goh *et al*. developed an injectable macroporous hydrogel by incorporating gelatin microgels in a PEG-based hydrogel [106]. The physically crosslinked gelatin microgels served as porogens (templates for pores), which could be leached out at body temperature as the microgels dissociated. This hydrogel was used for tissue engineering purposes such as cell recruitment.

However, the formation of this macroporous hydrogel relies on microgel leaching and the melted polymer presents a potential risk to the surrounding tissue.

One promising method of making an injectable macroporous hydrogel is assembling and curing microgels. In this case, the macropores are formed by the interstitial space in between the microgels [107]. Caldwell *et al*. reported a hydrogel which was made by self-assembly using modified PEG to form PEG-dibenzocyclooctyne microgels and PEG-N_3 microgels [108]. Griffin *et al*. reported a method using 4-arm PEG-vinyl sulfone crosslinked with lysine and glutamine residues to form microgels [109]. A similar method could be used to assemble HA microgels [107]. However, these methods require chemical modification of the polymer which is risky for cell behaviors.

2.6. Motivation of the research

Based on the current status of the field of hydrogels and their applications in medicine and biotechnology, the motivation of my research was the following.

- To develop a new microgel-based injectable macroporous hydrogel that is simple to make, cost-effective, and highly biofunctional, and that can be used for wound healing and tissue engineering.

In the following chapters, I demonstrate the feasibility of using this method for accelerated wound healing and tissue engineering.

2.7. Reference

1. Hoffman, A. S., Hydrogels for Biomedical Applications. *Adv. Drug Del. Rev.* 2012, *64*, 18-23.

2. Geckil, H.; Xu, F.; Zhang, X.; Moon, S.; Demirci, U., Engineering Hydrogels as Extracellular Matrix Mimics. *Nanomedicine* 2010, *5* (3), 469-484.

3. Allen, A. B.; Priddy, L. B.; Li, M.-T. A.; Guldberg, R. E., Functional Augmentation of Naturally-Derived Materials for Tissue Regeneration. *Ann. Biomed. Eng.* 2015, *43* (3), 555-567.

4. Lee, C. H.; Singla, A.; Lee, Y., Biomedical Applications of Collagen. *Int. J. Pharm.* 2001, *221* (1-2), 1-22.

5. Rammelt, S.; Illert, T.; Bierbaum, S.; Scharnweber, D.; Zwipp, H.; Schneiders, W., Coating of Titanium Implants with Collagen, Rgd Peptide and Chondroitin Sulfate. *Biomaterials* 2006, *27* (32), 5561-5571.

6. Krane, S. M., Collagenases and Collagen Degradation. *J. Invest. Dermatol.* 1982, *79* (1), 83-86.

7. Heo, J.; Koh, R. H.; Shim, W.; Kim, H. D.; Yim, H.-G.; Hwang, N. S., Riboflavin-Induced Photo-Crosslinking of Collagen Hydrogel and Its Application in Meniscus Tissue Engineering. *Drug Delivery Transl. Res.* 2016, *6* (2), 148-158.

8. Telis, V.; Wolf, K.; Sobral, P. In Characterizations of Collagen Fibers for Biodegradable Films Production, *13th World Congress of Food Science & Technology* 2006, 2006; pp 929-929.

9. Eaglstein, W. H.; Alvarez, O. M.; Auletta, M.; Leffel, D.; Rogers, G. S.; Zitelli, J. A.; Norris, J. E.; Thomas, I.; Irondo, M.; Fewkes, J., Acute Excisional Wounds Treated with a Tissue‐Engineered Skin (Apligraf). *Dermatol. Surg.* 1999, *25* (3), 195-201.

10. Huang, Y.; Onyeri, S.; Siewe, M.; Moshfeghian, A.; Madihally, S. V., In Vitro Characterization of Chitosan–Gelatin Scaffolds for Tissue Engineering. *Biomaterials* 2005, *26* (36), 7616-7627.

11. Xu, C.; Inokuma, M. S.; Denham, J.; Golds, K.; Kundu, P.; Gold, J. D.; Carpenter, M. K., Feeder-Free Growth of Undifferentiated Human Embryonic Stem Cells. *Nat. Biotechnol.* 2001, *19* (10), 971.

12. Tylingo, R.; Gorczyca, G.; Mania, S.; Szweda, P.; Milewski, S., Preparation and Characterization of Porous Scaffolds from Chitosan-Collagen-Gelatin Composite. *React. Funct. Polym.* 2016, *103*, 131-140.

13. Rebers, L.; Granse, T.; Tovar, G. E.; Southan, A.; Borchers, K., Physical Interactions Strengthen Chemical Gelatin Methacryloyl Gels. *Gels* 2019, *5* (1), 4.

14. Nichol, J. W.; Koshy, S. T.; Bae, H.; Hwang, C. M.; Yamanlar, S.; Khademhosseini, A., Cell-Laden Microengineered Gelatin Methacrylate Hydrogels. *Biomaterials* 2010, *31* (21), 5536-5544.

15. Shin, S. R.; Zihlmann, C.; Akbari, M.; Assawes, P.; Cheung, L.; Zhang, K.; Manoharan, V.; Zhang, Y. S.; Yüksekkaya, M.; Wan, K. t., Reduced Graphene Oxide-GelMa Hybrid Hydrogels as Scaffolds for Cardiac Tissue Engineering. *Small* 2016, *12* (27), 3677-3689.

16. Chen, P.; Xia, C.; Mei, S.; Wang, J.; Shan, Z.; Lin, X.; Fan, S., Intra-Articular Delivery of Sinomenium Encapsulated by Chitosan Microspheres and Photo-Crosslinked GelMa Hydrogel Ameliorates Osteoarthritis by Effectively Regulating Autophagy. *Biomaterials* 2016, *81*, 1-13.

17. Dong, Y.; Rodrigues, M.; Li, X.; Kwon, S. H.; Kosaric, N.; Khong, S.; Gao, Y.; Wang, W.; Gurtner, G. C., Injectable and Tunable Gelatin Hydrogels Enhance Stem Cell Retention and Improve Cutaneous Wound Healing. *Adv. Funct. Mater.* 2017, *27* (24), 1606619.

18. Chouhan, D.; Lohe, T. u.; Samudrala, P. K.; Mandal, B. B., *In Situ* Forming Injectable Silk Fibroin Hydrogel Promotes Skin Regeneration in Full Thickness Burn Wounds. *Adv. Healthcare Mater.* 2018, *7* (24), 1801092.

19. Keene, E. C.; Evans, J. S.; Estroff, L. A., Silk Fibroin Hydrogels Coupled with the N16n− B-Chitin Complex: An in Vitro Organic Matrix for Controlling Calcium Carbonate Mineralization. *Cryst. Growth Des.* 2010, *10* (12), 5169-5175.

20. Ribeiro, M.; de Moraes, M. A.; Beppu, M. M.; Garcia, M. P.; Fernandes, M. H.; Monteiro, F. J.; Ferraz, M. P., Development of Silk Fibroin/Nanohydroxyapatite Composite Hydrogels for Bone Tissue Engineering. *Eur. Polym. J.* 2015, *67*, 66-77.

21. Yucel, T.; Cebe, P.; Kaplan, D. L., Vortex-Induced Injectable Silk Fibroin Hydrogels. *Biophys. J.* 2009, *97* (7), 2044-2050.

22. Sun, W.; Incitti, T.; Migliaresi, C.; Quattrone, A.; Casarosa, S.; Motta, A., Viability and Neuronal Differentiation of Neural Stem Cells Encapsulated in Silk Fibroin Hydrogel Functionalized with an Ikvav Peptide. *J. Tissue Eng. Regener. Med.* 2017, *11* (5), 1532-1541.

23. Rowley, J. A.; Madlambayan, G.; Mooney, D. J., Alginate Hydrogels as Synthetic Extracellular Matrix Materials. *Biomaterials* 1999, *20* (1), 45-53.

24. García-Astrain, C.; Avérous, L., Synthesis and Evaluation of Functional Alginate Hydrogels Based on Click Chemistry for Drug Delivery Applications. *Carbohydr. Polym.* 2018, *190*, 271-280.

25. Jeon, O.; Bouhadir, K. H.; Mansour, J. M.; Alsberg, E., Photocrosslinked Alginate Hydrogels with Tunable Biodegradation Rates and Mechanical Properties. *Biomaterials* 2009, *30* (14), 2724-2734.

26. Tabriz, A. G.; Hermida, M. A.; Leslie, N. R.; Shu, W., Three-Dimensional Bioprinting of Complex Cell Laden Alginate Hydrogel Structures. *Biofabrication* 2015, *7* (4), 045012.

27. Crompton, K.; Goud, J.; Bellamkonda, R.; Gengenbach, T.; Finkelstein, D.; Horne, M.; Forsythe, J., Polylysine-Functionalised Thermoresponsive Chitosan Hydrogel for Neural Tissue Engineering. *Biomaterials* 2007, *28* (3), 441-449.

28. Fukuda, J.; Khademhosseini, A.; Yeo, Y.; Yang, X.; Yeh, J.; Eng, G.; Blumling, J.; Wang, C.-F.; Kohane, D. S.; Langer, R., Micromolding of Photocrosslinkable Chitosan Hydrogel for Spheroid Microarray and Co-Cultures. *Biomaterials* 2006, *27* (30), 5259-5267.

29. Lončarević, A.; Ivanković, M.; Rogina, A., Lysozyme-Induced Degradation of Chitosan: The Characterisation of Degraded Chitosan Scaffolds. *J.Tissue Repair Regen.* 2017, *1* (1), 12.

30. Kim, S.; Cui, Z.-K.; Koo, B.; Zheng, J.; Aghaloo, T.; Lee, M., Chitosan–Lysozyme Conjugates for Enzyme-Triggered Hydrogel Degradation in Tissue Engineering Applications. *ACS Appl. Mater. Interfaces* 2018, *10* (48), 41138-41145.

31. Schatz, C.; Bionaz, A.; Lucas, J.-M.; Pichot, C.; Viton, C.; Domard, A.; Delair, T., Formation of Polyelectrolyte Complex Particles from Self-Complexation of N-Sulfated Chitosan. *Biomacromolecules* 2005, *6* (3), 1642-1647.

32. Qu, J.; Zhao, X.; Ma, P. X.; Guo, B., Ph-Responsive Self-Healing Injectable Hydrogel Based on N-Carboxyethyl Chitosan for Hepatocellular Carcinoma Therapy. *Acta Biomater.* 2017, *58*, 168-180.

33. Chen, F.; Zhang, Z.-R.; Huang, Y., Evaluation and Modification of N-Trimethyl Chitosan Chloride Nanoparticles as Protein Carriers. *Int. J. Pharm.* 2007, *336* (1), 166-173.

34. Mohandas, A.; Sudheesh Kumar, P.; Raja, B.; Lakshmanan, V.-K.; Jayakumar, R., Exploration of Alginate Hydrogel/Nano Zinc Oxide Composite Bandages for Infected Wounds. *Int. J. Nanomed.* 2015, *10* (Suppl 1), 53.

35. Luo, Y.; Kirker, K. R.; Prestwich, G. D., Cross-Linked Hyaluronic Acid Hydrogel Films: New Biomaterials for Drug Delivery. *J. Controlled Release* 2000, *69* (1), 169-184.

36. Ouyang, L.; Highley, C. B.; Rodell, C. B.; Sun, W.; Burdick, J. A., 3D Printing of Shear-Thinning Hyaluronic Acid Hydrogels with Secondary Cross-Linking. *ACS Biomater. Sci. Eng.* 2016, *2* (10), 1743-1751.

37. Han, S.-S.; Yoon, H. Y.; Yhee, J. Y.; Cho, M. O.; Shim, H.-E.; Jeong, J.-E.; Lee, D.-E.; Kim, K.; Guim, H.; Lee, J. H., *In Situ* Cross-Linkable Hyaluronic Acid Hydrogels Using Copper Free Click Chemistry for Cartilage Tissue Engineering. *Polym. Chem.* 2018, *9* (1), 20-27.

38. Shim, W. S.; Kim, J.-H.; Park, H.; Kim, K.; Kwon, I. C.; Lee, D. S., Biodegradability and Biocompatibility of a Ph-and Thermo-Sensitive Hydrogel Formed from a Sulfonamide-Modified Poly (E-Caprolactone-Co-Lactide)–Poly (Ethylene Glycol)–Poly (E-Caprolactone-Co-Lactide) Block Copolymer. *Biomaterials* 2006, *27* (30), 5178-5185.

39. Sridhar, B. V.; Brock, J. L.; Silver, J. S.; Leight, J. L.; Randolph, M. A.; Anseth, K. S., Development of a Cellularly Degradable Peg Hydrogel to Promote Articular Cartilage Extracellular Matrix Deposition. *Adv. Healthcare Mater.* 2015, *4* (5), 702-713.

40. Henise, J.; Hearn, B. R.; Ashley, G. W.; Santi, D. V., Biodegradable Tetra-Peg Hydrogels as Carriers for a Releasable Drug Delivery System. *Bioconj. Chem.* 2015, *26* (2), 270-278.

41. Han, L.; Zhang, Y.; Lu, X.; Wang, K.; Wang, Z.; Zhang, H., Polydopamine Nanoparticles Modulating Stimuli-Responsive Pnipam Hydrogels with Cell/Tissue Adhesiveness. *ACS Appl. Mater. Interfaces* 2016, *8* (42), 29088-29100.

42. Kim, D. S.; Choi, A.; Seo, K. D.; Yoon, H.; Han, S., Bulk Poly (N-Isopropylacrylamide)(Pnipaam) Thermoresponsive Cell Culture Platform: Toward a New Horizon in Cell Sheet Engineering. *Biomater. Sci.* 2019.

43. Ekerdt, B. L.; Fuentes, C. M.; Lei, Y.; Adil, M. M.; Ramasubramanian, A.; Segalman, R. A.; Schaffer, D. V., Thermoreversible Hyaluronic Acid-Pnipaam Hydrogel Systems for 3D Stem Cell Culture. *Adv. Healthcare Mater.* 2018, *7* (12), 1800225.

44. Schmedlen, R. H.; Masters, K. S.; West, J. L., Photocrosslinkable Polyvinyl Alcohol Hydrogels That Can Be Modified with Cell Adhesion Peptides for Use in Tissue Engineering. *Biomaterials* 2002, *23* (22), 4325-4332.

45. Zhou, Y.; Zhang, C.; Liang, K.; Li, J.; Yang, H.; Liu, X.; Yin, X.; Chen, D.; Xu, W., Photopolymerized Water-Soluble Maleilated Chitosan/Methacrylated Poly (Vinyl Alcohol) Hydrogels as Potential Tissue Engineering Scaffolds. *Int. J. Biol. Macromol.* 2018, *106*, 227-233.

46. Chen, W.; Hou, Y.; Tu, Z.; Gao, L.; Haag, R., Ph-Degradable Pva-Based Nanogels Via Photo-Crosslinking of Thermo-Preinduced Nanoaggregates for Controlled Drug Delivery. *J. Controlled Release* 2017, *259*, 160-167.

47. Hwang, Y.; Kim, G., Evaluation of Stability and Biocompatibility of Phema-Pmma Keratoprosthesis by Penetrating Keratoplasty in Rabbits. *ILAR J.* 2016, *32* (4), 181-186.

48. Ciolino, J. B.; Ross, A. E.; Tulsan, R.; Watts, A. C.; Wang, R.-F.; Zurakowski, D.; Serle, J. B.; Kohane, D. S., Latanoprost-Eluting Contact Lenses in Glaucomatous Monkeys. *Ophthalmology* 2016, *123* (10), 2085-2092.

49. Cellesi, F.; Tirelli, N.; Hubbell, J. A., Materials for Cell Encapsulation Via a New Tandem Approach Combining Reverse Thermal Gelation and Covalent Crosslinking. *Macromol. Chem. Phys.* 2002, *203* (10-11), 1466-1472.

50. Jeong, B.; Bae, Y. H.; Kim, S. W., *In Situ* Gelation of Peg-Plga-Peg Triblock Copolymer Aqueous Solutions and Degradation Thereof. *J. Biomed. Mater. Res.* 2000, *50* (2), 171-177.

51. Bogdanov, B.; Vidts, A.; Van Den Buicke, A.; Verbeeck, R.; Schacht, E., Synthesis and Thermal Properties of Poly (Ethylene Glycol)-Poly (ϵ-Caprolactone) Copolymers. *Polymer* 1998, *39* (8-9), 1631-1636.

52. Kouchak, M., *In Situ* Gelling Systems for Drug Delivery. *Jundishapur J. Nat. Pharm. Prod.* 2014, *9* (3).

53. Sun, T.; Wang, G.; Feng, L.; Liu, B.; Ma, Y.; Jiang, L.; Zhu, D., Reversible Switching between Superhydrophilicity and Superhydrophobicity. *Angew. Chem., Int. Ed.* 2004, *43* (3), 357-360.

54. Azzaroni, O.; Brown, A. A.; Huck, W. T., Ucst Wetting Transitions of Polyzwitterionic Brushes Driven by Self‐Association. *Angew. Chem., Int. Ed.* 2006, *45* (11), 1770-1774.

55. Nagarkar, S.; Nicolai, T.; Chassenieux, C.; Lele, A., Structure and Gelation Mechanism of Silk Hydrogels. *Phys. Chem. Chem. Phys.* 2010, *12* (15), 3834-3844.

56. Huang, C.-C.; Ravindran, S.; Yin, Z.; George, A., 3-D Self-Assembling Leucine Zipper Hydrogel with Tunable Properties for Tissue Engineering. *Biomaterials* 2014, *35* (20), 5316-5326.

57. Shen, W.; Kornfield, J. A.; Tirrell, D. A., Structure and Mechanical Properties of Artificial Protein Hydrogels Assembled through Aggregation of Leucine Zipper Peptide Domains. *Soft Matter* 2007, *3* (1), 99-107.

58. Wheeldon, I. R.; Gallaway, J. W.; Barton, S. C.; Banta, S., Bioelectrocatalytic Hydrogels from Electron-Conducting Metallopolypeptides Coassembled with Bifunctional Enzymatic Building Blocks. *Proc. Natl. Acad. Sci. U. S. A.* 2008, *105* (40), 15275-15280.

59. Wang, C.; Liu, X.; Wulf, V.; Vázquez-González, M.; Fadeev, M.; Willner, I., DNA-Based Hydrogels Loaded with Au Nanoparticles or Au Nanorods: Thermoresponsive Plasmonic Matrices for Shape-Memory, Self-Healing, Controlled Release and Mechanical Applications. *ACS nano* 2019.

60. Kamoun, E. A.; El-Betany, A.; Menzel, H.; Chen, X., Influence of Photoinitiator Concentration and Irradiation Time on the Crosslinking Performance of Visible-Light Activated Pullulan-Hema Hydrogels. *Int. J. Biol. Macromol.* 2018, *120*, 1884-1892.

61. Noshadi, I.; Hong, S.; Sullivan, K. E.; Sani, E. S.; Portillo-Lara, R.; Tamayol, A.; Shin, S. R.; Gao, A. E.; Stoppel, W. L.; Black III, L. D., In Vitro and *in Vivo* Analysis of Visible Light Crosslinkable Gelatin Methacryloyl (GelMA) Hydrogels. *Biomater. Sci.* 2017, *5* (10), 2093-2105.

62. Lu, M.; Song, X.; Yang, M.; Kong, W.; Zhu, J., Combined Effects of Glutaraldehyde and Riboflavin/Uv365 on the Self-Assembly of Type I Collagen Molecules Observed with Atomic Force Microscopy. *Int. J. Food Prop.* 2018, *21* (1), 2181-2192.

63. Tan, G.; Wang, Y.; Li, J.; Zhang, S., Synthesis and Characterization of Injectable Photocrosslinking Poly (Ethylene Glycol) Diacrylate Based Hydrogels. *Polym. Bull.* 2008, *61* (1), 91-98.

64. Patra, L.; Toomey, R., Viscoelastic Response of Photo-Cross-Linked Poly (N-Isopropylacrylamide) Coatings by Qcm-D. *Langmuir* 2009, *26* (7), 5202-5207.

65. Sabnis, A.; Rahimi, M.; Chapman, C.; Nguyen, K. T., Cytocompatibility Studies of an *in Situ* Photopolymerized Thermoresponsive Hydrogel Nanoparticle System Using Human Aortic Smooth Muscle Cells. *J. Biomed. Mater. Res., Part A* 2009, *91* (1), 52-59.

66. Drzewiecki, K. E.; Malavade, J. N.; Ahmed, I.; Lowe, C. J.; Shreiber, D. I., A Thermoreversible, Photocrosslinkable Collagen Bio-Ink for Free-Form Fabrication of Scaffolds for Regenerative Medicine. *Technology* 2017, *5* (04), 185-195.

67. Hiemstra, C.; van der Aa, L. J.; Zhong, Z.; Dijkstra, P. J.; Feijen, J., Rapidly *in Situ*-Forming Degradable Hydrogels from Dextran Thiols through Michael Addition. *Biomacromolecules* 2007, *8* (5), 1548-1556.

68. Fu, Y.; Kao, W. J., *In Situ* Forming Poly (Ethylene Glycol)‐Based Hydrogels Via Thiol‐Maleimide Michael‐Type Addition. *J. Biomed. Mater. Res., Part A* 2011, *98* (2), 201-211.

69. Darling, N. J.; Hung, Y.-S.; Sharma, S.; Segura, T., Controlling the Kinetics of Thiol-Maleimide Michael-Type Addition Gelation Kinetics for the Generation of Homogenous Poly (Ethylene Glycol) Hydrogels. *Biomaterials* 2016, *101*, 199-206.

70. Kudva, A.; Luyten, F.; Patterson, J., *In Vitro* Screening of Molecularly Engineered Polyethylene Glycol Hydrogels for Cartilage Tissue Engineering Using Periosteum-Derived and Atdc5 Cells. *Int. J. Mol. Sci.* 2018, *19* (11), 3341.

71. Stewart, S.; Coulson, M.; Zhou, C.; Burke, N.; Stöver, H., Synthetic Hydrogels Formed by Thiol–Ene Crosslinking of Vinyl Sulfone-Functional Poly (Methyl Vinyl Ether-Alt-Maleic Acid) with A, Ω-Dithio-Polyethyleneglycol. *Soft matter* 2018, *14* (41), 8317-8324.

72. Goodarzi, H.; Jadidi, K.; Pourmotabed, S.; Sharifi, E.; Aghamollaei, H., Preparation and Characterization of Cross-Linked Collagen–Gelatin Hydrogel Using Edc/Nhs for Corneal Tissue Engineering Applications. *Int. J. Biol. Macromol.* 2019, *126*, 620-632.

73. Singh, T. R. R.; Laverty, G.; Donnelly, R., Engineering Hyaluronan (Ha) Hydrogels with Bioactive and Mechanical Signals. In *Hydrogels*, CRC Press: 2018; pp 162-177.

74. Rafat, M.; Li, F.; Fagerholm, P.; Lagali, N. S.; Watsky, M. A.; Munger, R.; Matsuura, T.; Griffith, M., Peg-Stabilized Carbodiimide Crosslinked Collagen–Chitosan Hydrogels for Corneal Tissue Engineering. *Biomaterials* 2008, *29* (29), 3960-3972.

75. Guo, P.; Anderson, J. D.; Bozell, J. J.; Zivanovic, S., The Effect of Solvent Composition on Grafting Gallic Acid onto Chitosan Via Carbodiimide. *Carbohydr. Polym.* 2016, *140*, 171-180.

76. Hanthamrongwit, M.; Reid, W.; Grant, M., Chondroitin-6-Sulphate Incorporated into Collagen Gels for the Growth of Human Keratinocytes: The Effect of Cross-Linking Agents and Diamines. *Biomaterials* 1996, *17* (8), 775-780.

77. Hao, Y.; Xu, P.; He, C.; Yang, X.; Huang, M.; Xing, J.; Chen, J., Impact of Carbondiimide Crosslinker Used for Magnetic Carbon Nanotube Mediated Gfp Plasmid Delivery. *Nanotechnology* 2011, *22* (28), 285103.

78. Zhao, L.; Li, X.; Zhao, J.; Ma, S.; Ma, X.; Fan, D.; Zhu, C.; Liu, Y., A Novel Smart Injectable Hydrogel Prepared by Microbial Transglutaminase and Human-Like Collagen: Its Characterization and Biocompatibility. *Mater. Sci. Eng. C Biomimetic Supramol. Syst.* 2016, *68*, 317-326.

79. Yang, G.; Xiao, Z.; Ren, X.; Long, H.; Qian, H.; Ma, K.; Guo, Y., Enzymatically Crosslinked Gelatin Hydrogel Promotes the Proliferation of Adipose Tissue-Derived Stromal Cells. *Peer J.* 2016, *4*, e2497.

80. Lee, F.; Bae, K. H.; Kurisawa, M., Injectable Hydrogel Systems Crosslinked by Horseradish Peroxidase. *Biomed. Mater. (Bristol, U. K.)* 2015, *11* (1), 014101.

81. Zhou, B.; Wang, P.; Cui, L.; Yu, Y.; Deng, C.; Wang, Q.; Fan, X., Self-Crosslinking of Silk Fibroin Using H 2 O 2-Horseradish Peroxidase System and the Characteristics of the Resulting Fibroin Membranes. *Appl. Biochem. Biotechnol.* 2017, *182* (4), 1548-1563.

82. Toh, W. S.; Lim, T. C.; Kurisawa, M.; Spector, M., Modulation of Mesenchymal Stem Cell Chondrogenesis in a Tunable Hyaluronic Acid Hydrogel Microenvironment. *Biomaterials* 2012, *33* (15), 3835-3845.

83. Li, J.; Mooney, D. J., Designing Hydrogels for Controlled Drug Delivery. *Nat. Rev. Mater.* 2016, *1* (12), 16071.

84. Ashley, G. W.; Henise, J.; Reid, R.; Santi, D. V., Hydrogel Drug Delivery System with Predictable and Tunable Drug Release and Degradation Rates. *Proc. Natl. Acad. Sci. U. S. A.* 2013, *110* (6), 2318-2323.

85. Kolambkar, Y. M.; Dupont, K. M.; Boerckel, J. D.; Huebsch, N.; Mooney, D. J.; Hutmacher, D. W.; Guldberg, R. E., An Alginate-Based Hybrid System for Growth Factor Delivery in the Functional Repair of Large Bone Defects. *Biomaterials* 2011, *32* (1), 65-74.

86. Khaliq, N. U.; Sandra, F. C.; Park, D. Y.; Lee, J. Y.; Oh, K. S.; Kim, D.; Byun, Y.; Kim, I.-S.; Kwon, I. C.; Kim, S. Y., Doxorubicin/Heparin Composite Nanoparticles for Caspase-Activated Prodrug Chemotherapy. *Biomaterials* 2016, *101*, 131-142.

87. Jones, S. T.; Walsh-Korb, Z.; Barrow, S. J.; Henderson, S. L.; del Barrio, J.; Scherman, O. A., The Importance of Excess Poly(N-Isopropylacrylamide) for the Aggregation of Poly(N-Isopropylacrylamide)-Coated Gold Nanoparticles. *ACS Nano* 2016, *10* (3), 3158-3165.

88. Badugu, R.; Reece, E. A.; Lakowicz, J. R., Glucose-Sensitive Silicone Hydrogel Contact Lens toward Tear Glucose Monitoring. *J. Biomed. Opt.* 2018, *23* (5), 057005.

89. Lee, D.; Cho, S.; Park, H. S.; Kwon, I., Ocular Drug Delivery through Phema-Hydrogel Contact Lenses Co-Loaded with Lipophilic Vitamins. *Sci. Rep.* 2016, *6*, 34194.

90. Hu, X.; Tan, H.; Hao, L., Functional Hydrogel Contact Lens for Drug Delivery in the Application of Oculopathy Therapy. *J. Mech. Behav. Biomed. Mater.* 2016, *64*, 43-52.

91. Malakooti, N.; Alexander, C.; Alvarez-Lorenzo, C., Imprinted Contact Lenses for Sustained Release of Polymyxin B and Related Antimicrobial Peptides. *J. Pharm. Sci.* 2015, *104* (10), 3386-3394.

92. Diegelmann, R. F.; Evans, M. C., Wound Healing: An Overview of Acute, Fibrotic and Delayed Healing. *Front Biosci* 2004, *9*, 283-289.

93. Goodson, W. H., 3rd; Hung, T. K., Studies of Wound Healing in Experimental Diabetes Mellitus. *J. Surg. Res.* 1977, *22* (3), 221-227.

94. Zhao, X.; Sun, X.; Yildirimer, L.; Lang, Q.; Lin, Z. Y. W.; Zheng, R.; Zhang, Y.; Cui, W.; Annabi, N.; Khademhosseini, A., Cell Infiltrative Hydrogel Fibrous Scaffolds for Accelerated Wound Healing. *Acta Biomater.* 2017, *49*, 66-77.

95. Steed, D. L., The Role of Growth Factors in Wound Healing. *Surg Clin North Am* 1997, *77* (3), 575-586.

96. Thakur, T.; Xavier, J. R.; Cross, L.; Jaiswal, M. K.; Mondragon, E.; Kaunas, R.; Gaharwar, A. K., Photocrosslinkable and Elastomeric Hydrogels for Bone Regeneration. *J. Biomed. Mater. Res., Part A* 2016, *104* (4), 879-888.

97. Pok, S.; Stupin, I. V.; Tsao, C.; Pautler, R. G.; Gao, Y.; Nieto, R. M.; Tao, Z. W.; Fraser, C. D., Jr.; Annapragada, A. V.; Jacot, J. G., Full-Thickness Heart Repair with an Engineered Multilayered Myocardial Patch in Rat Model. *Adv. Healthcare Mater.* 2017, *6* (5).

98. Nicodemus, G. D.; Bryant, S. J., Cell Encapsulation in Biodegradable Hydrogels for Tissue Engineering Applications. *Tissue Eng Part B Rev* 2008, *14* (2), 149-165.

99. Lutolf, M. P.; Lauer-Fields, J. L.; Schmoekel, H. G.; Metters, A. T.; Weber, F. E.; Fields, G. B.; Hubbell, J. A., Synthetic Matrix Metalloproteinase-Sensitive Hydrogels for the Conduction of Tissue Regeneration: Engineering Cell-Invasion Characteristics. *Proc. Natl. Acad. Sci. USA* 2003, *100* (9), 5413-5418.

100. Patterson, J.; Hubbell, J. A., Enhanced Proteolytic Degradation of Molecularly Engineered Peg Hydrogels in Response to Mmp-1 and Mmp-2. *Biomaterials* 2010, *31* (30), 7836-7845.

101. Schultz, K. M.; Kyburz, K. A.; Anseth, K. S., Measuring Dynamic Cell-Material Interactions and Remodeling During 3D Human Mesenchymal Stem Cell Migration in Hydrogels. *Proc. Natl. Acad. Sci. USA* 2015, *112* (29), E3757-3764.

102. Raeber, G. P.; Lutolf, M. P.; Hubbell, J. A., Molecularly Engineered Peg Hydrogels: A Novel Model System for Proteolytically Mediated Cell Migration. *Biophys. J.* 2005, *89* (2), 1374-1388.

103. Koshy, S. T.; Ferrante, T. C.; Lewin, S. A.; Mooney, D. J., Injectable, Porous, and Cell-Responsive Gelatin Cryogels. *Biomaterials* 2014, *35* (8), 2477-2487.

104. Bencherif, S. A.; Sands, R. W.; Bhatta, D.; Arany, P.; Verbeke, C. S.; Edwards, D. A.; Mooney, D. J., Injectable Preformed Scaffolds with Shape-Memory Properties. *Proc. Natl. Acad. Sci. USA* 2012, *109* (48), 19590-19595.

105. Koshy, S. T.; Zhang, D. K. Y.; Grolman, J. M.; Stafford, A. G.; Mooney, D. J., Injectable Nanocomposite Cryogels for Versatile Protein Drug Delivery. *Acta Biomater.* 2018, *65*, 36-43.

106. Goh, M.; Kim, Y.; Gwon, K.; Min, K.; Hwang, Y.; Tae, G., *In Situ* Formation of Injectable and Porous Heparin-Based Hydrogel. *Carbohydr Polym* 2017, *174*, 990-998.

107. Sideris, E.; Griffin, D. R.; Ding, Y.; Li, S.; Weaver, W. M.; Di Carlo, D.; Hsiai, T.; Segura, T., Particle Hydrogels Based on Hyaluronic Acid Building Blocks. *ACS Biomater. Sci. Eng.* 2016, *2* (11), 2034-2041.

108. Caldwell, A. S.; Campbell, G. T.; Shekiro, K. M. T.; Anseth, K. S., Clickable Microgel Scaffolds as Platforms for 3D Cell Encapsulation. *Adv. Healthcare Mater.* 2017, *6* (15).

109. Griffin, D. R.; Weaver, W. M.; Scumpia, P. O.; Di Carlo, D.; Segura, T., Accelerated Wound Healing by Injectable Microporous Gel Scaffolds Assembled from Annealed Building Blocks. *Nat Mater* 2015, *14* (7), 737-744.

Chapter 3:

Injectable Macroporous Hydrogel Formed by Enzymatic Crosslinking of Gelatin Microgels

---

Shujie Hou, Rachel Lake, Shiwha Park, Seth Edwards, Chante Jones, and Kyung Jae Jeong

Key words: injectable hydrogel, porous, wound healing, microgels, gelatin, mTG, controlled release

3.1. Introduction

Due to their hydrophilic nature, hydrogels generally absorb a large quantity of water [1], which makes them ideal materials to interface human tissues, such as in wound dressings [2-5], contact lens [6-10], drug delivery [11-14], and tissue engineering [15-19]. Hydrogels can be made injectable through various in situ crosslinking mechanisms and conform to the irregular topography of the applied site [20]. This makes hydrogels an attractive option for use in wound healing applications.

Wound healing is a complex cellular and biochemical process, typically involving inflammation, new tissue formation, and remodeling phases [21]. When the wound size exceeds a critical value, or when the patient has compromised health conditions such as diabetes, proper wound healing process is seriously impeded. Biodegradable hydrogels applied to wounds can serve as a temporary matrix to facilitate the wound healing process. One of the major challenges regarding injectable hydrogels for such applications is the lack of inherent macropores to allow the migration of cells from neighboring tissue since the gel is formed on the wound site directly from a continuous liquid phase. The typical mesh size of hydrogels is a few nanometers to a few tens of nanometers [22-23], which is orders of magnitude smaller than the dimension of cells (~10μm).

A number of methods have been developed to make macroporous injectable hydrogels in order to enhance the hydrogels' ability to interact with surrounding cells. Hydrogels that are crosslinked in a frozen state can be thawed and made into a highly porous scaffold which can be injected through a needle and regain its original shape [24-26]. However, the shape of the hydrogel must be pre-determined and it is a challenge to tailor the shape of the hydrogel to the wound site. Injectable hydrogels that are formed by crosslinking biocompatible polymers with enzyme-sensitive peptides can also enable the migration of cells within the hydrogel through the cleavage of peptides by the cell-secreted enzymes, such as matrix metalloproteinases (MMPs) [27-29]. Pores

for cell migration are formed as the cells secrete MMPs and cleave the peptide crosslinkers. However, one drawback of this approach is that the mechanical integrity of the hydrogel can be compromised as its enzymatic degradation by the infiltrating cells progresses. Photocuring of gelatin-derived injectable hydrogels has been shown to result in inherent pore structures and to enhance wound healing [30], but the pore size of such hydrogels is not large enough for rapid cell migration as can be demonstrated by the prolonged round cell morphologies when the cells are encapsulated in such hydrogels [30-31]. Another approach of forming macropores within the hydrogels is by assembling microgels. The idea has been explored for regenerative medicine [32-35] and tissue engineering [36-39]. Recently, a novel injectable macroporous hydrogel using a microgel-assembly for accelerated wound healing was reported [40]. In this case, monodisperse polyethylene glycol (PEG) microgels were enzymatically crosslinked through cell adhesive peptides, creating macropores through the interstitial space among microgels. When applied to a rat skin wound model *in vivo*, this porous hydrogel induced more rapid cell migration and wound healing compared to the nonporous counterpart. Due to the inherent macropores, this formulation could also encapsulate cells in the pores and induce rapid cell spreading and proliferation within the hydrogel. However, this method requires a series of chemical modifications of synthetic materials to make the hydrogel bioactive and enzymatically curable.

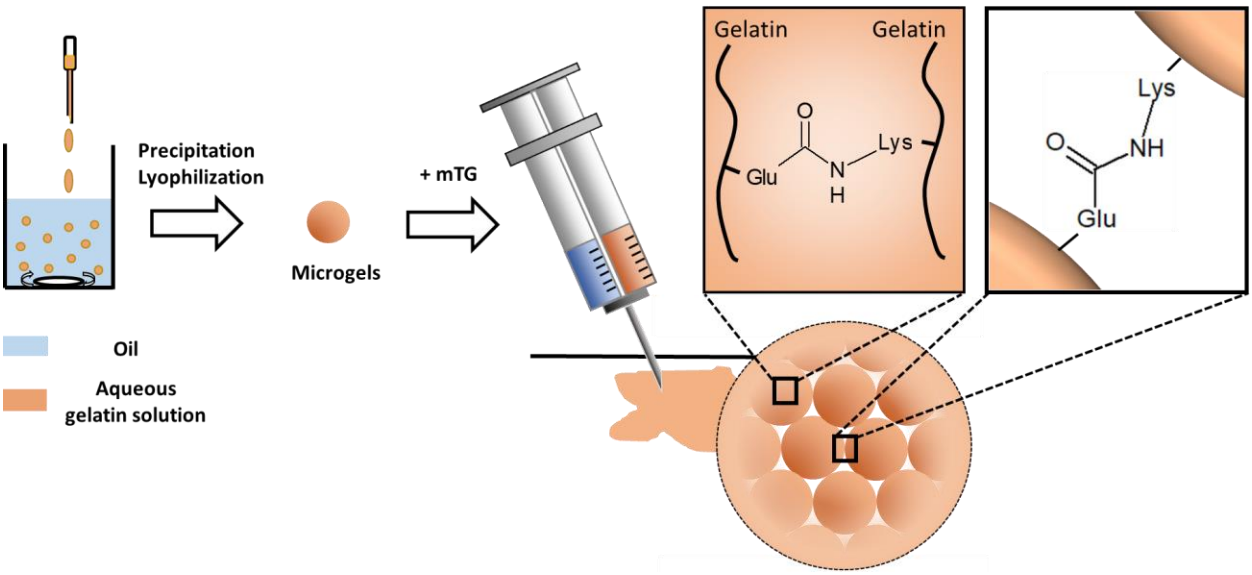

Figure 3.1: Schematic diagram of the microgel synthesis and the formation of porous hydrogel by crosslinking gelatin microgels with mTG. mTG crosslinks gelatins within the microgels and between microgels by creating amide bonds between glutamine (Glu) and lysine (Lys) residues.

In this research, I introduce an injectable macroporous hydrogel by annealing physically crosslinked gelatin microgels by an enzyme - microbial transglutaminase (mTG) (Fig 3.1). Gelatin is a natural protein derived from collagen, and various forms of gelatin hydrogels have been made for applications in wound healing in skin [5, 41] or ocular tissues [30, 42] due to its low cost and well-known bioactivity and biocompatibility. mTG creates covalent bonds between glutamine and lysine residues of gelatin, and forms covalent crosslinks between and within the gelatin microgels [43]. Similar to annealed PEG microgels, pores for cell migration are created by the interstitial space among the gelatin microgels. However, unlike the PEG-based macroporous hydrogel, the gelatin-based macroporous hydrogel introduced here displays inherent bioactivity for cell adhesion and proliferation without any chemical modifications of the raw materials, such as the use of cell adhesive peptides. I also demonstrate the macroporous hydrogel's capability of controlled release of growth factors, which makes this novel formulation even more promising for the applications in wound healing.

3.2. Materials and methods

All materials were purchased from Sigma-Aldrich (St. Louis, MO) unless specified. Microbial transglutaminase (mTG) was purchased from Ajinomoto (Fort Lee, NJ). Sterile phosphate buffer saline (PBS, pH 7.4) was purchased from Gibco (Carlsbad, CA). Dulbecco's Modified Eagle's Medium (DMEM), fetal bovine serum (FBS), penicillin/streptomycin, alamarBlue, actinRed 555, albumin–fluorescein isothiocyanate conjugate (FITC-BSA), and betadine were purchased from Invitrogen (Frederick, MD). The four-arm polyethylene glycol maleimide (20k) (PEG-MAL) was purchased from JenKem technology (Plano, TX). Human dermal fibroblasts (hDFs) were purchased from Lonza (Portsmouth, NH). Platelet-derived growth factor BB (PDGF-BB) was purchased from Boster Bio (Pleasanton, CA). The fresh pig eyeballs were obtained from Frist Visiontech (Sunnyvale, Texas).

3.2.1. Microgel synthesis and mTG crosslinking

Gelatin microgel was prepared by the water-in-oil emulsion method described by Li *et al.* [44]. Briefly, gelatin (Type 1, from bovine and porcine bones) was dissolved in 20 mL deionized water at 50−55 °C to make 10% (w/v) solution. The gelatin solution then was added dropwise to 200 mL olive oil at 50−55 °C and stirred for 1 hour. The temperature of the mixture was lowered to reach room temperature for 30 min with stirring. Then the mixture was placed in an icewater bath for additional 30 min with stirring to solidify the microgels by inducing physical crosslinking. 100 mL of precooled acetone (4 °C) was added into the mixture to precipitate the microgels with stirring for 30 min in the icewater bath. The microgels were separated from the olive oil and acetone through vacuum filtration and further washed twice with 60 mL of precooled acetone. The microgels were lyophilized and kept dry until use. mTG at 20% (w/v)

concentration in PBS was mixed with 10% (w/v) gelatin microgel in PBS at 1:5 ratio to form a porous hydrogel, or mixed with 10% (w/v) gelatin solution in PBS at 1:5 ratio to form a non-porous hydrogel. The final concentration of mTG and gelatin was 3.3% and 8.3%, respectively.

3.2.2. Rheological characterization

The viscoelastic properties of the porous hydrogel and non-porous hydrogel were characterized with a rheometer (TA Instruments AR 550, New Castle, DE). Either gelatin microgel solution or plain gelatin solution was mixed with mTG and placed under a plane stainless steel geometry (diameter = 2cm). The linear viscoelastic regime was first determined by a stress sweep. The gelation kinetics was observed by the time sweep, with an oscillatory stress of 1 Pa at 10 rad/s and 37°C. Once the gelation was completed, the frequency sweep was performed between 0.1 and 100 rad/s with an oscillatory stress of 1 Pa at 37°C. For the temperature sweep, temperature was changed from 4°C to 45°C with an oscillatory stress of 1 Pa at 10 rad/s.

3.2.3. Characterization of the gelatin microgels and porous hydrogel

The microgels were visualized with an optical microscope (EVOS XL, Life Technologies, Carlsbad, CA), and scanning electron microscope (SEM) (Tescan Lyra3 GMU FIB SEM, Brno, Czech Republic). For SEM, the microgels were lyophilized and coated with gold/palladium to avoid charging. Size distribution of the microgels was obtained from the optical microscope and SEM images using ImageJ. After the porous hydrogel was formed, the detailed structure of the hydrogel was visualized with optical microscope, SEM, and confocal microscope (Nikon A1R HD, Melville, NY). For the SEM imaging, the hydrogel was dried by critical point drying. For the confocal microscopy, the porous hydrogel was formed from the microgels mixed with fluorescein isothiocyanate-labelled bovine serum albumin (FTIC-BSA) (0.1%).

3.2.4. Enzymatic degradation of hydrogels

The kinetics of the enzymatic degradation of porous and nonporous gelatin hydrogels was obtained by incubating hydrogels in collagenase type II solution (concentration = 0.5 U/mL) [45]. At different time points (0h, 4h, 24 h), the hydrogels were collected, lyophilized and weighed to calculate the amount of degraded gelatin.

3.2.5. Human dermal fibroblast (hDF) culture on the hydrogels

Human dermal fibroblasts (hDFs) were cultured in T75 flasks using Dulbecco's Modified Eagle Medium (DMEM) supplemented with 10% fetal bovine serum (FBS) and 1% penicillin/streptomycin (pen/strep). The culture was performed in a humidified chamber with 5% CO_2 at 37°C. Cells under passage 4 were used for all the experiments.

To test cellular proliferation on the hydrogels, the porous and non-porous hydrogels (600 μL) were formed in 24-well plates, followed by sterilization in 70% ethanol overnight. Human dermal fibroblasts (hDFs) were seeded on the hydrogel surface with the seeding density of 1×10^4 cells/cm^2. The media was changed twice a day. The proliferation of hDFs was measured by almarBlue on day 7 and 14 by measuring the fluorescence at 595 nm (excitation at 555 nm).

The three-dimensional distribution of hDFs in the hydrogels was visualized by confocal microscopy. After 14 days from the initial seeding, the samples were fixed in 4% formaldehyde in PBS overnight, and stained with actinRed 555 to stain the actin cytoskeleton of hDFs. The Z-section images were obtained using confocal microscope (Nikon A1R HD, Melville, NY) and 2D-projection, 3D images and cross-sectional images were obtained using ImageJ.

3.2.6. Application of the hydrogel to the porcine cornea tissues

Fresh pig eyeballs were sterilized by immersion in povidone-iodine and rinsing several times with sterile PBS. Cornea tissues were collected from the eyeballs using surgical scissors. A hole was created in the middle of the cornea using a biopsy punch (8 mm in diameter). The hole in the cornea was filled by injecting either gelatin microgel solution or plain gelatin solution with mTG to create porous or non-porous hydrogel, respectively. The assembly was incubated for 1 hour at 37°C for curing, after which DMEM supplemented with FBS and pen/strep was added. The tissue-hydrogel assembly was fed daily for 14 days before fixation in formaldehyde. The corneas were stained with actinRed555 and DAPI and imaged by confocal microscope.

3.2.7. Controlled release of FITC-BSA and platelet-derived growth factor (PDGF)

In order to understand the nature of protein loading in the porous hydrogel, the microgels were incubated in a FITC-BSA solution (100 μg/mL) for 48 hours at room temperature. After the supernatant was removed, the distribution of FITC-BSA within the microgels was visualized with a confocal microscope.

PDGF loading into the microgels was achieved using the same method except that the concentration of PDGF was reduced to 20 μg/mL. A PDGF-loaded porous hydrogel was formed by mixing these microgels with unloaded gelatin microgels at 1:9 ratio (v:v) and crosslinking it using mTG. PDGF-loaded non-porous hydrogel was created by adding PDGF to a gelatin solution, which was crosslinked by mTG. After the hydrogels were formed, the release of PDGF was measured at day 1, 2, 3, 7 and 14 by enzyme-linked immunosorbent assay (ELISA).

3.2.8. hDF proliferation with the controlled release of PDGF from the hydrogels

hDFs were seeded on the 24 well plates with the seeding density of 1500 cells/cm^2. On day 2, PDGF-loaded porous and nonporous hydrogels were added to the cell culture through the transwell inserts with semi-permeable membranes. The proliferation of hDFs was measured by almarBlue assay on day 7.

3.2.9. Statistics

The data are presented as means ± standard deviation unless stated otherwise. The statistical significance of the difference among multiple sample groups was tested by ANOVA followed by Tukey's *post hoc* test using Origin 8.1.

3.3. Results and Discussion

3.3.1. Characterization of gelatin microgels

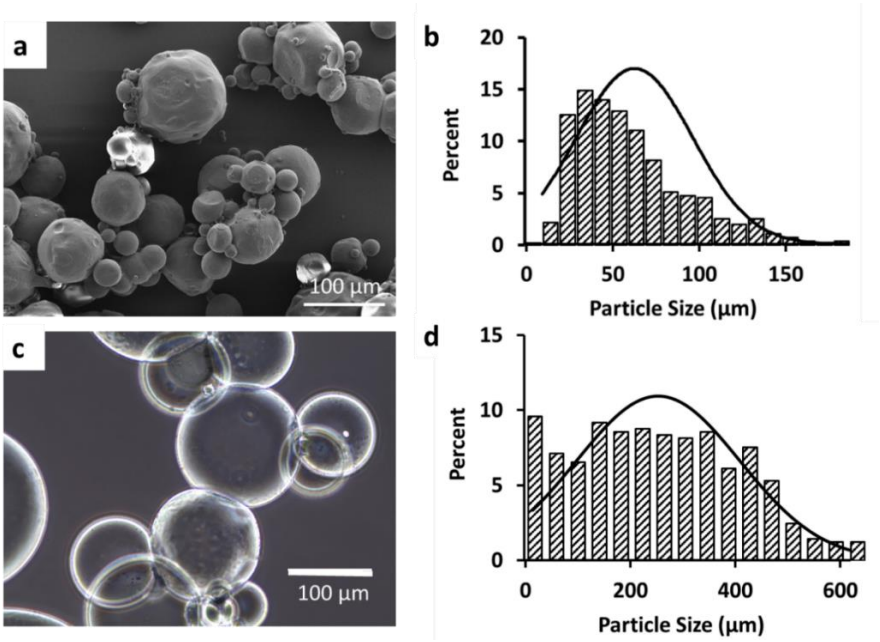

Figure 3.2: Gelatin microgels. a) SEM image of lyophilized (dry) microgels. b) Size distribution of the dry microgels. The average diameter of the dry microgels was 63µm (± 34µm). c) Optical microscope image of the gelatin microgels after swelling in PBS. d) Size distribution of the microgels after swelling. The average diameter was 253µm (± 155µm).

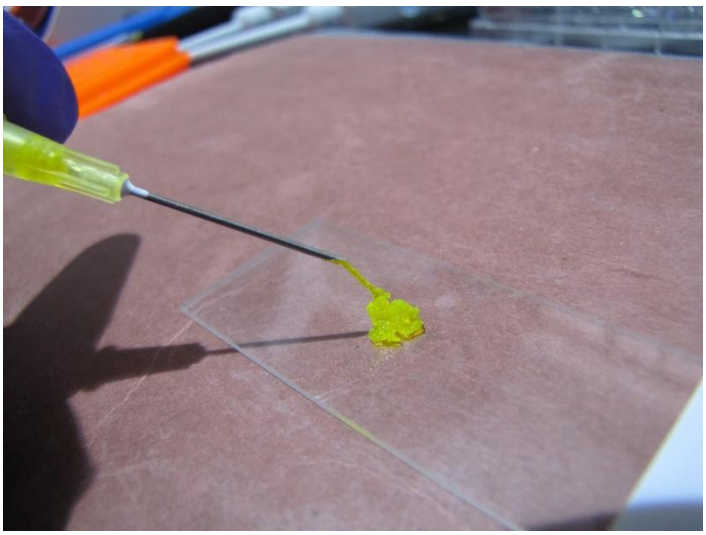

Figure 3.3: Gelatin microgels injected through the needle. Fluorescein was added to the solution for enhanced visualization.

The microgels were synthesized by the water-in-oil emulsion method. The size distribution of the dry microgels were measured by SEM images after lyophilization. The microgels were spherical in shape (Fig 3.2a) and polydisperse with the average diameter of 63 µm (Fig 3.2b). When the microgels were dispersed in water, they swelled significantly (Fig 3.2c) to an average diameter of 253 µm (Fig 3.2d). The swelling ratio was 14.7. At 10% (w/v) concentration and at 37°C, gelatin microgels formed a viscous solution, making them injectable through a gauge 26 needle (Fig 3.3).

3.3.2. Formation and characterization of the macroporous hydrogel.

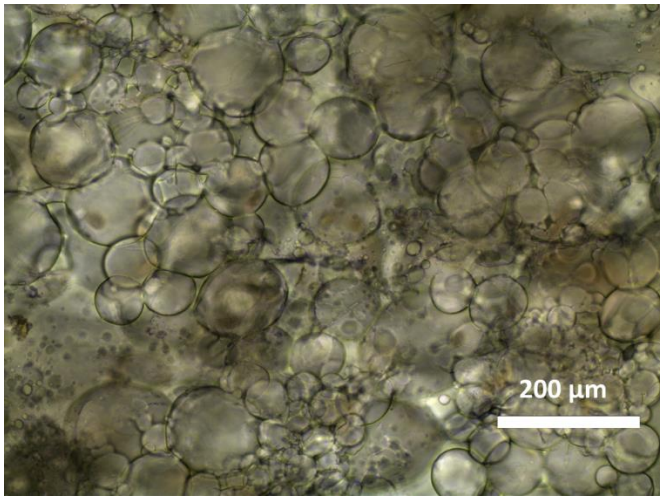

Figure 3.4: Optical microscope image of the porous gelatin hydrogel. The hydrogel was formed by mixing gelatin microgels with mTG. Gelatin microspheres within the hydrogel are evident.

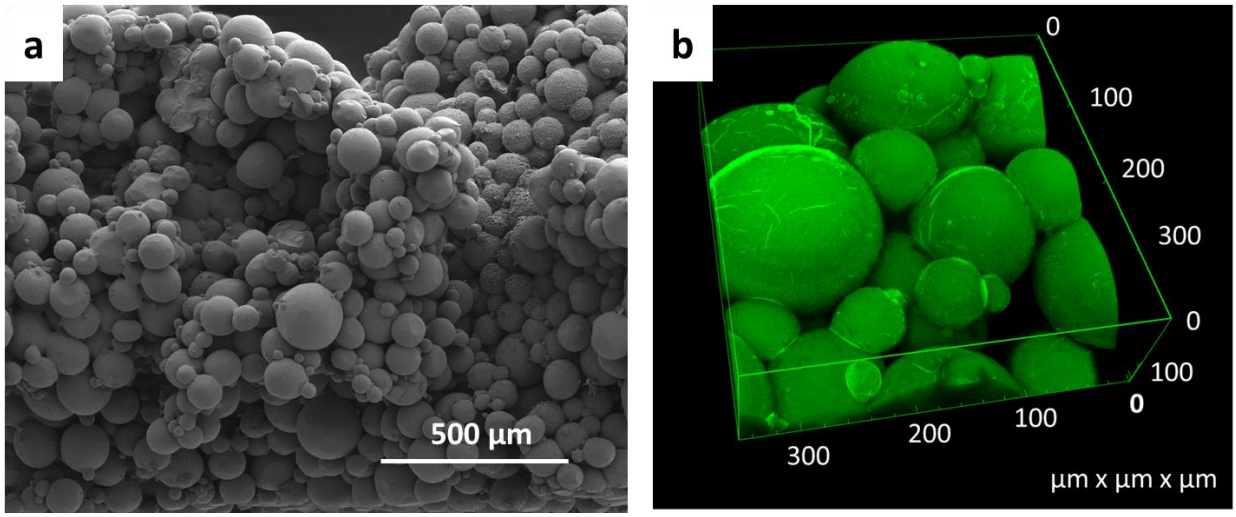

Figure 3.5: 3D structure of the porous hydrogel made of the crosslinked gelatin microgels. a) SEM image of the porous hydrogel after critical point drying. b) 3D rendition of the confocal microscope images of the porous hydrogel. Green fluorescence was obtained by the inclusion of FITC-BSA in the microgels.

A bulk macroporous hydrogel was formed by annealing the gelatin microgels with mTG. When mixed with mTG, the microgel solution became more viscous over time (< 5 min) and eventually became a bulk gel. When viewed under the optical microscope, the assembly of spherical microgels within the hydrogel was evident (Fig 3.4). The SEM image clearly demonstrates a three-dimensional network of spherical microgels with void space between microgels (Fig 3.5a). Confocal microscope images of the hydrogel further confirmed these findings (Fig 3.5b). The pore size was mostly in the range of tens of microns, which is large enough for cell migration [46]. The porosity of the hydrogel was estimated to be 0.43 by the confocal microscope images. This value is in good agreement with the void fraction of random packing of spheres, which is around ~0.4 for various sphere size distributions and materials [47].

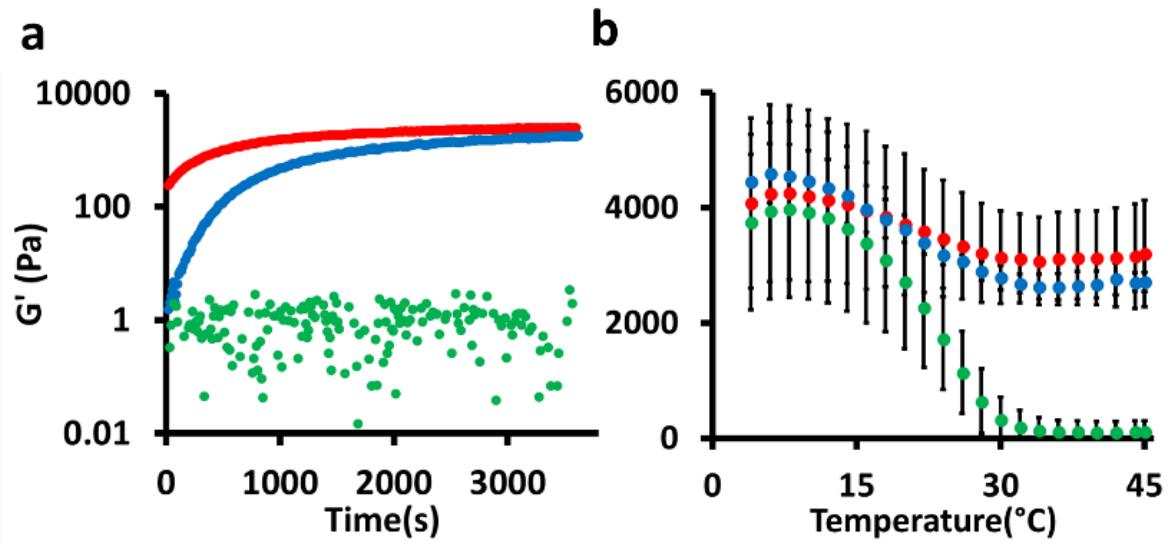

Figure 3.6: Rheological characterization of the hydrogels. a) Time sweep. b) Temperature sweep. Data are means with standard deviation (n = 3). Red: gelatin microgels + mTG (= macroporous hydrogel). Blue: gelatin solution + mTG (nonporous hydrogel). Green: gelatin microgels solution.

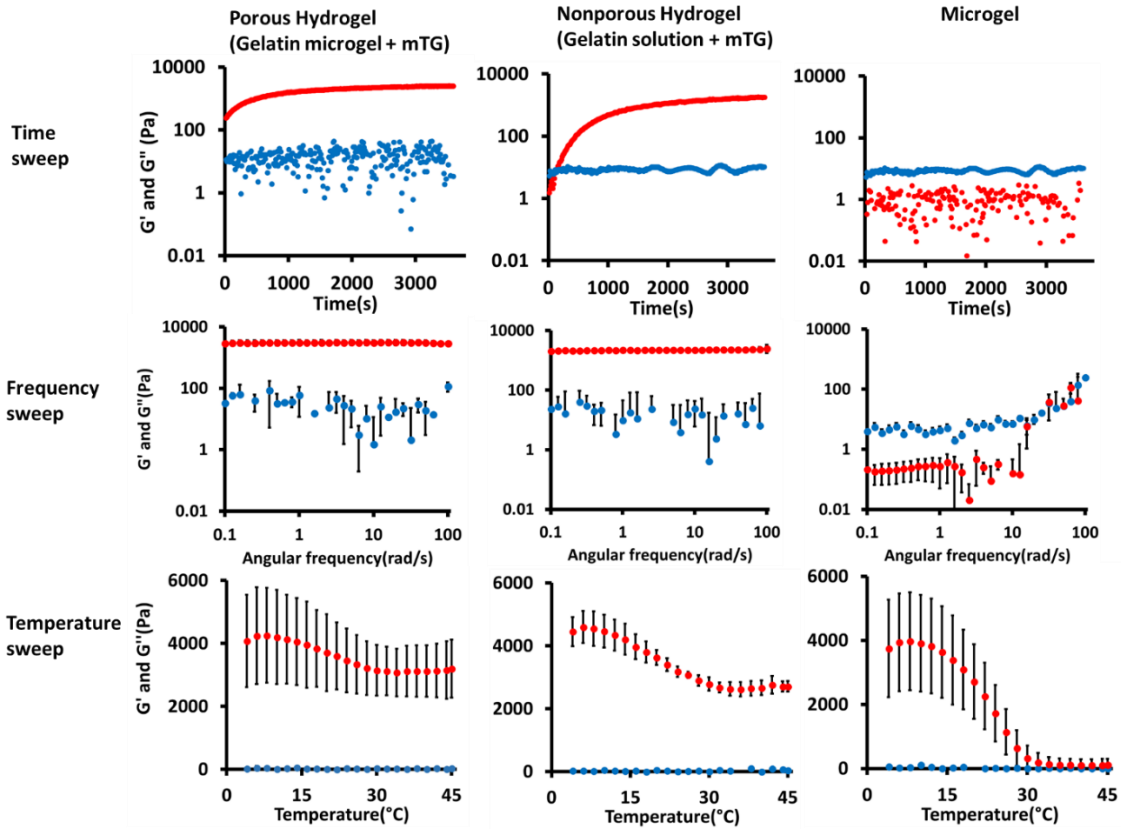

Figure 3.7: Storage modulus (G') and loss modulus (G''). Red: storage modulus (G') and Blue: loss modulus (G'').

Viscoelastic properties of the hydrogels were characterized to understand the nature of the crosslinks created by mTG (Fig 3.6, Fig 3.7). The time-sweep measurements show the kinetics of the covalent crosslinking by mTG. Both G' and G'' of the porous hydrogel (gelatin microgel + mTG) at t = 0 were higher than the nonporous hydrogel (gelatin solution + mTG) because of the following two reasons: (i) Data collection for the porous hydrogel was more delayed than for the nonporous hydrogel (~3 min) due to the longer sample preparation time. (ii) In addition, gelatin concentration in the microgels was higher than that of the bulk gelatin solution because there was void space within the microgel solution even though its weight per volume concentration was the same (10%) as the bulk gelatin solution. In another recent study, the inclusion of gelatin microgels in a covalently crosslinked PEG hydrogel also resulted in a much higher initial G' and G'' in a time sweep [44], although direct comparisons are difficult to be made due to the differences in the overall hydrogel structures. However, the final G' values after 1 hour were comparable to each other (Fig 3.6a). G' of the microgels without mTG remained unchanged due to the lack of chemical crosslinking, indicating the microgels alone without crosslinking by mTG do not form a bulk hydrogel.

Once the gelation was completed, G' was measured as a function of temperature (Fig 3.6b). The temperature-sweep measurements provide more information about the nature of crosslinks. As temperature decreased, G' increased for both porous and nonporous hydrogels due to the formation of physical crosslinks by hydrogen bonding. G' of gelatin microgels without mTG also increased for the same reason. As the temperature increased, the physical crosslinks were weakened resulting in a continuous decrease in G' for both the porous and nonporous hydrogels. This trend continued until ~30°C at which G' reached a plateau at ~3000 Pa. This is attributed to the presence of the covalent bonds created by the actions of mTG because covalent crosslinks by

amide bonds in this temperature regime are stable. The fact that G' of the porous hydrogel is comparable to that of the nonporous hydrogel indicates that the chemical crosslinking by mTG occurred within the microgels as well as between microgels. In comparison, G' of microgels without mTG decreased until the microgels completely melted. The frequency sweep further confirmed that the viscoelastic properties of the porous hydrogel are similar to the nonporous hydrogel (Fig 3.7). The slight increase of G' as a function of frequency is a characteristic of the hydrogels that are crosslinked both physically and chemically [48].

3.3.3. Enzymatic degradation of the porous hydrogel.

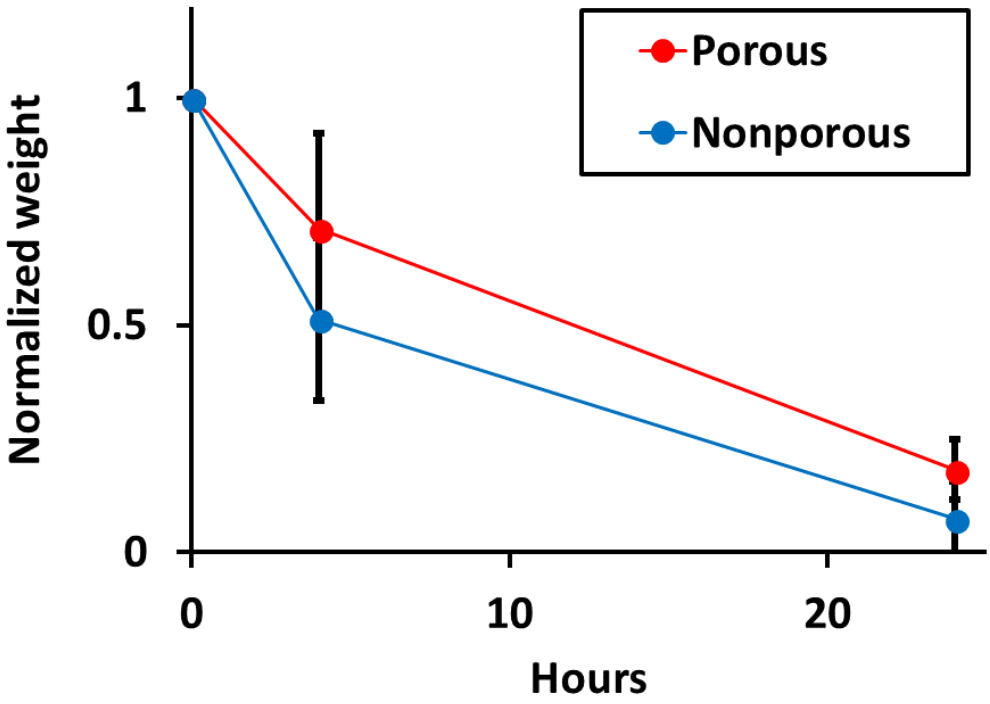

Figure 3.8: Degradation of porous (red) and nonporous (blue) gelatin hydrogels by collagenase type II. (n=4) Each hydrogel was lyophilized and weighed, and the values were normalized to the initial weight.

It is essential that a hydrogel added to a wound is able to degrade over the course of the wound healing process. Gelatin can be degraded by many cell-secreted enzymes, such as collagenases and gelatinases [49-50]. When incubated in collagenase type II solution, the porous gelatin hydrogel degraded slightly slower than the nonporous hydrogel than the nonporous hydrogel (82% degradation for porous hydrogel vs 93% degradation for nonporous hydrogel at 24 hour) (Fig 3.8). This is possibly due to the fact that the porous hydrogel has an increased local gelatin concentration than the nonporous hydrogel at the same bulk gelatin concentration (8.3% w/v) because of the presence of pores. However, there was no statistical significance of the difference ($p = 0.198$ at 4 hours and 0.086 at 24 hours). This result indicates that the porous gelatin hydrogel can serve as a temporary matrix during the wound healing process.

3.3.4. *In vitro* culture of human dermal fibroblasts (hDFs) on the hydrogels.

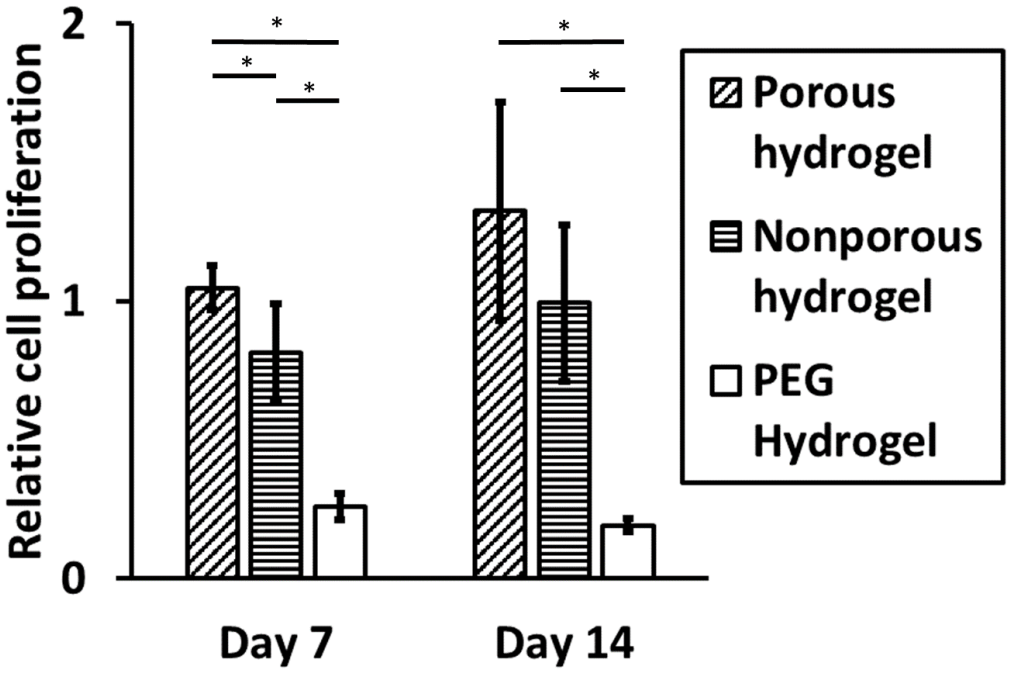

Figure 3.9: hDF proliferation on the hydrogels. Proliferation measured by alamarBlue assay was normalized to the proliferation on tissue culture polystyrene (TCPS). The data are means and standard deviation ($n = 4$, $*p<0.05$).

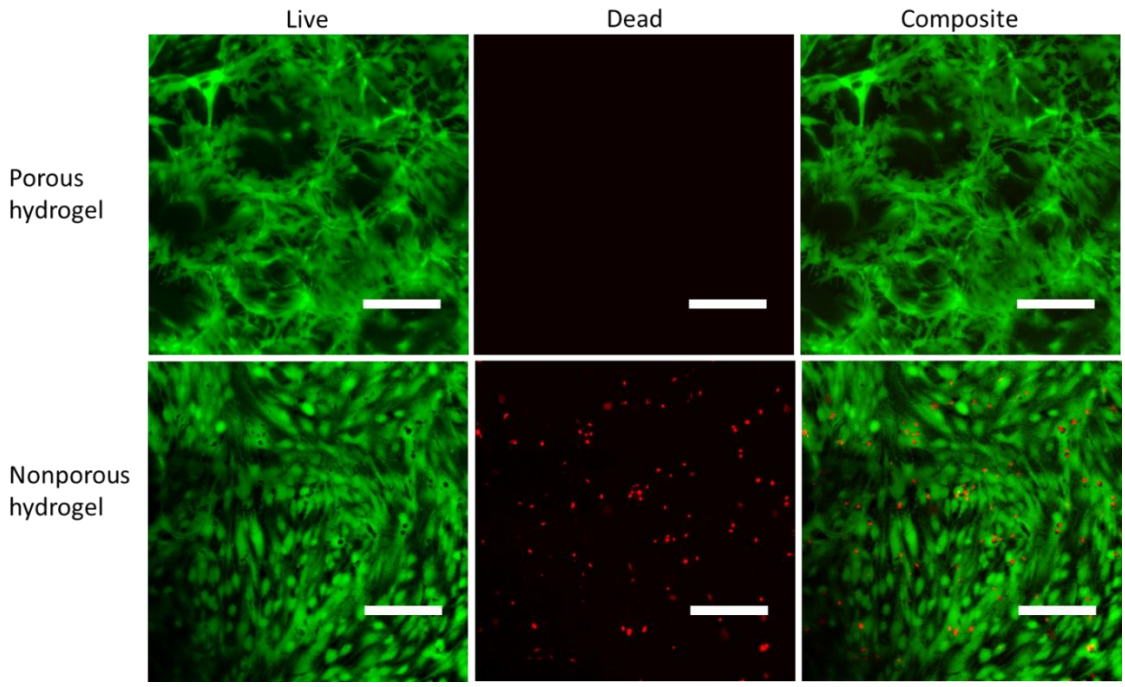

Figure 3.10: Cell viability of hDFs on the porous and nonporous hydrogels 14 days after the initial seeding. Viable cells were stained green by calcein-AM, and dead cells were stained red by ethidium homodimer-1. The scale bar is 200 μm.

Bioactivity of the macroporous hydrogel was compared to the nonporous hydrogel by seeding hDFs on the surface of the hydrogels and monitoring cell proliferation over two weeks using alamarBlue assay (Fig 3.9). Proliferation of hDFs on the porous hydrogel was higher than on the nonporous hydrogel over the two-week period, and there was no statistical significance between the two groups at week 2. Various studies have shown that mTG-crosslinked nonporous gelatin hydrogel supports cell adhesion and proliferation [51-52]. The fact that the macroporous gelatin hydrogel resulted in a higher cellular proliferation than the nonporous gelatin hydrogel proves its excellent bioactivity properties and its potential use in biological systems such as for wound healing. The excellent hDF proliferation on the gelatin macroporous hydrogel is comparable to the PEG-based macroporous hydrogel, which also supported robust proliferation of hDFs encapsulated in the hydrogel [40]. The advantage of using gelatin as a base material for the

injectable macroporous hydrogel as opposed to other synthetic polymers is highlighted by comparing the proliferation of hDF on nonporous PEG hydrogel created by crosslinking maleimide functionalized 4-arm polyethylene glycol (20kDa) by dithiothreitol. Hydrogels made of synthetic polymers typically do not support cell adhesion or proliferation without chemical modifications with bioactive moieties, such as cell adhesive RGD peptides [53-55]. In contrast, the gelatin-based injectable porous hydrogel does not require any chemical modifications to promote cell adhesion and proliferation because of innate cell adhesive ligands, such as RGD, present in gelatin. The live/dead assay showed that the cells in both porous and nonporous hydrogels were viable (Fig 3.10).

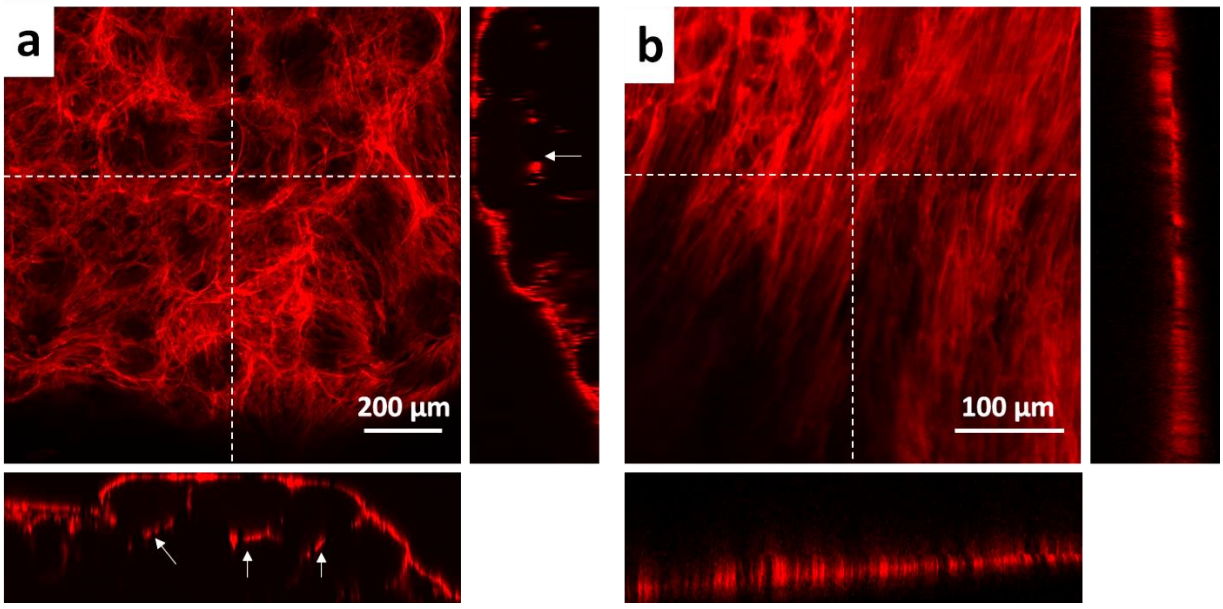

Figure 3.11: Maximum intensity projection of confocal microscope images a) porous hydrogel b) nonporous hydrogel. Actin cytoskeleton of hDFs was stained with actinRed555. The insets on the right and at the bottom of each image are the cross-sectional images corresponding to the vertical and horizontal dotted lines, respectively. The white arrows in the insets indicate the cells that grew underneath the microgels through the interstitial space.

When the hDFs were stained for actin cytoskeleton and visualized by confocal microscopy, some hDFs were found to grow beyond the first layer of the microgels despite the fact that all cells

were initially added on the hydrogel surface (Fig 3.11a). This shows that the gelatin macroporous hydrogel not only supports cell adhesion and proliferation, but also allows cell migration through the pores. This is an important feature of the macroporous hydrogel because cell migration is an essential phenomenon during the wound healing process. In contrast, the cells on the nonporous gelatin hydrogel grew exclusively on the surface of the hydrogel (Fig 3.11b). Due to the small polymer mesh size, the hydrogel must be degraded first for the cell migration into the nonporous hydrogel [44], which was not observed during the time frame of our study.

3.3.5. Application of the macroporous hydrogel to the porcine cornea *ex vivo*.

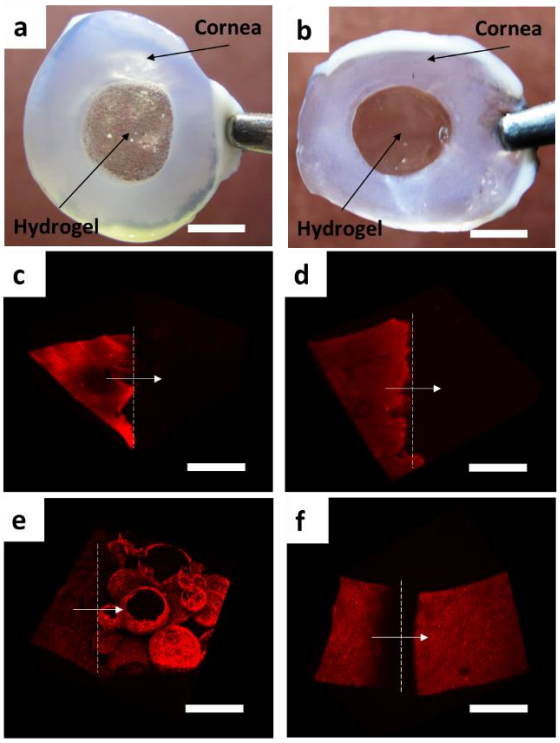

Figure 3.12: Tissue adhesion of the porous and nonporous gelatin hydrogels and cell migration. a) Porous and b) nonporous hydrogels were injected into a hole in an excised porcine cornea and were cultured for 14 days. The hydrogels stably adhered to the cornea tissues during that period. The cornea tissues turned opaque during the culture. Confocal microscope images of the cornea-hydrogel interface of the c) porous and d) nonporous hydrogels on day 0 and e) porous and f) nonporous hydrogels on day 14. Actin cytoskeleton was stained red using actinRed555. Dotted lines indicate the cornea-hydrogel interface with the arrows indicating the direction from cornea to hydrogel. The scale bar for (a, b) is 5 mm and for (c-f) is 200 μm.

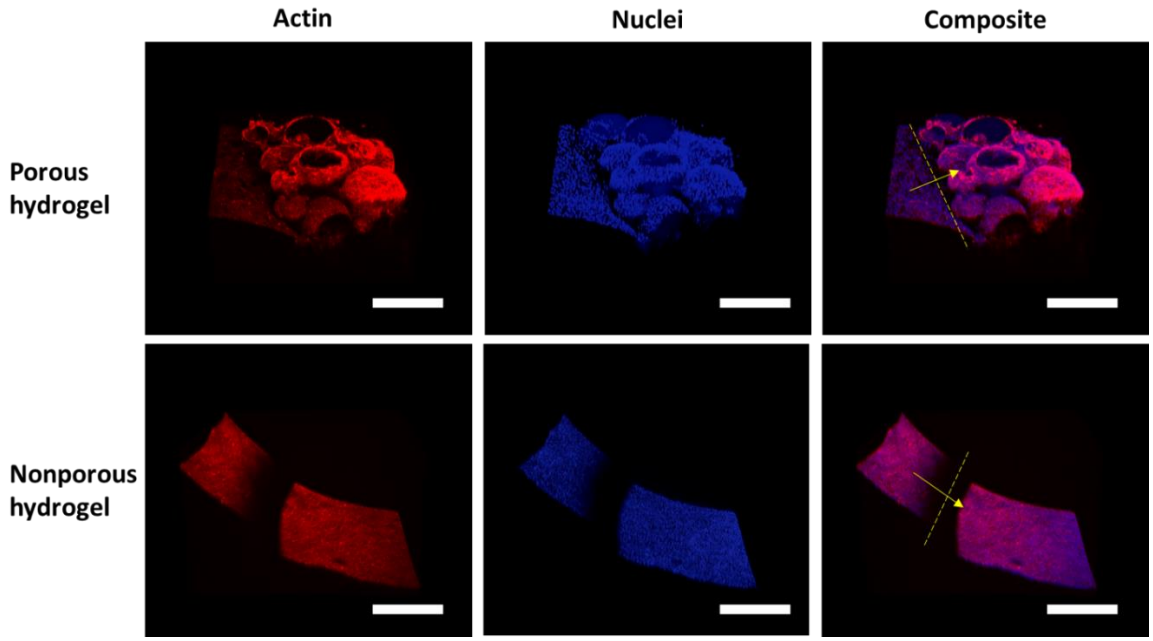

Figure 3.13: 3D images constructed from the Z-sections taken by confocal microscopy. Actin cytoskeleton was stained red using actinRed555 and cell nuclei were stained using DAPI. The yellow dotted lines in the composite images indicate the cornea-hydrogel interface with the yellow arrows pointing the direction from the cornea to the hydrogel. The scale bar is 200 µm.

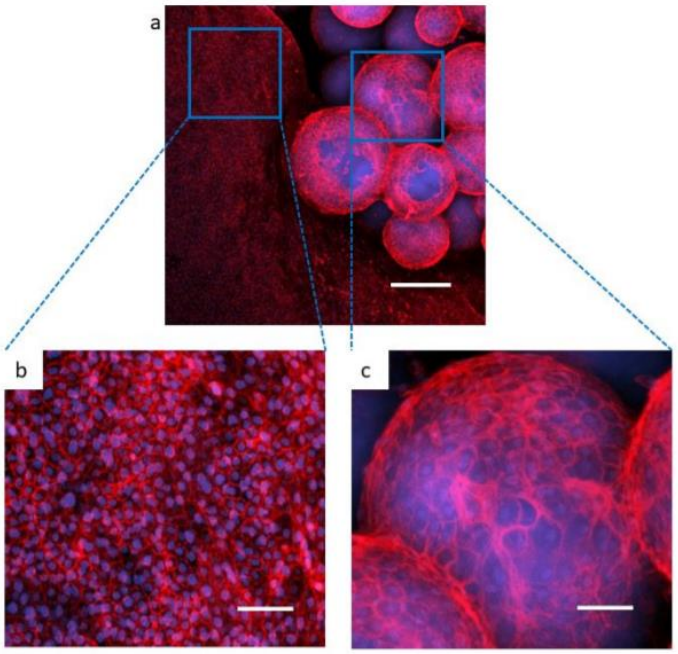

Figure 3.14: a) Maximum intensity projection of confocal microscope image at the cornea-hydrogel interface of a porous hydrogel. The scale bar is 200 µm. b) and c) are the high resolution images of the selected areas of a) demonstrating the specificity of the actin staining. The scale bar is 50 µm.

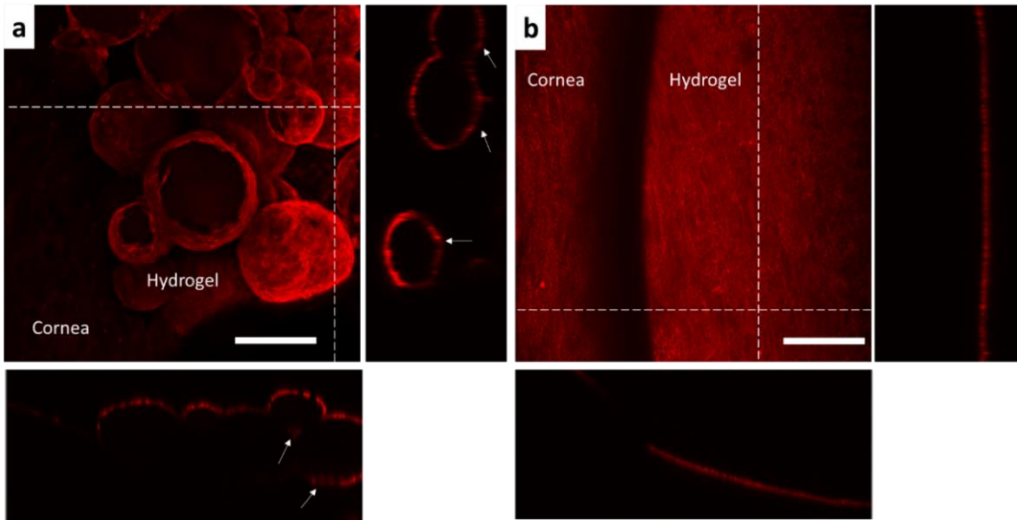

Figure 3.15: Maximum intensity projection of confocal microscope images at the cornea-hydrogel interface for a) porous hydrogel b) nonporous hydrogel on day 14. Actin cytoskeleton was stained red using actinRed555. The insets on the right and at the bottom of each image are the cross-sections along the vertical and horizontal dotted lines, respectively. The white arrows in the insets indicate the cells that grew underneath the microgels through the interstitial space. The scale bar is 200 μm.

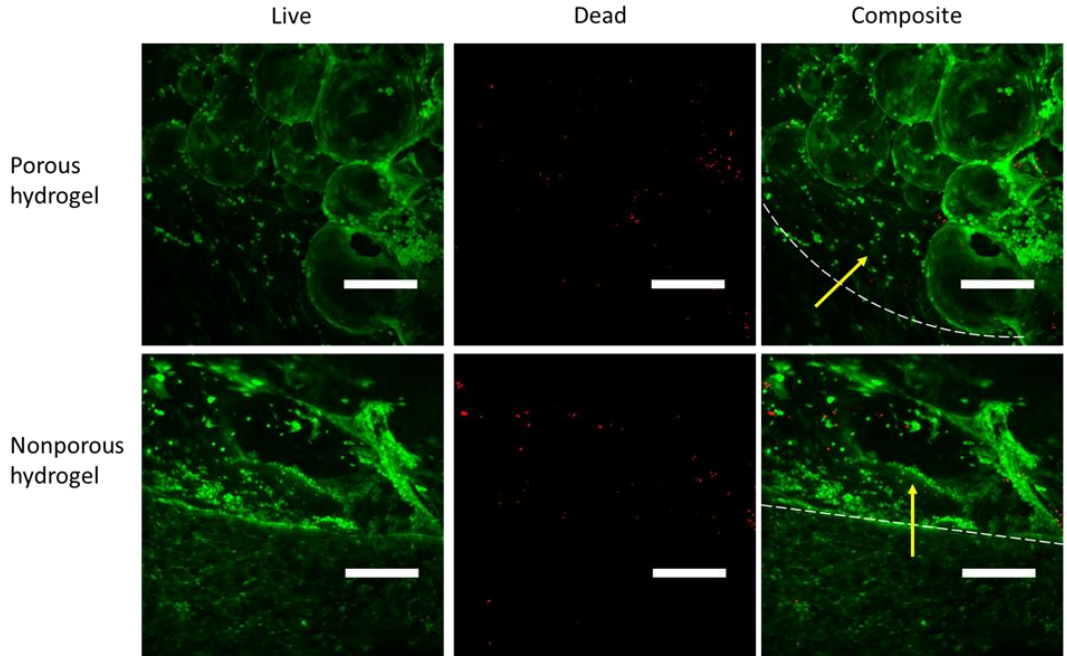

Figure 3.16: Cell viability at the interface between the porcine cornea and the porous/nonporous hydrogels on day 14. Viable cells were stained green by calcein-AM, and dead cells were stained red by ethidium homodimer-1. The dotted lines in the composite images indicate the cornea-microgel interface with the yellow arrows indicating the direction from the cornea to the hydrogel. The images are maximum intensity projections of confocal microscope images. The scale bar is 200 μm.

To test the feasibility of using this injectable porous hydrogel in facilitating cell migration and wound healing in a damaged tissue, I applied the hydrogel (without cells) to a freshly cut porcine cornea tissue. A small hole (8mm in diameter) was punctured in the middle of the cornea and the gelatin microgel solution or gelatin solution was injected into the hole with mTG to form a porous or nonporous hydrogel. The hydrogel stably adhered to the tissue through the action of mTG during the two weeks' span of tissue culture (Fig 3.12a, b). On day 0, cells were found only in the cornea tissue as no cells were present in the hydrogels (Fig 3.12c, d). On day 14, the hydrogel phase was densely populated by the cells, mainly the corneal epithelial cells, that migrated from the cornea tissue (Fig 3.12e, f, Fig 3.13, Fig 3.14). As in the *in vitro* culture of hDFs, cells were found not only on the hydrogel surface but also inside the void space of the porous hydrogel, whereas migrated cells were found exclusively on the surface of the nonporous hydrogel (Fig 3.15). The live/dead assay showed that the majority of the cells in the cornea tissue and the hydrogels (both porous and nonporous) were viable (Fig 3.16).

It should be noted that the current form of porous gelatin hydrogel can only be used for small-sized peripheral corneal wounds due to its low transmittance in the visible range (~ 30 %). In this study, porcine cornea was chosen as a model tissue for their ready accessibility and ease of tissue culture [56-57]. Considering the necessity of porous structure for the facilitated cell migration and wound healing [40], our results point to the potential of this porous hydrogel formulation being used to facilitate the wound healing process in non-ocular tissues (e.g. skin) as well by allowing cell migration and proliferation within the hydrogel.

Another limitation of the current formulation for the clinical applications is a relatively slow curing time by mTG (~ 30 min). Potential solutions to address this issue are (i) the use of a composite material between gelatin and alginate for microgels [58], which can be rapidly

crosslinked by calcium, followed by the covalent crosslinking by mTG, and (ii) the incorporation of photocurable gelatin (e.g. methacrylated gelatin [59]) in the microgels followed by UV crosslinking.

3.3.6. Controlled release of platelet-derived growth factor (PDGF) from the macroporous hydrogel.

Various growth factors play essential roles during the wound healing process. For example, platelet-derived growth factor (PDGF) is released during wound healing and induces the proliferation of fibroblasts for the secretion of a new extracellular matrix (ECM) [60-62]. An ideal hydrogel formulation to facilitate wound healing, therefore, should have the capability of controlled release of growth factors.

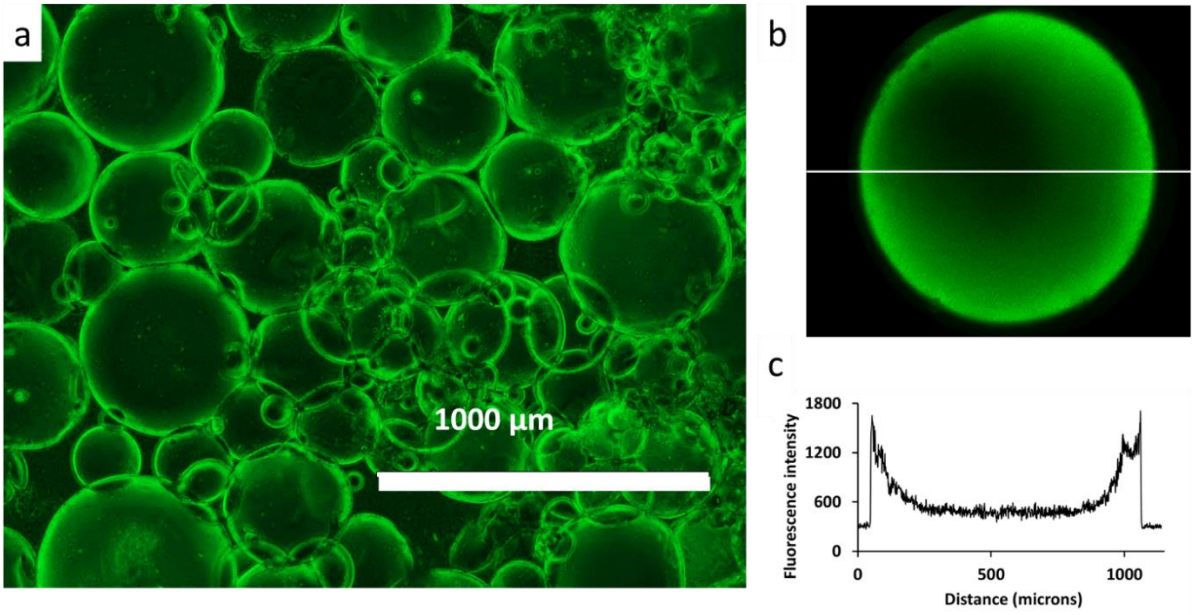

Figure 3.17: a) FITC-BSA-loaded gelatin microgels. b) Confocal microscope image of a microgel. c) Fluorescence intensity along the lateral line in b).

Hydrogels are ideal materials for the controlled release of protein drugs [11, 63-64] because the hydrated environment of the hydrogels allows the proteins to maintain their native 3D structures

and functions [65]. For the characterization of the nature of protein loading in the gelatin microgels, the gelatin microgels were incubated with FITC-labeled bovine serum albumin (FITC-BSA) for 48 hours to induce diffusion-driven loading of the protein in the microgels. The proteins were found mainly on the surface of the microgels as the diffusion of the protein occurred through the surface (Fig 3.17).

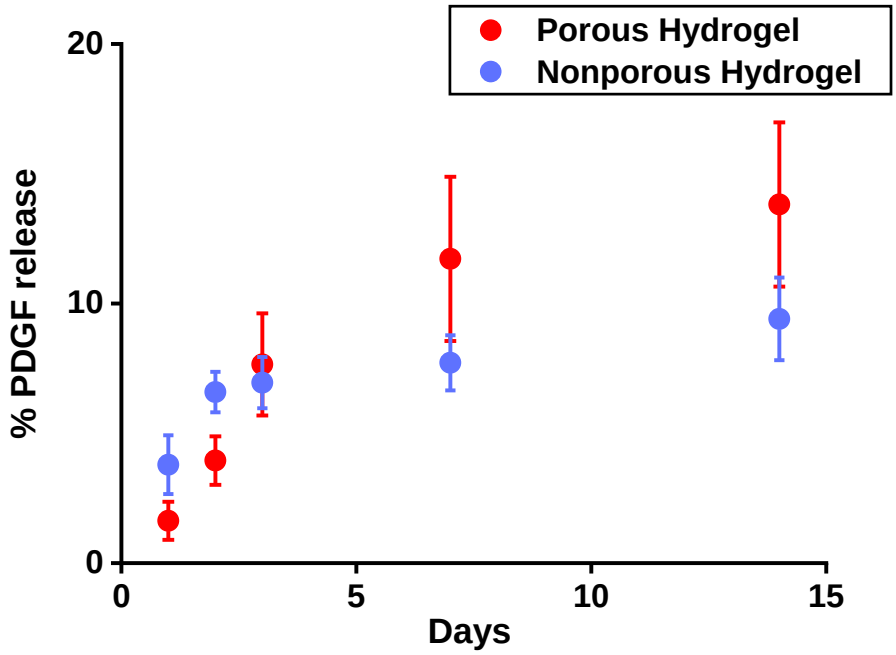

Figure 3.18: Cumulative release profile of PDGF from the hydrogels. The initial loading was 1.6 µg in 250 µL hydrogel. (n = 4)

Human PDGF was loaded in the microgels in the same way as FITC-BSA. The PDGF-loaded microgels were crosslinked by mTG to form a PDGF-loaded macroporous hydrogel. PDGF was loaded in the nonporous hydrogel by mixing PDGF with the gelatin solution before crosslinking with mTG. For both hydrogels, the overall release of PDGF was inefficient over two weeks (13% and 9% release of the initial loading from the porous and nonporous hydrogel, respectively) (Fig 3.18). The reason for such inefficient release is likely due to covalent

immobilization of PDGF to the hydrogels by the action of mTG during the crosslinking process. Covalent attachment of proteins within the hydrogel during the crosslinking process is common for the covalently crosslinked injectable hydrogels [66]. It is also known that the positively charged growth factors are strongly bound to the negatively charged gelatin hydrogels, making the growth factor release inefficient even if the loading is performed after the covalent crosslinking of the hydrogel [67]. Nonetheless, the porous hydrogel released a higher amount of PDGF at a steadier rate than the nonporous hydrogel. Considering that the gelatin hydrogels degrade in the presence of collagenases and there exist various kinds of collagenases and gelatinases *in vivo* [68], I expect that the growth factor release from the gelatin hydrogels will be more efficient *in vivo* with the degradation of the hydrogel [69].

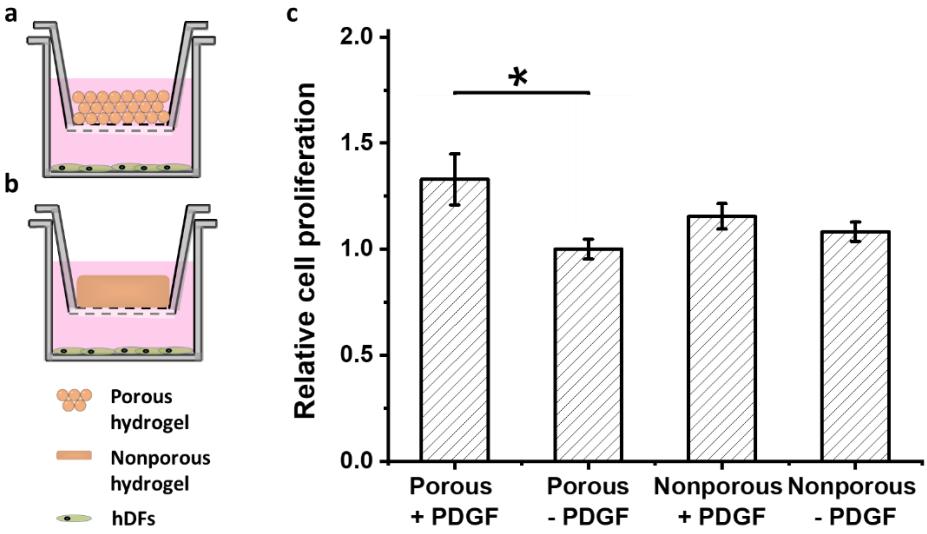

Figure 3.19: hDF proliferation with the controlled release of PDGF from the hydrogels. Schematic of the experimental design for a) porous and b) nonporous hydrogels. c) Relative proliferation at day 14. The proliferation was normalized to that of porous hydrogel without PDGF (n =4, *p<0.05).

When the PDGF was released into the culture medium of hDFs for two weeks through semi-permeable membranes (Fig 3.19a,b), the cellular proliferation increased by 1.3 times for the

porous hydrogel when compared to the culture without PDGF (Fig 3.19c) ($p = 0.039$). No significant differences were observed at earlier time points. PDGF release from the nonporous hydrogel also increased the proliferation of hDFs, but there was no statistical significance compared to the culture without PDGF ($p = 0.900$).

3.4. Conclusion

Addition of mTG to gelatin microgels induced covalent crosslinks within and between microgels, forming a bulk network of macroporous hydrogel. This injectable hydrogel did not require any chemical modification before the gelation. The hydrogel was noncytotoxic to hDFs and allowed adhesion and proliferation of hDFs on the hydrogel surface and cell migration into the hydrogel pores. Upon injection into a hole in porcine corneal tissue, a large number of cells from the surrounding cornea tissue migrated to the porous hydrogel and proliferated both on the surface and in the pores of the hydrogel. Controlled release of PDGF over two weeks was achieved using this hydrogel, which enhanced the proliferation of hDFs. Although I did not show the facilitated wound healing *in vivo*, the fact that this simple and low-cost hydrogel allows the cellular adhesion and migration into the porous structure indicates its potential applications in wound healing and tissue engineering.

3.5. Reference

1. Maitra, J.; Shukla, V. K., Cross-Linking in Hydrogels-a Review. *Am. J. Polym. Sci.* **2014,** *4* (2), 25-31.

2. Zhao, X.; Wu, H.; Guo, B.; Dong, R.; Qiu, Y.; Ma, P. X., Antibacterial Anti-Oxidant Electroactive Injectable Hydrogel as Self-Healing Wound Dressing with Hemostasis and Adhesiveness for Cutaneous Wound Healing. *Biomaterials* **2017,** *122*, 34-47.

3. Xu, J.; Tam, M.; Samaei, S.; Lerouge, S.; Barralet, J.; Stevenson, M. M.; Cerruti, M., Mucoadhesive Chitosan Hydrogels as Rectal Drug Delivery Vessels to Treat Ulcerative Colitis. *Acta Biomater.* **2017,** *48*, 247-257.

4. Tavakoli, J.; Mirzaei, S.; Tang, Y., Cost-Effective Double-Layer Hydrogel Composites for Wound Dressing Applications. *Polymers* **2018,** *10* (3), 305.

5. Balakrishnan, B.; Mohanty, M.; Umashankar, P.; Jayakrishnan, A., Evaluation of an *in Situ* Forming Hydrogel Wound Dressing Based on Oxidized Alginate and Gelatin. *Biomaterials* **2005,** *26* (32), 6335-6342.

6. Schroeder, T. B.; Guha, A.; Lamoureux, A.; VanRenterghem, G.; Sept, D.; Shtein, M.; Yang, J.; Mayer, M., An Electric-Eel-Inspired Soft Power Source from Stacked Hydrogels. *Nature* **2017,** *552* (7684), 214.

7. Horne, R. R.; Judd, K. E.; Pitt, W. G., Rapid Loading and Prolonged Release of Latanoprost from a Silicone Hydrogel Contact Lens. *J. Drug Deliv. Sci. Technol.* **2017,** *41*, 410-418.

8. Nicolson, P. C.; Vogt, J., Soft Contact Lens Polymers: An Evolution. *Biomaterials* **2001,** *22* (24), 3273-3283.

9. Ciolino, J. B.; Stefanescu, C. F.; Ross, A. E.; Salvador-Culla, B.; Cortez, P.; Ford, E. M.; Wymbs, K. A.; Sprague, S. L.; Mascoop, D. R.; Rudina, S. S.; Trauger, S. A.; Cade, F.; Kohane, D. S., *In Vivo* Performance of a Drug-Eluting Contact Lens to Treat Glaucoma for a Month. *Biomaterials* **2014,** *35* (1), 432-439.

10. Ciolino, J. B.; Hoare, T. R.; Iwata, N. G.; Behlau, I.; Dohlman, C. H.; Langer, R.; Kohane, D. S., A Drug-Eluting Contact Lens. *Invest. Ophthalmol. Visual Sci.* **2009,** *50* (7), 3346-3352.

11. Yamamoto, M.; Ikada, Y.; Tabata, Y., Controlled Release of Growth Factors Based on Biodegradation of Gelatin Hydrogel. *J. Biomater. Sci., Polym. Ed.* **2001,** *12* (1), 77-88.

12. Cai, S.; Liu, Y.; Zheng Shu, X.; Prestwich, G. D., Injectable Glycosaminoglycan Hydrogels for Controlled Release of Human Basic Fibroblast Growth Factor. *Biomaterials* **2005,** *26* (30), 6054-6067.

13. Koutsopoulos, S.; Unsworth, L. D.; Nagai, Y.; Zhang, S., Controlled Release of Functional Proteins through Designer Self-Assembling Peptide Nanofiber Hydrogel Scaffold. *Proc. Natl. Acad. Sci. USA* **2009,** *106* (12), 4623-4628.

14. Zhang, Y.; Tao, L.; Li, S.; Wei, Y., Synthesis of Multiresponsive and Dynamic Chitosan-Based Hydrogels for Controlled Release of Bioactive Molecules. *Biomacromolecules* **2011,** *12* (8), 2894-2901.

15. Tan, H.; Chu, C. R.; Payne, K. A.; Marra, K. G., Injectable *in Situ* Forming Biodegradable Chitosan-Hyaluronic Acid Based Hydrogels for Cartilage Tissue Engineering. *Biomaterials* **2009,** *30* (13), 2499-2506.

16. Rafat, M.; Li, F.; Fagerholm, P.; Lagali, N. S.; Watsky, M. A.; Munger, R.; Matsuura, T.; Griffith, M., PEG-Stabilized Carbodiimide Crosslinked Collagen-Chitosan Hydrogels for Corneal Tissue Engineering. *Biomaterials* **2008,** *29* (29), 3960-3972.

17. Eke, G.; Mangir, N.; Hasirci, N.; MacNeil, S.; Hasirci, V., Development of a Uv Crosslinked Biodegradable Hydrogel Containing Adipose Derived Stem Cells to Promote Vascularization for Skin Wounds and Tissue Engineering. *Biomaterials* **2017,** *129*, 188-198.

18. Xavier, J. R.; Thakur, T.; Desai, P.; Jaiswal, M. K.; Sears, N.; Cosgriff-Hernandez, E.; Kaunas, R.; Gaharwar, A. K., Bioactive Nanoengineered Hydrogels for Bone Tissue Engineering: A Growth-Factor-Free Approach. *ACS Nano* **2015,** *9* (3), 3109-3118.

19. Van Vlierberghe, S.; Dubruel, P.; Schacht, E., Biopolymer-Based Hydrogels as Scaffolds for Tissue Engineering Applications: A Review. *Biomacromolecules* **2011,** *12* (5), 1387-1408.

20. Ruel-Gariepy, E.; Leroux, J.-C., *In Situ*-Forming Hydrogels—Review of Temperature-Sensitive Systems. *Eur. J. Pharm. Biopharm.* **2004,** *58* (2), 409-426.

21. Gurtner, G. C.; Werner, S.; Barrandon, Y.; Longaker, M. T., Wound Repair and Regeneration. *Nature* **2008,** *453* (7193), 314.

22. Canal, T.; Peppas, N. A., Correlation between Mesh Size and Equilibrium Degree of Swelling of Polymeric Networks. *J. Biomed. Mater. Res.* **1989,** *23* (10), 1183-1193.

23. Zustiak, S. P.; Leach, J. B., Hydrolytically Degradable Poly (Ethylene Glycol) Hydrogel Scaffolds with Tunable Degradation and Mechanical Properties. *Biomacromolecules* **2010,** *11* (5), 1348-1357.

24. Bencherif, S. A.; Sands, R. W.; Bhatta, D.; Arany, P.; Verbeke, C. S.; Edwards, D. A.; Mooney, D. J., Injectable Preformed Scaffolds with Shape-Memory Properties. *Proc. Natl. Acad. Sci. USA* **2012,** *109* (48), 19590-19595.

25. Koshy, S. T.; Ferrante, T. C.; Lewin, S. A.; Mooney, D. J., Injectable, Porous, and Cell-Responsive Gelatin Cryogels. *Biomaterials* **2014,** *35* (8), 2477-2487.

26. Koshy, S. T.; Zhang, D. K.; Grolman, J. M.; Stafford, A. G.; Mooney, D. J., Injectable Nanocomposite Cryogels for Versatile Protein Drug Delivery. *Acta Biomater.* **2018,** *65*, 36-43.

27. Lutolf, M. P.; Lauer-Fields, J. L.; Schmoekel, H. G.; Metters, A. T.; Weber, F. E.; Fields, G. B.; Hubbell, J. A., Synthetic Matrix Metalloproteinase-Sensitive Hydrogels for the Conduction of Tissue Regeneration: Engineering Cell-Invasion Characteristics. *Proc. Natl. Acad. Sci. USA* **2003,** *100* (9), 5413-5418.

28. Patterson, J.; Hubbell, J. A., Enhanced Proteolytic Degradation of Molecularly Engineered PEG Hydrogels in Response to MMP-1 and MMP-2. *Biomaterials* **2010,** *31* (30), 7836-7845.

29. Schultz, K. M.; Kyburz, K. A.; Anseth, K. S., Measuring Dynamic Cell-Material Interactions and Remodeling During 3D Human Mesenchymal Stem Cell Migration in Hydrogels. *Proc. Natl. Acad. Sci. USA* **2015,** *112* (29), E3757-3764.

30. Li, L.; Lu, C.; Wang, L.; Chen, M.; White, J.; Hao, X.; McLean, K. M.; Chen, H.; Hughes, T. C., Gelatin-Based Photocurable Hydrogels for Corneal Wound Repair. *ACS Appl. Mater. Interfaces* **2018,** *10* (16), 13283-13292.

31. Benton, J. A.; DeForest, C. A.; Vivekanandan, V.; Anseth, K. S., Photocrosslinking of Gelatin Macromers to Synthesize Porous Hydrogels That Promote Valvular Interstitial Cell Function. *Tissue Eng., Part A* **2009,** *15* (11), 3221-3230.

32. McGuigan, A. P.; Sefton, M. V., Modular Tissue Engineering: Fabrication of a Gelatin-Based Construct. *J. Tissue Eng. Regener. Med.* **2007,** *1* (2), 136-145.

33. Du, Y.; Lo, E.; Ali, S.; Khademhosseini, A., Directed Assembly of Cell-Laden Microgels for Fabrication of 3D Tissue Constructs. *Proc. Natl. Acad. Sci. USA* **2008,** *105* (28), 9522-9527.

34. Xu, F.; Wu, C. a. M.; Rengarajan, V.; Finley, T. D.; Keles, H. O.; Sung, Y.; Li, B.; Gurkan, U. A.; Demirci, U., Three-Dimensional Magnetic Assembly of Microscale Hydrogels. *Adv Mater.* **2011,** *23* (37), 4254-4260.

35. Qi, H.; Ghodousi, M.; Du, Y.; Grun, C.; Bae, H.; Yin, P.; Khademhosseini, A., DNA-Directed Self-Assembly of Shape-Controlled Hydrogels. *Nat. Commun.* **2013,** *4*, 2275.

36. Roam, J. L.; Yan, Y.; Nguyen, P. K.; Kinstlinger, I. S.; Leuchter, M. K.; Hunter, D. A.; Wood, M. D.; Elbert, D. L., A Modular, Plasmin-Sensitive, Clickable Poly (Ethylene Glycol)-Heparin-Laminin Microsphere System for Establishing Growth Factor Gradients in Nerve Guidance Conduits. *Biomaterials* **2015,** *72*, 112-124.

37. Zhou, W.; Stukel, J. M.; Cebull, H. L.; Willits, R. K., Tuning the Mechanical Properties of Poly (Ethylene Glycol) Microgel-Based Scaffolds to Increase 3D Schwann Cell Proliferation. *Macromol. Biosci.* **2016,** *16* (4), 535-544.

38. Xin, S.; Wyman, O. M.; Alge, D. L., Assembly of PEG Microgels into Porous Cell-Instructive 3D Scaffolds Via Thiol-Ene Click Chemistry. *Adv. Healthcare Mater.* **2018,** *7* (11), e1800160.

39. Zhou, W.; Stukel, J. M.; AlNiemi, A.; Willits, R. K., Novel Microgel-Based Scaffolds to Study the Effect of Degradability on Human Dermal Fibroblasts. *Biomed. Mater. (Bristol, U. K.)* **2018,** *13* (5), 055007.

40. Griffin, D. R.; Weaver, W. M.; Scumpia, P. O.; Di Carlo, D.; Segura, T., Accelerated Wound Healing by Injectable Microporous Gel Scaffolds Assembled from Annealed Building Blocks. *Nat. Mater.* **2015,** *14* (7), 737.

41. Zhao, X.; Lang, Q.; Yildirimer, L.; Lin, Z. Y.; Cui, W.; Annabi, N.; Ng, K. W.; Dokmeci, M. R.; Ghaemmaghami, A. M.; Khademhosseini, A., Photocrosslinkable Gelatin Hydrogel for Epidermal Tissue Engineering. *Adv. Healthcare Mater.* **2016,** *5* (1), 108-118.

42. Mimura, T.; Amano, S.; Yokoo, S.; Uchida, S.; Yamagami, S.; Usui, T.; Kimura, Y.; Tabata, Y., Tissue Engineering of Corneal Stroma with Rabbit Fibroblast Precursors and Gelatin Hydrogels. *Mol. Vision* **2008,** *14*, 1819.

43. Yung, C.; Wu, L.; Tullman, J.; Payne, G.; Bentley, W.; Barbari, T., Transglutaminase Crosslinked Gelatin as a Tissue Engineering Scaffold. *J. Biomed. Mater. Res., Part A* **2007,** *83* (4), 1039-1046.

44. Li, Y.; Meng, H.; Liu, Y.; Narkar, A.; Lee, B. P., Gelatin Microgel Incorporated Poly (Ethylene Glycol)-Based Bioadhesive with Enhanced Adhesive Property and Bioactivity. *ACS Appl. Mater. Interfaces* **2016,** *8* (19), 11980-11989.

45. Shin, S. R.; Aghaei-Ghareh-Bolagh, B.; Dang, T. T.; Topkaya, S. N.; Gao, X.; Yang, S. Y.; Jung, S. M.; Oh, J. H.; Dokmeci, M. R.; Tang, X., Cell-Laden Microengineered and Mechanically Tunable Hybrid Hydrogels of Gelatin and Graphene Oxide. *Adv Mater.* **2013,** *25* (44), 6385-6391.

46. Murphy, C. M.; Haugh, M. G.; O'Brien, F. J., The Effect of Mean Pore Size on Cell Attachment, Proliferation and Migration in Collagen–Glycosaminoglycan Scaffolds for Bone Tissue Engineering. *Biomaterials* **2010,** *31* (3), 461-466.

47. Scott, G.; Kilgour, D., The Density of Random Close Packing of Spheres. *J. Phys. D: Appl. Phys.* **1969,** *2* (6), 863.

48. Jeong, K. J.; Panitch, A., Interplay between Covalent and Physical Interactions within Environment Sensitive Hydrogels. *Biomacromolecules* **2009,** *10* (5), 1090-1099.

49. Bányai, L.; Tordai, H.; Patthy, L., Structure and Domain-Domain Interactions of the Gelatin-Binding Site of Human 72-Kilodalton Type Iv Collagenase (Gelatinase a, Matrix Metalloproteinase 2). *J. Biol. Chem.* **1996,** *271* (20), 12003-12008.

50. Mladenovska, K.; Kumbaradzi, E.; Dodov, G.; Makraduli, L.; Goracinova, K., Biodegradation and Drug Release Studies of Bsa Loaded Gelatin Microspheres. *Int. J. Pharm.* **2002,** *242* (1-2), 247-249.

51. Maddaus, A.; Curley, P.; Griswold, M. A.; Costa, B. D.; Hou, S.; Jeong, K. J.; Song, E.; Deravi, L. F., Design and Fabrication of Bio-Hybrid Materials Using Inkjet Printing. *Biointerphases* **2016,** *11* (4), 041002.

52. Yang, G.; Xiao, Z.; Long, H.; Ma, K.; Zhang, J.; Ren, X.; Zhang, J., Assessment of the Characteristics and Biocompatibility of Gelatin Sponge Scaffolds Prepared by Various Crosslinking Methods. *Sci. Rep.* **2018,** *8* (1), 1616.

53. Burdick, J. A.; Anseth, K. S., Photoencapsulation of Osteoblasts in Injectable RGD-Modified PEG Hydrogels for Bone Tissue Engineering. *Biomaterials* **2002,** *23* (22), 4315-4323.

54. Groll, J.; Fiedler, J.; Engelhard, E.; Ameringer, T.; Tugulu, S.; Klok, H. A.; Brenner, R. E.; Moeller, M., A Novel Star PEG-Derived Surface Coating for Specific Cell Adhesion. *J. Biomed. Mater. Res., Part A* **2005,** *74* (4), 607-617.

55. Weber, L. M.; Hayda, K. N.; Haskins, K.; Anseth, K. S., The Effects of Cell-Matrix Interactions on Encapsulated Beta-Cell Function within Hydrogels Functionalized with Matrix-Derived Adhesive Peptides. *Biomaterials* **2007,** *28* (19), 3004-3011.

56. Salvador-Culla, B.; Jeong, K. J.; Kolovou, P. E.; Chiang, H. H.; Chodosh, J.; Dohlman, C. H.; Kohane, D. S., Titanium Coating of the Boston Keratoprosthesis. *Transl Vis Sci Techn* **2016,** *5* (2), 17.

57. Wang, L.; Jeong, K. J.; Chiang, H. H.; Zurakowski, D.; Behlau, I.; Chodosh, J.; Dohlman, C. H.; Langer, R.; Kohane, D. S., Hydroxyapatite for Keratoprosthesis Biointegration. *Invest. Ophthalmol. Visual Sci.* **2011,** *52* (10), 7392-7399.

58. Wen, C.; Lu, L.; Li, X., Mechanically Robust Gelatin–a Lginate Ipn Hydrogels by a Combination of Enzymatic and Ionic Crosslinking Approaches. *Macromol. Mater. Eng.* **2014,** *299* (4), 504-513.

59. Nichol, J. W.; Koshy, S. T.; Bae, H.; Hwang, C. M.; Yamanlar, S.; Khademhosseini, A., Cell-Laden Microengineered Gelatin Methacrylate Hydrogels. *Biomaterials* **2010,** *31* (21), 5536-5544.

60. Bonner, J. C.; Badgett, A.; Osornio-Vargas, A. R.; Hoffman, M.; Brody, A. R., Pdgf-Stimulated Fibroblast Proliferation Is Enhanced Synergistically by Receptor-Recognized *Alpha* 2-Macroglobulin. *J. Cell. Physiol.* **1990,** *145* (1), 1-8.

61. Deuel, T. F.; Kawahara, R. S.; Mustoe, T. A.; Pierce, A. F., Growth Factors and Wound Healing: Platelet-Derived Growth Factor as a Model Cytokine. *Annu. Rev. Med.* **1991,** *42*, 567-584.

62. Agren, M. S.; Steenfos, H. H.; Dabelsteen, S.; Hansen, J. B.; Dabelsteen, E., Proliferation and Mitogenic Response to PDGF-BB of Fibroblasts Isolated from Chronic Venous Leg Ulcers Is Ulcer-Age Dependent. *J. Invest. Dermatol.* **1999,** *112* (4), 463-469.

63. Hori, K.; Sotozono, C.; Hamuro, J.; Yamasaki, K.; Kimura, Y.; Ozeki, M.; Tabata, Y.; Kinoshita, S., Controlled-Release of Epidermal Growth Factor from Cationized Gelatin Hydrogel Enhances Corneal Epithelial Wound Healing. *J. Controlled Release* **2007,** *118* (2), 169-176.

64. Li, Z.; Qu, T.; Ding, C.; Ma, C.; Sun, H.; Li, S.; Liu, X., Injectable Gelatin Derivative Hydrogels with Sustained Vascular Endothelial Growth Factor Release for Induced Angiogenesis. *Acta Biomater.* **2015,** *13*, 88-100.

65. Vermonden, T.; Censi, R.; Hennink, W. E., Hydrogels for Protein Delivery. *Chem. Rev.* **2012,** *112* (5), 2853-2888.

66. Lin, C.-C.; Anseth, K. S., PEG Hydrogels for the Controlled Release of Biomolecules in Regenerative Medicine. *Pharm. Res.* **2009,** *26* (3), 631-643.

67. Tabata, Y.; Ikada, Y., Vascularization Effect of Basic Fibroblast Growth Factor Released from Gelatin Hydrogels with Different Biodegradabilities. *Biomaterials* **1999,** *20* (22), 2169-2175.

68. Thrailkill, K. M.; Moreau, C. S.; Cockrell, G.; Simpson, P.; Goel, R.; North, P.; Fowlkes, J. L.; Bunn, R. C., Physiological Matrix Metalloproteinase Concentrations in Serum During Childhood and Adolescence, Using Luminex® Multiplex Technology. *Clin. Chem. Lab. Med.* **2005,** *43* (12), 1392-1399.

69. Nguyen, A. H.; McKinney, J.; Miller, T.; Bongiorno, T.; McDevitt, T. C., Gelatin Methacrylate Microspheres for Controlled Growth Factor Release. *Acta Biomater.* **2015,** *13*, 101-110.

Chapter 4:

Injectable Macroporous Gelatin Hydrogel for Tissue Engineering Applications

4.1. Introduction

Tissue engineering, which is focused on organ or tissue regeneration, is a field of great interest in biomaterials, and important for the advancement of modern medicine [1]. To accomplish tissue regeneration, biomaterials can serve as synthetic extracellular matrix that support cell function and differentiation [2]. Hydrogel, due to its high water content and potential as a drug delivery vehicle, is a widely used biomaterial for manufacturing scaffolds [3]. There are two general approaches in terms of making cell-seeded hydrogel scaffolds: i) the hydrogel scaffold is premade and then cells are seeded on top of it; ii) cells are mixed with the solution before the hydrogel is crosslinked, and the seeded cells will be trapped in the hydrogel upon gel formation via crosslinking [4]. By the first approach, because cells are added at a later stage, potential cytotoxicity of the hydrogel scaffold synthesis steps is not a concern [5]. In contrast, by the second method, care must be taken to ensure that crosslinking methods are non-cytotoxic. However, this method allows encapsulated cells to be evenly distributed throughout the hydrogel [6], and the size and shape of the hydrogel system is easily controlled, which makes it more viable for clinical applications [7].

Macroporous hydrogel can facilitate the transport of nutrients and oxygen, as well as promote cell adhesion and migration due to its large pore size and interconnectivity [8]. Among the various methods of making macroporous hydrogel, the method of curing microgel spheres is of particular interest because it can be injectable [9]. By this method, interconnected pores are formed by the interstitial space between microgel particles. In this case, microgel size is directly related to pore size when it is monodispersed, and thus pore size can be optimized accordingly [9]. Synthetic polymers, for example poly(ethylene glycol) (PEG), can be used for synthesizing microgels, but the synthetic polymers in general do not allow cell attachment without chemical modification [10].

With the addition of cell adhesive ligand to enhance cell adhesion, this functionality is improved but it generally requires chemical modification [9, 11-12]. Alternatively, hyaluronic acid (HA) was another material that people used to make microgels [13-15].

Previously, I demonstrated an injectable macroporous hydrogel system by crosslinking gelatin microgels with microbial transglutaminase (mTG) for wound healing applications [16]. In the study, no cells were provided at the hydrogel gelation step. Instead, cells were either seeded from the top after hydrogel gelation, or cells migrated in from the live tissues. Either way, in order for cells to occupy the pore space of the scaffold, cell infiltration from the outside was required. However, the homogeneous cell distribution is important when applying for tissue engineering [6]. In this case, cell encapsulation within the hydrogel is more suitable. Meanwhile, similar to wound healing application, since porosity is also very important in terms of cell spreading and proliferation, I wanted to test whether this injectable macroporous hydrogel could be used for tissue engineering applications.

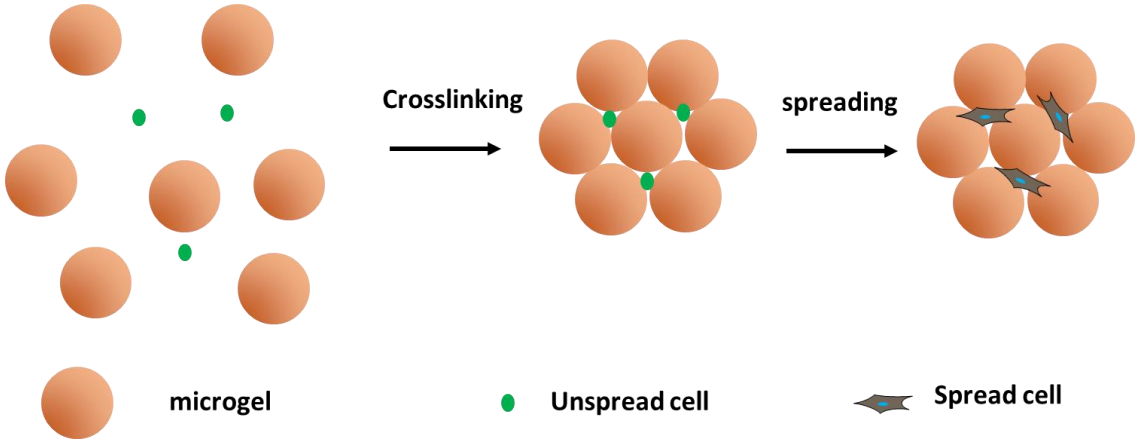

Figure 4.1: Schematic of cell encapsulated in the injectable macroporous hydrogel.

In the present study, cell encapsulation in injectable macroporous hydrogel was examined. Here, cell suspension was mixed with gelatin microgel solution before crosslinking. mTG was then

added to enzymatically crosslink the gelatin microgels into macroporous hydrogel (Fig 4.1). By this method, cells can be evenly distributed throughout the hydrogel, specifically trapped in the pores of the macroporous hydrogel. Gelatin has been shown to allow for cell adhesion and spreading [17], indicating that encapsulated cells should rapidly adhere to the microgel surface and spread. After gelatin microgels were prepared, they were mixed with cell suspension before being crosslinked into hydrogel, and then this crosslinked hydrogel was cultured in media to allow cell spreading and proliferation (Fig 4.1). Human dermal fibroblasts (hDFs) were first used to test the feasibility of *in situ* cell encapsulation in the macroporous hydrogel. Then several other cell types were also encapsulated in this manner, including adipose-derived stem cells (ADSCs), human umbilical vein endothelial cells (HUVECs), and the HL-1 cell line of cardiac muscle cells (HL-1).

ADSCs are isolated from adipose tissue and can differentiate into many cell types including osteogenic [18], adipogenic [19], and chondrogenic [20], showing promise for use in tissue engineering, especially for bone [21] or cartilage related research [22]. ADSCs osteogenic differentiation is very important for bone regeneration [23]. Although the gelatin hydrogels are relatively soft (G' ~ 3000 Pa), which is not conducive for osteogenic differentiation of ADSCs [24-25], we wanted to study the effects of macropores on the osteogenic differentiation of ADSCs.

When building an engineered tissue, blood vessel formation within the tissue is critical, because without the blood vessels, the nutrition supply and the waste removal of the tissue should rely on the diffusion [26] which is a highly inefficient mechanism of mass transfer. In general, a tissue thicker than 200 μm cannot survive long-term without the presence of blood vessels [27]. One solution for the issue of blood vessel formation is to pre-vascularize the engineered tissues by encapsulating vascular endothelial cells in hollow templates within the scaffold and induce

neovascularization. Here, we wanted to explore the possibility of utilizing the interconnected pore network of the macroporous hydrogel as a template for the blood vessel formation. HUVECs, one type of vascular endothelial cells [26] were used as model vascular endothelial cells.

HL-1 encapsulation was performed to test the feasibility of producing functional engineered cardiac muscle tissue [28]. Myocardial infarction is caused by the clot in the coronary artery which halts blood flow to the muscle tissues of the heart [29]. Lack of blood supply causes ischemia and causes cell death and tissue loss [30]. However, unlike the cell types that can be regenerated by itself, the loss of the cardiac muscle cell (cardiomyocytes) is irreversible, which can cause heart failure [31]. Engineered cardiac muscle tissue, or cardiac patch, is made of cardiomyocytes embedded in a 3D scaffold, which can be attached to the patient's damaged heart for the functional recovery [32]. To produce a functional cardiac patch, the formation of gap junction, which is the electrical and biochemical coupling among cells, is an important factor for the synchronous contraction of cardiomyocytes within the cardiac patch [33]. We hypothesized that encapsulating cardiomyocytes in the interconnected pore network of the macroporous hydrogel will be beneficial to induce gap junction formation among the encapsulated cardiomyocytes and build a functional cardiac patch.

4.2. Materials and Methods

All materials were purchased from Sigma-Aldrich (St. Louis, MO) unless specified. Microbial transglutaminase (mTG) was purchased from Ajinomoto (Fort Lee, NJ). Sterile phosphate buffer saline (PBS, pH 7.4) was purchased from Gibco (Carlsbad, CA). Human dermal fibroblasts (hDFs), human adipose derived stem cells (ADSCs), ADSC growth medium, human mesenchymal stem cells (hMSC) osteogenic differentiation medium, human umbilical vein endothelial cells (HUVECs), EGM™-PLUS medium, and EGM™-2 medium were purchased

from Lonza (Portsmouth, NH). Cell Viability kit, Dulbecco's Modified Eagle's Medium (DMEM), fetal bovine serum (FBS), penicillin/streptomycin (pen/strep), ActinRed 555, NucBlue fixed cell ReadyProbes™ reagent, and ActinGreen 488 were purchased from Invitrogen (Frederick, MD). Mouse anti-human osteocalcin antibody, goat anti-mouse IgG, goat anti-CX43 antibody, rabbit anti-sarcomeric *alpha* actinin antibody, donkey anti-goat IgG, donkey anti-rabbit IgG, and anti-CD31 (Alexa Fluor 488) antibody were purchased from Abcam (Cambridge, United Kingdom).

4.2.1. Synthesis of gelatin microgels

Gelatin microgel was prepared by using the same method discussed previously [16]. Briefly, gelatin (Type 1, from bovine and porcine bones) was dissolved in 20 mL deionized water at 50−55 °C to make a 10% (w/v) solution. This was added dropwise to 200 mL olive oil at 50−55 °C and stirred for 1 hour. The mixture was cooled to room temperature and then placed in an ice−water bath for 30 min with stirring to solidify the microgels by inducing physical crosslinking. To precipitate the microgels, 100 mL precooled acetone (4 °C) was added to the mixture with stirring for 30 min in the ice−water bath. The microgels were separated from the olive oil and acetone by vacuum filtration and further washed with two 60 mL aliquots of precooled acetone. The microgels were lyophilized and kept dry until used.

4.2.2. Cell encapsulation and characterization

hDFs were cultured in T75 flasks using DMEM, supplemented with FBS and pen/strep. hDFs under passage 4 were used for all experiments. ADSCs were cultured in T75 flasks with ADSC growth medium, and ADSCs under passage 4 were used for all experiments. HUVECs were cultured in T75 flasks with EGM™-PLUS medium, and HUVECs under passage 4were used for

all experiments. HL-1 were cultured in T75 flasks with its growth medium, and HL-1 under passage 3 were used for all experiments.

Prior to cell encapsulation, the gelatin microgels were sterilized by incubation in 70% ethanol overnight. 10% w/v nonporous gelatin and 20% w/v mTG solution were sterilized by syringe filters (pore size = 220 nm). For encapsulation, 10% w/v microgel or nonporous gelatin solution was mixed with cells and then mixed with 20% w/v mTG (5:1 microgel/gelatin:mTG) to make the final seeding density 500 cells/μL. Gels were incubated at 37 °C for 1 hour. Hydrogels containing encapsulated cells were cultured with the appropriate growth media.

The three-dimensional distribution of cells in a hydrogel was visualized by Nikon A1R-HD confocal laser-scanning microscope using a cell viability kit, which stained live and dead cells with green (by calcein-AM) and red fluorescence (by ethidium homodimer), respectively. Z-stacked images were obtained using the confocal microscope. 2D average intensity projections were generated using Fiji software. hDFs were stained exclusively for cell viability; other cell types were stained for cell viability and as described below.

For culture of ADSCs, after the sample was cultured in the growth medium for a week, the medium was switched to hMSC osteogenic differentiation medium for 2 more weeks. The hydrogels were then fixed in 4% formaldehyde (in PBS) overnight at room temperature. For fluorescence staining, the hydrogels were permeabilized with 0.05% Triton X-100 for 5 mins and blocked with 1% bovine serum albumin (BSA) before staining. To test for ADSCs' osteogenic differentiation, the fixed hydrogel was stained with mouse anti-human osteocalcin antibody for 16 hours followed by fluorescence labeled goat anti-mouse IgG for 1 hour, and then stained with ActinGreen 488 and DAPI for 1 hour before collecting Z-stacks by confocal microscopy imaging. 2D projections were generated using Fiji. Alizarin red (2 wt % pH 4), a dye that binds

to calcium deposits, was used to stain fixed samples for 30 mins followed by 48 hours of washing in DI water. Then, images were taken using Canon PowerShot SX20 IS to compare the porous and nonporous conditions.

For HUVECs, after cell encapsulation, the cells were cultured in EGM™-PLUS medium for a week to allow further proliferation before switching to EGM™-2 medium containing vascular endothelial growth factor (VEGF) to promote neovascularization. After 14 days culture in EGM™-2 medium, the hydrogels were fixed in 4% formaldehyde (in PBS) overnight. Fixed samples were permeabilized for 5 mins and blocked in 1% BSA before fluorescence staining. The hydrogel was then stained with fluorescence labeled anti-CD31 antibody for 16 hours followed by DAPI and ActinRed 555 staining. Confocal Z-stacks and average intensity projections were obtained as described above.

For HL-1, after culturing in the media for 9 days, the hydrogels were fixed in 4% formaldehyde (in PBS) overnight, permeabilized for 5 mins, and blocked in 1% BSA, before fluorescence staining. To test for HL-1 CX-43 and sarcomeric α-actinin, the fixed hydrogel was stained with goat anti-CX43 antibody and rabbit anti-sarcomeric α-actinin antibody for 16 hours followed by fluorescence labeled donkey anti-goat IgG and donkey anti-rabbit IgG, and DAPI for 1 hour before confocal microscopy imaging as above.

4.3 Results and discussion

4.3.1. hDFs encapsulation

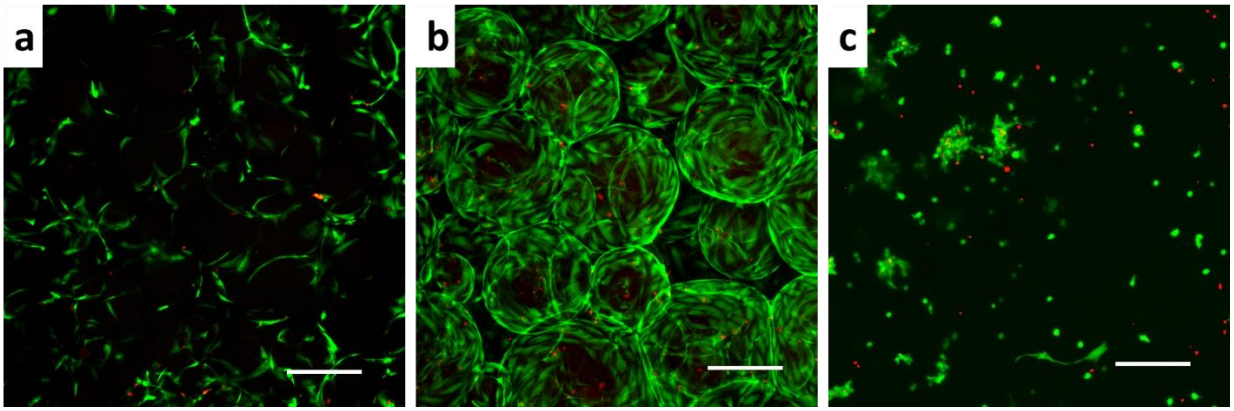

Figure 4.2: Cell viability of hDFs encapsulated in the a) macroporous hydrogel at day 1, b) macroporous hydrogel at day 4, c) nonporous hydrogel at day 4. Green: live cells. Red: dead cells. scale bar: 200 µm.

hDF cells were tested first to demonstrate whether the hydrogel system would be able to accommodate cell encapsulation. hDFs encapsulated in the macroporous hydrogel system are shown in Fig 4.2. By day 1, the cells encapsulated in the macroporous hydrogel adhered and fully spread on the microgel surfaces (Fig 4.2a). On day 4, the cells in the macroporous hydrogel significantly increased in number and they wrapped around the microgels (Fig 4.2b). In comparison, cells encapsulated in the nonporous hydrogel remained ball-shaped and showed far less spreading and proliferation at day 4 (Fig 4.2c). This clear difference between the macroporous and nonporous hydrogel systems indicates that a macroporous system was necessary for achieving rapid spreading and healthy cell morphology.

4.3.2. ADSCs encapsulation and osteogenic differentiation

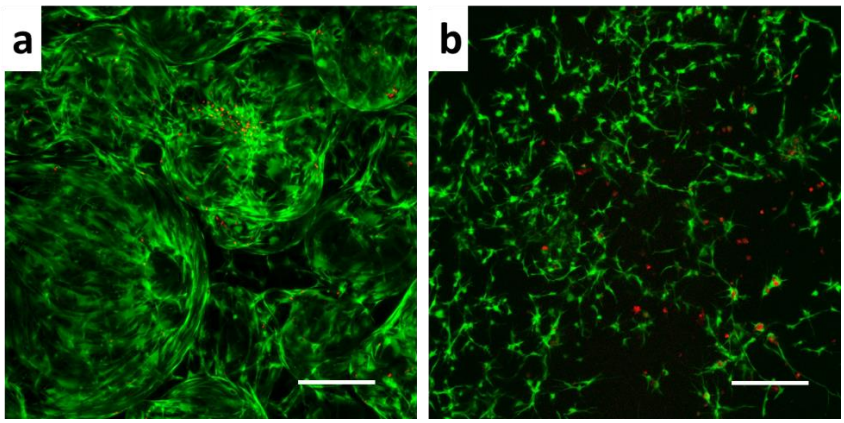

Figure 4.3: Day 21 cell viability of ADSCs encapsulated in the a) macroporous hydrogel, b) nonporous hydrogel. Green: live cells. Red: dead cells. scale bar: 200 µm.

After the rapid cell spreading and proliferation in the macroporous hydrogel was demonstrated using hDFs, other cell types were also tested. Here, ADSCs were encapsulated in the described macroporous hydrogel system to test the effect of macropores on the viability and osteogenic differentiation of ADSCs. By day 21, ADSCs still showed higher viability and spreading within macroporous hydrogel (Fig 4.3a) than within nonporous hydrogel (Fig 4.3b).

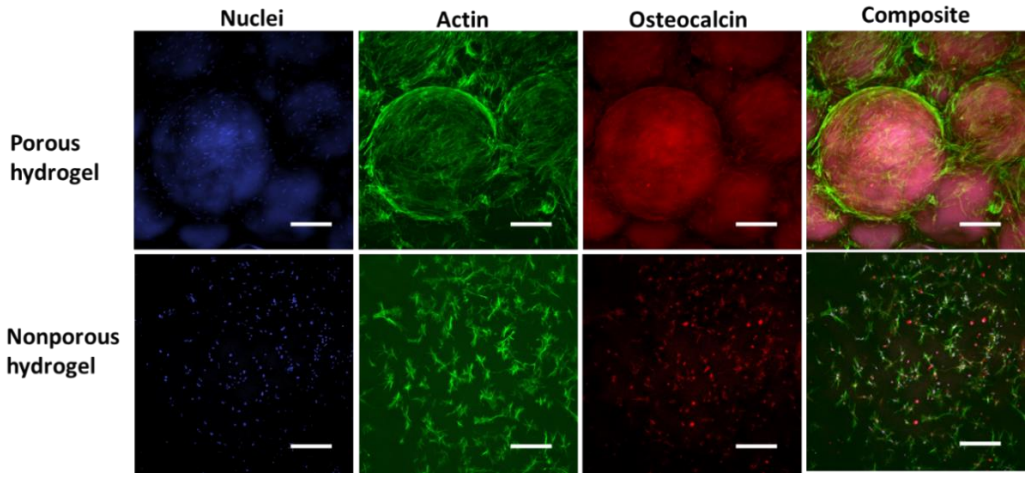

Figure 4.4: Day 21 cell fluorescence image of ADSCs encapsulated in hydrogel. Scale bar: 200 µm.

The same hydrogel was also tested for the ADSCs' osteogenic differentiation. The osteogenic differentiation was induced by the dexamethasone in the differentiation media [34]. Cells encapsulated in macroporous hydrogel showed higher nuclei signal, indicating better cell proliferation, higher actin cytoskeleton signal, representing better spreading, and higher osteocalcin signal, demonstrating more osteogenic differentiation, than cells encapsulated in nonporous hydrogel. (Fig 4.4). These results indicate there was more efficient osteogenic differentiation in the macroporous hydrogel than in the nonporous hydrogel.

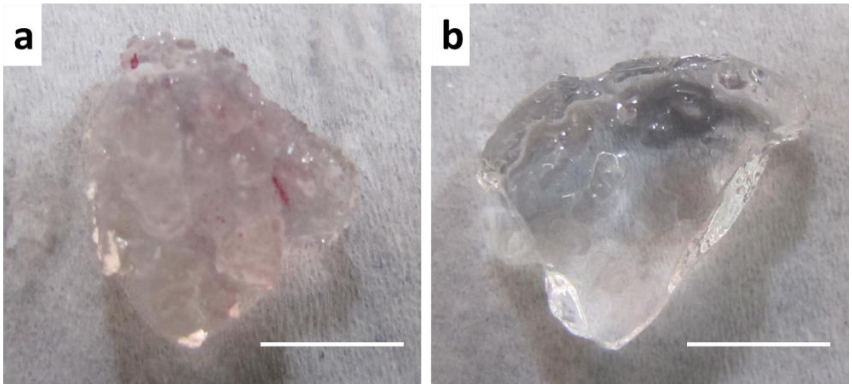

Figure 4.5: Day 21 alizarin red image of ADSCs encapsulated in the a) macroporous hydrogel, b) nonporous hydrogel. Scale bar: 5 mm.

Alizarin red results were consistent with the fluorescence staining results above which showed more osteogenic differentiation within the macroporous hydrogel. Alizarin red dye binds to calcium deposits secreted from the cells, an indicator for osteogenic differentiation. Hydrogels were fixed and stained with alizarin red solution [35]. The macroporous hydrogel (Fig 4.5a) showed more strong red staining compared to the nonporous hydrogel (Fig 4.5b), which indicates that there was more osteogenic differentiation in the macroporous hydrogel. It is known that osteogenic differentiation of stem cells encapsulated in a hydrogel is enhanced by cell spreading [36]. More efficient osteogenic differentiation of mesenchymal stem cells (MSCs) was

achieved when the MSCs were allowed to spread in alginate hydrogels by faster stress relaxation of the surrounding polymers. (Explain here in one or two sentences how it is related to our results). Several spots of thick staining in the macroporous hydrogel (Fig. 4.5a) is possibly due to the cell aggregates within the hydrogel.

4.3.3. HUVECs encapsulation

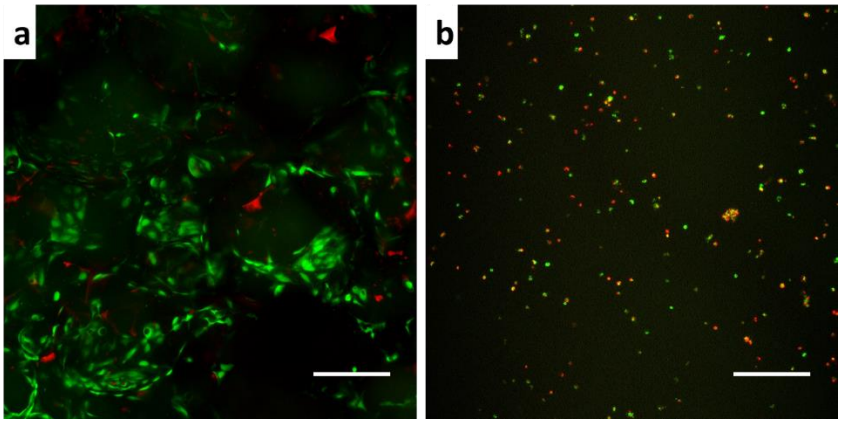

Figure 4.6: Day 21 cell viability of HUVECs encapsulated in the a) macroporous hydrogel, b) nonporous hydrogel. Green: live cells. Red: dead cells. scale bar: 200 µm.

Here, HUVECs were encapsulated in macroporous hydrogel and differentiated to prove neovascularization. After 21 days, similar to other cell types, cell viability and cell spreading in the macroporous hydrogel (Fig 4.6a) was better than in the nonporous hydrogel (Fig 4.6b).

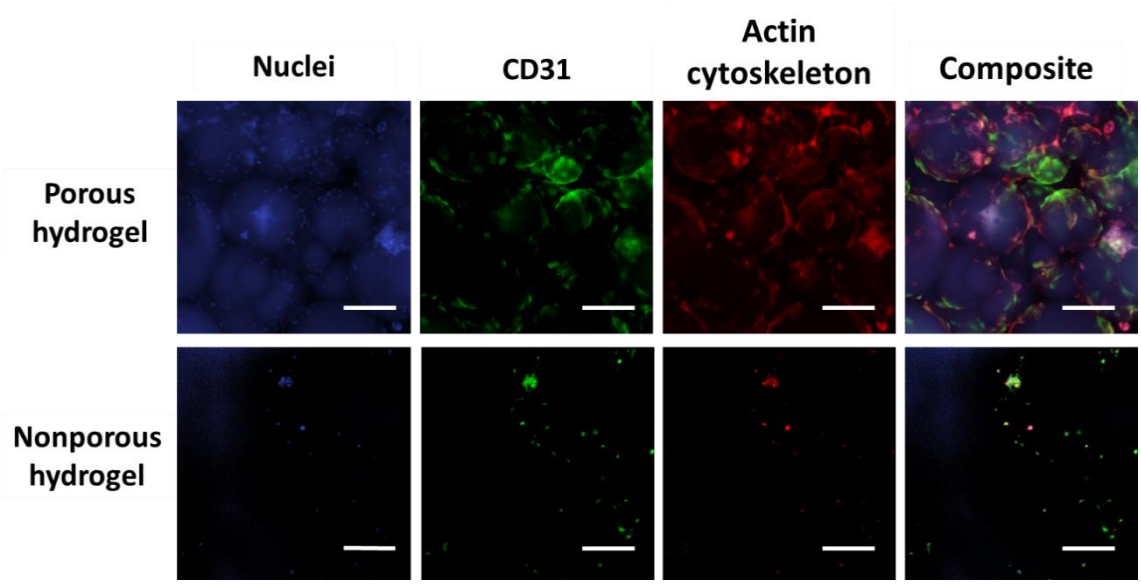

Figure 4.7: Day 21 fluorescence image of HUVECs encapsulated in the hydrogel. Scale bar: 100 µm.

CD31, platelet/endothelial cell adhesion molecule-1, is a cell surface molecule expressed by endothelial cells [37]. For endothelial cells to be incorporated into a blood vessel, it is very important for the cells to be connected with each other. CD31 expression is indicative of cell junction having formed among HUVECs. Within macroporous hydrogel, CD31 signal was higher, and connections among the endothelial cells were more obvious (Fig 4.7). This was likely due to the faster spreading of HUVECs and their subsequent physical contacts among the cells in the porous hydrogel condition. Furthermore, these increased connections among cells in the macroporous system would presumably translate into enhanced neovascular formation.

4.3.4. HL-1 encapsulation and gap junction formation

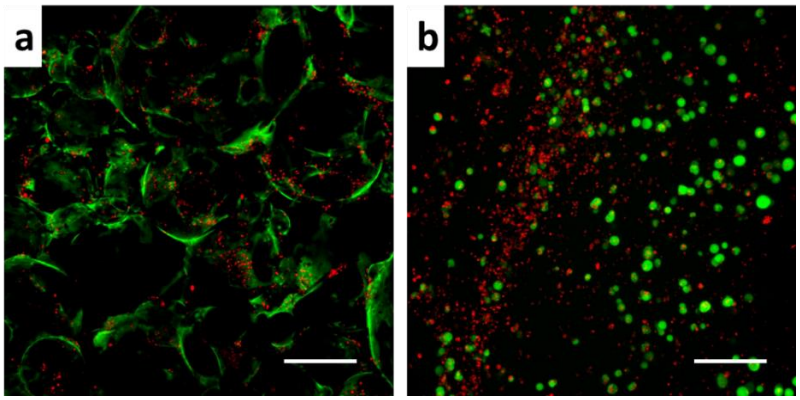

Figure 4.8: Cell viability of HL-1 encapsulated in the a) macroporous hydrogel, b) nonporous hydrogel on day 9. Green: live cells. Red: dead cells. Scale bar: 200 µm.

HL-1 is a mouse cardiac muscle cell line which can continuously divide and spontaneously contract while maintaining a differentiated cardiac phenotype [38]. It was chosen here to test if the macroporous hydrogel will enhance the gap junction formation among the encapsulated cells. After culturing cells for 9 days, similar to the cell types shown above (hDF, HUVEC and ADSC), there was more spreading and proliferation of HL-1 in the macroporous hydrogel (Fig 4.8a) than in the nonporous hydrogel (Fig 4.8b) as evidenced by live/dead confocal microscopy images.

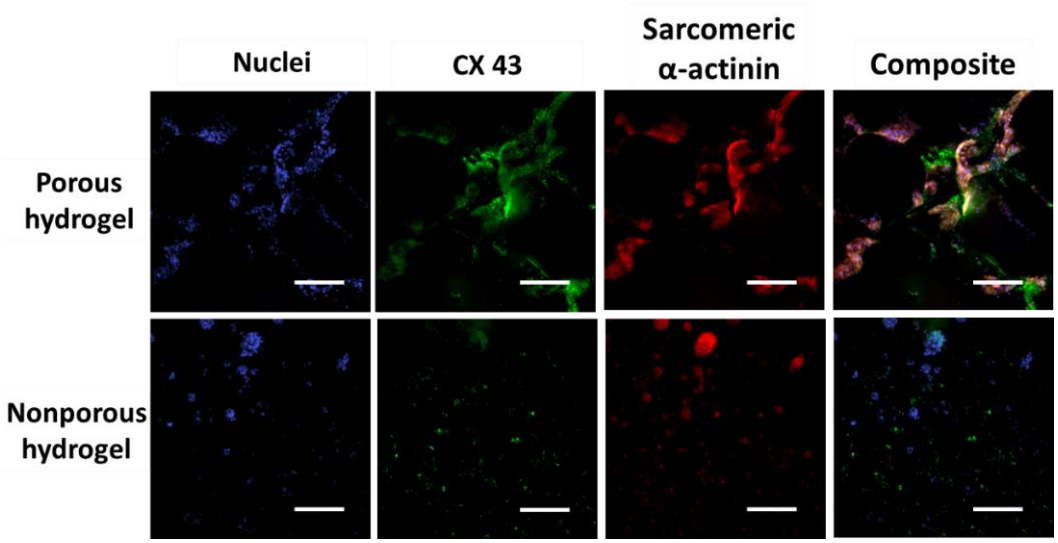

Figure 4.9: Day 9 cell fluorescence image of HL-1 encapsulated in the hydrogel. scale bar: 200 µm.

Especially for cardiomyocytes, cell spreading is vital because cells must be physically connected in order to form gap junctions to promote coordinated beating as is found in the normal cardiac muscle tissue [32]. By cell-cell coupling, cardiomyocytes fuse into a unit of striated muscle tissue called myofibers with the repeating sections of sarcomeres [39]. Connexin 43 (CX-43) and sarcomeric α-actinin are used to visualize the cell-cell coupling [40]. Fluorescence indicating the presence of CX-43, a gap junction protein [40], was more evident in cells encapsulated in macroporous hydrogel than in nonporous hydrogel, providing evidence for better cell-cell interaction in the former condition (Fig 4.9). The sarcomeric α-actinin is a protein that indicates the formation of sarcomere [41]. However, the result here did not show clear repeating unit of sarcomeric α-actinin, which might be due to the fact that HL-1 is a modified cell line, not primary cardiomyocytes.

4.4 Conclusion

Multiple cell types, including hDFs, ADSCs, HUVECs, and HL-1 were successfully encapsulated into the previously reported gelatin macroporous hydrogel system. The

macroporous hydrogel allowed for more rapid cell spreading compared with the nonporous hydrogel. Additionally, the macroporous hydrogel enhanced osteogenic differentiation in encapsulated ADSCs, neovascularization among HUVECs, and the formation of cell connections among HL-1, necessary for synchronized beating. In summary, this macroporous hydrogel system promoted increased cell viability for multiple types of encapsulated cells, important for tissue engineering applications, and thus shows potential as a 3D culture scaffold for tissue engineering.

4.5 Reference

1. Thakur, T.; Xavier, J. R.; Cross, L.; Jaiswal, M. K.; Mondragon, E.; Kaunas, R.; Gaharwar, A. K., Photocrosslinkable and Elastomeric Hydrogels for Bone Regeneration. *J. Biomed. Mater. Res., Part A* **2016,** *104* (4), 879-888.

2. Rowley, A. T.; Nagalla, R. R.; Wang, S. W.; Liu, W. F., Extracellular Matrix-Based Strategies for Immunomodulatory Biomaterials Engineering. *Adv. Healthcare Mater.* **2019**, 1801578.

3. Pok, S.; Stupin, I. V.; Tsao, C.; Pautler, R. G.; Gao, Y.; Nieto, R. M.; Tao, Z. W.; Fraser Jr, C. D.; Annapragada, A. V.; Jacot, J. G., Full-Thickness Heart Repair with an Engineered Multilayered Myocardial Patch in Rat Model. *Adv. Healthcare Mater.* **2017,** *6* (5), 1600549.

4. Nicodemus, G. D.; Bryant, S. J., Cell Encapsulation in Biodegradable Hydrogels for Tissue Engineering Applications. *Tissue Eng., Part B* **2008,** *14* (2), 149-165.

5. Bejleri, D.; Streeter, B. W.; Nachlas, A. L.; Brown, M. E.; Gaetani, R.; Christman, K. L.; Davis, M. E., A Bioprinted Cardiac Patch Composed of Cardiac-Specific Extracellular Matrix and Progenitor Cells for Heart Repair. *Adv. Healthcare Mater.* **2018,** *7* (23), 1800672.

6. Zhu, J.; Marchant, R. E., Design Properties of Hydrogel Tissue-Engineering Scaffolds. *Expert Rev. Med. Devices* **2011,** *8* (5), 607-626.

7. Ruel-Gariepy, E.; Leroux, J.-C., In Situ-Forming Hydrogels—Review of Temperature-Sensitive Systems. *Eur. J. Pharm. Biopharm.* **2004,** *58* (2), 409-426.

8. Wang, L.; Deng, F.; Wang, W.; Li, A.; Lu, C.; Chen, H.; Wu, G.; Nan, K.; Li, L., Construction of Injectable Self-Healing Macroporous Hydrogels Via a Template-Free Method for Tissue Engineering and Drug Delivery. *ACS Appl. Mater. Interfaces* **2018,** *10* (43), 36721-36732.

9. Caldwell, A. S.; Campbell, G. T.; Shekiro, K. M.; Anseth, K. S., Clickable Microgel Scaffolds as Platforms for 3D Cell Encapsulation. *Adv. Healthcare Mater.* **2017,** *6* (15), 1700254.

10. Zhang, M.; Desai, T.; Ferrari, M., Proteins and Cells on Peg Immobilized Silicon Surfaces. *Biomaterials* **1998,** *19* (10), 953-960.

11. Scott, E. A.; Nichols, M. D.; Kuntz-Willits, R.; Elbert, D. L., Modular Scaffolds Assembled around Living Cells Using Poly (Ethylene Glycol) Microspheres with Macroporation Via a Non-Cytotoxic Porogen. *Acta Biomater.* **2010,** *6* (1), 29-38.

12. Griffin, D. R.; Weaver, W. M.; Scumpia, P. O.; Di Carlo, D.; Segura, T., Accelerated Wound Healing by Injectable Microporous Gel Scaffolds Assembled from Annealed Building Blocks. *Nat. Mater.* **2015,** *14* (7), 737.

13. Sideris, E.; Griffin, D. R.; Ding, Y.; Li, S.; Weaver, W. M.; Di Carlo, D.; Hsiai, T.; Segura, T., Particle Hydrogels Based on Hyaluronic Acid Building Blocks. *ACS Biomater. Sci. Eng.* **2016,** *2* (11), 2034-2041.

14. Darling, N. J.; Sideris, E.; Hamada, N.; Carmichael, S. T.; Segura, T., Injectable and Spatially Patterned Microporous Annealed Particle (MAP) Hydrogels for Tissue Repair Applications. *Adv. Sci.* **2018,** *5* (11), 1801046.

15. Nih, L. R.; Sideris, E.; Carmichael, S. T.; Segura, T., Injection of Microporous Annealing Particle (MAP) Hydrogels in the Stroke Cavity Reduces Gliosis and Inflammation and Promotes Npc Migration to the Lesion. *Adv Mater.* **2017,** *29* (32), 1606471.

16. Hou, S.; Lake, R.; Park, S.; Edwards, S.; Jones, C.; Jeong, K. J., Injectable Macroporous Hydrogel Formed by Enzymatic Cross-Linking of Gelatin Microgels. *ACS Appl. Bio Mater.* **2018,** *1* (5), 1430-1439.

17. Tseng, H. J.; Tsou, T. L.; Wang, H. J.; Hsu, S. h., Characterization of Chitosan–Gelatin Scaffolds for Dermal Tissue Engineering. *J. Tissue Eng. Regener. Med.* **2013,** *7* (1), 20-31.

18. Sarker, B.; Zehnder, T.; Rath, S. N.; Horch, R. E.; Kneser, U.; Detsch, R.; Boccaccini, A. R., Oxidized Alginate-Gelatin Hydrogel: A Favorable Matrix for Growth and Osteogenic Differentiation of Adipose-Derived Stem Cells in 3D. *ACS Biomater. Sci. Eng.* **2017,** *3* (8), 1730-1737.

19. Gwon, K.; Kim, E.; Tae, G., Heparin-Hyaluronic Acid Hydrogel in Support of Cellular Activities of 3D Encapsulated Adipose Derived Stem Cells. *Acta Biomater.* **2017,** *49*, 284-295.

20. Fan, L.; Lin, C.; Zhao, P.; Wen, X.; Li, G., An Injectable Bioorthogonal Dextran Hydrogel for Enhanced Chondrogenesis of Primary Stem Cells. *Tissue Eng., Part C* **2018,** *24* (9), 504-513.

21. Sayin, E.; Rashid, R. H.; Rodríguez-Cabello, J. C.; Elsheikh, A.; Baran, E. T.; Hasirci, V., Human Adipose Derived Stem Cells Are Superior to Human Osteoblasts (Hob) in Bone Tissue Engineering on a Collagen-Fibroin-Elr Blend. *Bioact. Mater.* **2017,** *2* (2), 71-81.

22. Fernández-Muiños, T.; Recha-Sancho, L.; López-Chicón, P.; Castells-Sala, C.; Mata, A.; Semino, C. E., Bimolecular Based Heparin and Self-Assembling Hydrogel for Tissue Engineering Applications. *Acta Biomater.* **2015,** *16*, 35-48.

23. Heo, D. N.; Castro, N. J.; Lee, S.-J.; Noh, H.; Zhu, W.; Zhang, L. G., Enhanced Bone Tissue Regeneration Using a 3d Printed Microstructure Incorporated with a Hybrid Nano Hydrogel. *Nanoscale* **2017,** *9* (16), 5055-5062.

24. Chaudhuri, O.; Gu, L.; Klumpers, D.; Darnell, M.; Bencherif, S. A.; Weaver, J. C.; Huebsch, N.; Lee, H.-p.; Lippens, E.; Duda, G. N., Hydrogels with Tunable Stress Relaxation Regulate Stem Cell Fate and Activity. *Nat. Mater.* **2016,** *15* (3), 326.

25. Huebsch, N.; Arany, P. R.; Mao, A. S.; Shvartsman, D.; Ali, O. A.; Bencherif, S. A.; Rivera-Feliciano, J.; Mooney, D. J., Harnessing Traction-Mediated Manipulation of the Cell/Matrix Interface to Control Stem-Cell Fate. *Nat. Mater.* **2010,** *9* (6), 518.

26. Kang, Y.; Chang, J., Channels in a Porous Scaffold: A New Player for Vascularization. *Regener. Med.* **2018,** *13* (06), 705-715.

27. Rouwkema, J.; Koopman, B. F.; Blitterswijk, C. A. V.; Dhert, W. J.; Malda, J., Supply of Nutrients to Cells in Engineered Tissues. *Biotechnol. Genet. Eng. Rev.* 2009, 26 (1), 163-178.

28. Smith, A. W.; Segar, C. E.; Nguyen, P. K.; MacEwan, M. R.; Efimov, I. R.; Elbert, D. L., Long-Term Culture of HL-1 Cardiomyocytes in Modular Poly (Ethylene Glycol) Microsphere-Based Scaffolds Crosslinked in the Phase-Separated State. *Acta Biomater.* **2012,** *8* (1), 31-40.

29. Hasan, A.; Waters, R.; Roula, B.; Dana, R.; Yara, S.; Alexandre, T.; Paul, A., Engineered Biomaterials to Enhance Stem Cell‐Based Cardiac Tissue Engineering and Therapy. *Macromol. Biosci.* **2016,** *16* (7), 958-977.

30. O'Neill, H. S.; Gallagher, L. B.; O'Sullivan, J.; Whyte, W.; Curley, C.; Dolan, E.; Hameed, A.; O'Dwyer, J.; Payne, C.; O'Reilly, D., Biomaterial‐Enhanced Cell and Drug Delivery: Lessons Learned in the Cardiac Field and Future Perspectives. *Adv Mater.* **2016,** *28* (27), 5648-5661.

31. Laflamme, M. A.; Murry, C. E., Heart Regeneration. *Nature* **2011,** *473* (7347), 326.

32. Shin, S. R.; Zihlmann, C.; Akbari, M.; Assawes, P.; Cheung, L.; Zhang, K.; Manoharan, V.; Zhang, Y. S.; Yüksekkaya, M.; Wan, K. t., Reduced Graphene Oxide‐Gelma Hybrid Hydrogels as Scaffolds for Cardiac Tissue Engineering. *Small* **2016,** *12* (27), 3677-3689.

33. Sun, H.; Tang, J.; Mou, Y.; Zhou, J.; Qu, L.; Duval, K.; Huang, Z.; Lin, N.; Dai, R.; Liang, C., Carbon Nanotube-Composite Hydrogels Promote Intercalated Disc Assembly in Engineered Cardiac Tissues through B1-Integrin Mediated Fak and Rhoa Pathway. *Acta Biomater.* **2017,** *48*, 88-99.

34. Vater, C.; Kasten, P.; Stiehler, M., Culture Media for the Differentiation of Mesenchymal Stromal Cells. *Acta Biomater.* **2011,** *7* (2), 463-477.

35. Li, J.; Liu, X.; Crook, J. M.; Wallace, G. G., Development of a Porous 3D Graphene-Pdms Scaffold for Improved Osseointegration. *Colloids Surf. B. Biointerfaces* **2017,** *159*, 386-393.

36. Chaudhuri, O.; Gu, L.; Darnell, M.; Klumpers, D.; Bencherif, S. A.; Weaver, J. C.; Huebsch, N.; Mooney, D. J., Substrate Stress Relaxation Regulates Cell Spreading. *Nat. Commun.* **2015,** *6*, 6365.

37. Righi, L.; Deaglio, S.; Pecchioni, C.; Gregorini, A.; Horenstein, A. L.; Bussolati, G.; Sapino, A.; Malavasi, F., Role of CD31/Platelet Endothelial Cell Adhesion Molecule-1

Expression in *in Vitro* and *in Vivo* Growth and Differentiation of Human Breast Cancer Cells. *Am. J. Pathol.* **2003,** *162* (4), 1163-1174.

38. White, S. M.; Constantin, P. E.; Claycomb, W. C., Cardiac Physiology at the Cellular Level: Use of Cultured HL-1 Cardiomyocytes for Studies of Cardiac Muscle Cell Structure and Function. *AJP-Heart* **2004,** *286* (3), H823-H829.

39. Shin, S. R.; Jung, S. M.; Zalabany, M.; Kim, K.; Zorlutuna, P.; Kim, S. B.; Nikkhah, M.; Khabiry, M.; Azize, M.; Kong, J., Carbon-Nanotube-Embedded Hydrogel Sheets for Engineering Cardiac Constructs and Bioactuators. *ACS nano* **2013,** *7* (3), 2369-2380.

40. Sottas, V.; Wahl, C.-M.; Trache, M. C.; Bartolf-Kopp, M.; Cambridge, S.; Hecker, M.; Ullrich, N. D., Improving Electrical Properties of IPSC-Cardiomyocytes by Enhancing CX43 Expression. *J. Mol. Cell. Cardiol.* **2018,** *120*, 31-41.

41. Hsu, C. P.; Moghadaszadeh, B.; Hartwig, J. H.; Beggs, A. H., Sarcomeric and Nonmuscle *a*-Actinin Isoforms Exhibit Differential Dynamics at Skeletal Muscle Z-Lines. *Cytoskeleton* **2018,** *75* (5), 213-228.

Chapter 5:

Fast Curing Macroporous Gelatin and Gelatin Methacryloyl (GelMA) Hydrogel

5.1. Introduction

Injectable hydrogels are useful tools in regenerative medicine, such as wound healing, due to their ability to conform to the irregular topography of target sites and thereby serve as a temporary scaffold for the healing process [1]. Injectable hydrogels can also be used to encapsulate cells *in situ* for tissue engineering [2-6]. An injectable hydrogel starts as a viscous polymer solution and becomes a viscoelastic solid upon injection by the crosslinking of the polymer chains. Ideally, the crosslinking chemistry should be rapid and non-cytotoxic and the resulting hydrogel should adhere to the applied tissue [7]. The hydrogel should also allow adhesion, spreading, and migration of surrounding [8] or encapsulated cells [4].

One drawback of most injectable hydrogels is lack of macropores, which results in two major issues when it comes to applications in wound healing and tissue engineering. (1) When the hydrogel is applied to a target tissue, the host cells are prevented from migrating into the hydrogel phase to use it as a temporary scaffold for tissue regeneration, slowing down the wound healing process. (2) When cells are encapsulated in the hydrogel for cell delivery or tissue engineering, they are trapped in the polymer mesh, the size of which is orders of magnitude smaller than the size of cells [9]. This significantly delays the spreading and proper functioning of the encapsulated cells. It is inherently difficult to create macropores in injectable hydrogels because the starting material is a viscous solution. To overcome this problem, a typical strategy has been to keep the polymer concentration low (< 5% w/v) [10-11]. Although such an approach improves the interaction between cells and hydrogel, the mechanical integrity of the hydrogels is compromised due to the low polymer concentration, with the resulting storage moduli ~ 500 Pa.

Recently, microgel-based macroporous hydrogels have gained attention [12-17]. In this class of hydrogels, preformed microgels are used as building blocks which are assembled and cured to

form a bulk hydrogel. Macropores are formed by the interstitial space between the microgels. The microgels can be made of modified synthetic polymers (e.g. polyethylene glycol (PEG)) [12-14] or natural polymers (e.g. hyaluronic acid, gelatin) [15-17], and curing of the microgels can be achieved by click chemistry [14], or enzymatic reactions [18]. These microgel-based macroporous hydrogels have been shown to be useful for accelerated wound healing [13], nerve regeneration [16], and *in situ* cell encapsulation for tissue engineering [17]. In theory, the microgel-based macroporous hydrogels can be made injectable as long as the microgel solution is injectable.

Previously, I reported an injectable macroporous hydrogel, composed of gelatin microgels enzymatically crosslinked by microbial transglutaminase (mTG), for use in wound healing [18]. The method used to create this hydrogel was simple, requiring no chemical modifications to the starting reagents, and it yielded a highly biofunctional material that allowed human cells to migrate and proliferate in the hydrogel. However, despite displaying many advantageous qualities, this technology required a lengthy curing time (~ 60 minutes), limiting its usefulness *in vivo*.

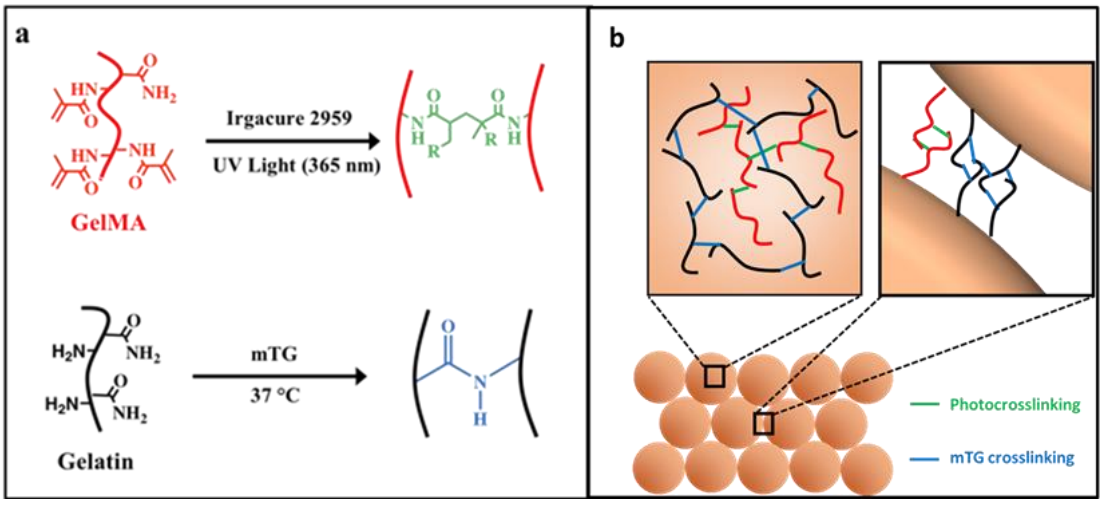

Figure 5.1: Schematic representation of hydrogel formation. a) Mechanism of crosslinking GelMA by UV irradiation and gelatin by enzymatic catalysis. b) Microgel inter- and intra-crosslinking to form an interpenetrating network.

In the present study we address this limitation by introducing a composite gelatin/gelatin methacryloyl (GelMA)-based injectable macroporous hydrogel that cures fast, is minimally cytotoxic, and stably adheres to the applied tissue. This fast-curing hydrogel utilizes dual crosslinking - enzymatic crosslinking of gelatin by mTG [19] and photocrosslinking of GelMA [20-22] by ultraviolet (UV) irradiation (Fig 5.1). Each microgel contains both (1) unmodified gelatin which can be crosslinked by mTG, and (2) GelMA which can be crosslinked by UV photopolymerization in the presence of photoinitiators. Curing of these composite microgels is achieved by both crosslinking mechanisms. UV photopolymerization is fast and allows rapid hydrogel formation; the enzymatic crosslinking by mTG is relatively slow and gradually strengthens the hydrogel. mTG, which forms an amide bond between a glutamine and a lysine residue on proteins, also allows the hydrogel to adhere to target tissues [18, 23]. We also demonstrate that this method can be used for *in situ* cell encapsulation with minimal cytotoxicity, which enables rapid cell spreading and proliferation.

5.2. Materials and methods

All materials were purchased from Sigma-Aldrich (St. Louis, MO) unless specified. Microbial transglutaminase (mTG) was purchased from Ajinomoto (Fort Lee, NJ). Sterile phosphate buffer saline (PBS, pH 7.4) was purchased from Gibco (Carlsbad, CA). Human dermal fibroblasts (hDFs) were purchased from Lonza (Portsmouth, NH). Cell Viability kit, Dulbecco's Modified Eagle's Medium (DMEM), fetal bovine serum (FBS), penicillin/streptomycin (pen/strep), alamarBlue, and ActinRed 555 were purchased from Invitrogen (Frederick, MD). Fresh pig eyeballs were obtained from Visiontech (Sunnyvale, TX).

5.2.1. Synthesis of gelatin/GelMA composite microgels

The gelatin/GelMA composite microgels were prepared using a method similar to the previously reported method [13]. Due to the photoactive nature of GelMA, all procedures involving GelMA were performed in the dark. A 2:1 mixture (by weight) of gelatin (type 1, from bovine and porcine bones) and gelatin methacryloyl (bloom 300, 80% degree of substitution) was dissolved in 20 mL of deionized water at 50−55 °C to make a total 10% (w/v) aqueous solution. This solution was added dropwise to 200 mL of olive oil at 50−55 °C and stirred for 1 h. The temperature of the mixture was lowered to reach room temperature for 30 min with stirring. Then the mixture was placed in an ice−water bath for an additional 30 min with stirring to solidify the microgels by inducing physical cross-linking. To precipitate the microgels, 100 mL of precooled acetone (4 °C) was added to the mixture with stirring for 30 min in the ice−water bath. The microgels were separated from the olive oil and acetone by vacuum filtration and further washed with two 60 mL aliquots of precooled (4°C) acetone. The microgels were lyophilized and kept dry until used.

5.2.2. Characterization of microgels

Microgels were visualized using a scanning electron microscope (SEM) (Tescan Lyra3 GMU FIB SEM, Brno, Czech Republic) and an optical microscope (EVOS XL, Life Technologies, Carlsbad, CA). For SEM, the lyophilized microgels were coated with gold/palladium to avoid charging. For the size distribution of microgels after hydration, a dilute microgel solution was prepared in PBS and 20 uL of this solution was observed using the optical microscope. Size distribution of microgels was obtained from the SEM and optical microscope images using ImageJ.

5.2.3. Crosslinking microgels

Macroporous hydrogels were made by mixing gelatin/GelMA composite microgels (10% w/v) with irgacure 2959 at varying concentrations (0.03-0.1%). Ascorbic acid was added to a final concentration of 0.005% (w/v) to minimize cytotoxicity during the UV irradiation. This mixture was mixed with 20% (w/v) mTG in a 5:1 ratio. The final concentration of gelatin/GelMA and mTG was 8.3% and 3.3%, respectively. For photocrosslinking, UV (365nm, up to 250 mW/cm^2) was applied for 2.5 mins. Nonporous hydrogels were made using the same method except that a gelatin/GelMA solution was used instead of gelatin/GelMA microgels.

5.2.4. Characterization of hydrogels

After the hydrogels were formed, their detailed structure was visualized with SEM. Prior to SEM imaging, the hydrogels were dehydrated through an ethanol series (30%, 50%, 60%, 70%, 80%, and 90% once each, and then 100% twice) before dried by critical point drying and coated with gold/palladium.

The viscoelastic properties of the hydrogels were characterized with a rheometer (TA Instruments AR 550, New Castle, DE). Either a gelatin/GelMA microgel suspension (for macroporous hydrogels) or a gelatin/GelMA solution (for nonporous hydrogels) was mixed with irgacure, ascorbic acid, and mTG, then irradiated by UV for 2.5 mins before being placed under a plane stainless steel geometry (diameter = 2 cm) and measured. The linear viscoelastic regime was first determined by a stress sweep. The gelation kinetics were observed at 37 °C by a time sweep, with an oscillatory stress of 1 Pa at 10 rad/s. Once gelation was completed, a frequency sweep was performed between 0.1 and 100 rad/s with an oscillatory stress of 1 Pa at 37 °C. For

the temperature sweep, the temperature was changed from 4 to 45 °C with an oscillatory stress of 1 Pa at 10 rad/s.

The enzymatic degradation of macroporous and nonporous gelatin/GelMA hydrogels and macroporous gelatin-only hydrogel was examined by incubating the hydrogels in collagenase type II solution (concentration = 0.5 U/mL). At different time points (0h, 4h, 24 h), the hydrogels were collected, lyophilized, and weighed to calculate the amount of degraded gelatin.

5.2.5. Tissue adhesion of the hydrogels

Porcine corneal tissues were used to test tissue adhesion of the hydrogels. Corneal tissues were collected from freshly obtained pig eyeballs using surgical scissors. A hole was created in the middle of the cornea using a biopsy punch (diameter = 8 mm) and was filled by injecting an uncrosslinked solution of microgels, irgacure 2959, ascorbic acid, and mTG, followed by 2.5 min of UV irradiation. To test the gelation and tissue adhesion, the tissue was transferred to 45 °C PBS.

5.2.6. Cell encapsulation and characterization

Human dermal fibroblasts (hDFs) were cultured in T75 flasks using DMEM, supplemented with FBS and pen/strep. Cells of passage 3 were used for all experiments.

Prior to cell encapsulation, the gelatin/GelMA microgels and GelMA powders were sterilized by incubating them in 70% ethanol overnight. Gelatin, mTG, irgacure 2959, and ascorbic acid solutions were sterilized by syringe filters (pore size = 220 nm). For encapsulation, the microgels, mTG, irgacure 2959, and ascorbic acid were mixed with hDFs at 5 x 10^5 cells/mL, followed by 2.5 mins of UV irradiation. These were further incubated at 37 °C for 1 hour. The encapsulated cells were cultured with DMEM supplemented with FBS and pen/strep.

The three-dimensional distribution of hDFs in hydrogel was visualized by confocal microscopy on days 3 and 6 using a cell viability kit, which stains live and dead cells with green (by calcein-AM) and red fluorescence (by ethidium homodimer), respectively. To visualize the details of cell spreading and morphology inside the hydrogel, each sample was fixed in 4% formaldehyde (in PBS) overnight and stained with ActinRed 555 and DAPI. Z-stacked images were then obtained using the confocal microscope. 2D maximum intensity projections, 3D reconstructions, and cross-sectional images were generated from Z-stacks in Fiji.

5.2.7. Statistics

The data are presented as means ± standard deviation unless stated otherwise. The statistical significance of the difference among multiple sample groups was tested by ANOVA followed by Tukey's *post hoc* test.

5.3. Results and discussion

5.3.1. Gelatin/GelMA microgel characterization

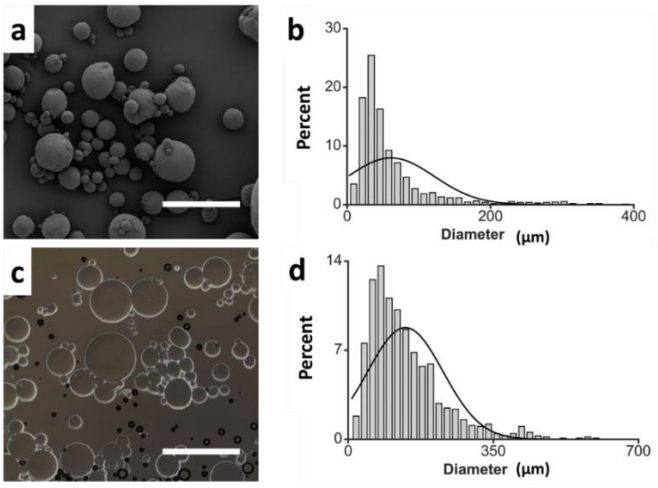

Figure 5.2: Microscope images and size distribution of microgels. a) SEM image and b) size distribution of lyophilized microgels. c) Optical microscope image and d) size distribution of hydrated microgels. Scale bars = 200 μm.

The composite microgels made from gelatin/GelMA were synthesized by a water-in-oil emulsion method, which generates polydisperse microspheres. The freeze-dried microgels were spherical in shape (Fig 5.2a) with an average diameter of 61 (± 60) μm (Fig 5.2b). When equilibrated in an aqueous environment (Fig 5.2c), the average diameter increased to 139 (± 90) μm (Fig 5.2d).

5.3.2. Hydrogel gelling, tissue binding, and rheology

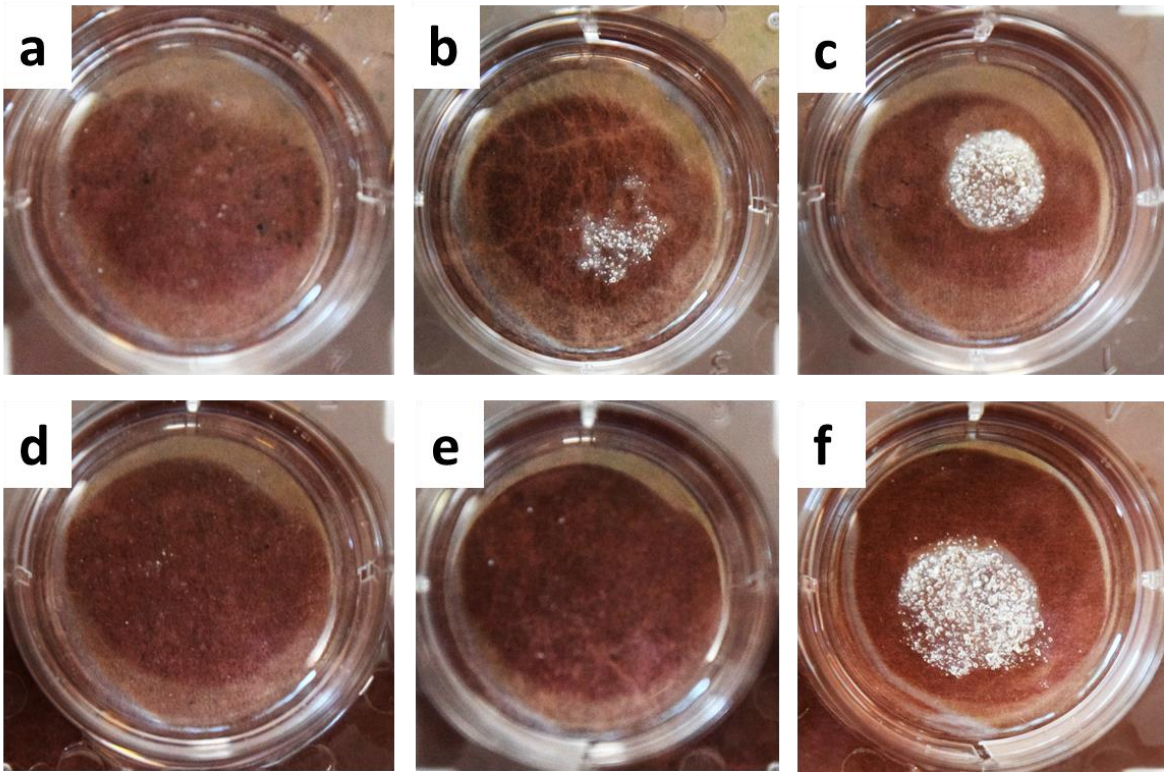

Figure 5.3: Stability test of hydrogels. After curing, hydrogels were immersed and shaken in a 45 °C water bath, in which all physical crosslinks are broken. The microgels were cured by a) mTG + 0.5% photoinitiator (no UV irradiation) b) 0.5% photoinitiator with UV irradiation (no mTG) c) 0.5% photoinitiator with UV irradiation + mTG d) mTG + 0.05% photoinitiator (no UV irradiation) e) 0.05% photoinitiator with UV irradiation (no mTG) (f) 0.05% photoinitiator with UV irradiation + mTG. In all cases, the crosslinking time was 2.5 min. The scale bar = 10 mm.

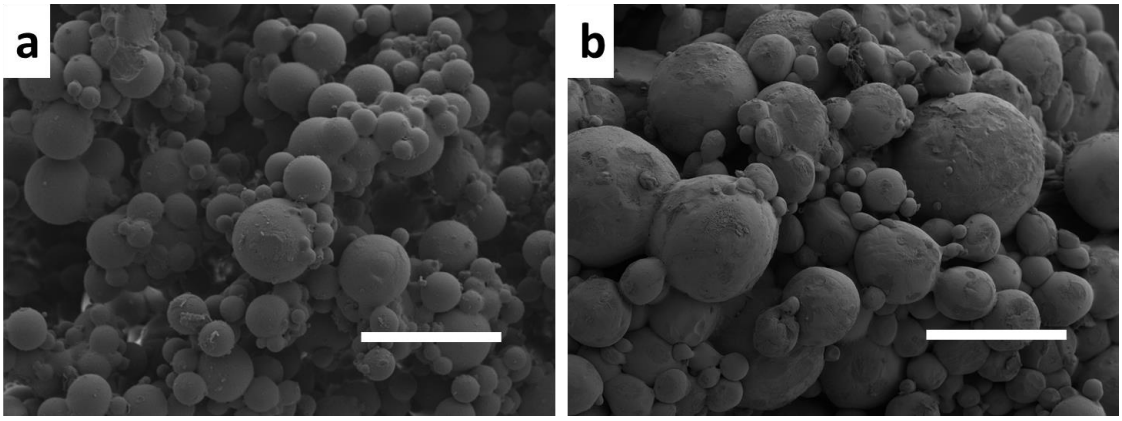

Figure 5.4: SEM images of the macroporous hydrogels crosslinked with mTG and a) 0.5% w/v photoinitiator b) 0.05% w/v photoinitiator.

Curing of the composite microgels and the stability of the resulting bulk hydrogel were tested under various crosslinking conditions by immersing the hydrogels in a warm water bath (45 °C). Gelatin itself physically crosslinks by hydrogen bonds and forms a hydrogel at low temperatures (< 30 °C) but quickly melts at high temperatures. In this test, a bulk hydrogel will remain intact only if there are enough covalent crosslinks. When the composite microgels were mixed with mTG (3.3%) for 2.5 min and immersed in the warm water bath, the microgel assembly dissociated completely, meaning the mTG-based crosslinking was not fast enough to cure the microgels within 2.5 min (Fig 5.3a). On the contrary, when the same composite microgels were cured by 2.5 min UV irradiation with 0.5% photoinitiator, a stable bulk hydrogel was formed (Fig 5.3b). This is attributed to the rapid formation of covalent crosslinks within and between microgels by photopolymerization. A similar result was obtained when the microgels were cured by mTG in addition to the UV irradiation (with 0.5% photoinitiator) (Fig 5.3c). When viewed by SEM, the hydrogel was clearly made of the composite microspheres, with macropores created by the interstitial space (Fig 5.4a).

A similar set of experiments was performed using a much lower photoinitiator concentration (0.05%). Photoinitiator is known to be cytotoxic [24], and minimizing its concentration is important for the utilization of this hydrogel in biological systems. As in the case of 0.5% photoinitiator concentration, the composite microgels did not result in a stable hydrogel with mTG crosslinking alone for 2.5 min (Fig 5.3d). When the microgels were cured by UV irradiation alone with 0.05% photoinitiator, the microgel assembly completely dissociated (Fig 5.3e). This means that photopolymerization alone was insufficient to cure the microgels at this photoinitiator concentration. When the mTG crosslinking was added to the UV irradiation with 0.05% photoinitiator, the resulting assembly was stable in a warm water bath (Fig 5.3f). As in the case of 0.5% photoinitiator, the hydrogel as viewed by SEM was clearly made of individual microspheres with macropores created by the interstitial space (Fig 5.4b) Comparing Fig 5.3e and 5.3f, we can conclude that the dual crosslinking by UV photopolymerization and enzymatic crosslinking by mTG allows rapid curing of the composite microgels even with a highly dilute photoinitiator concentration (0.05%).

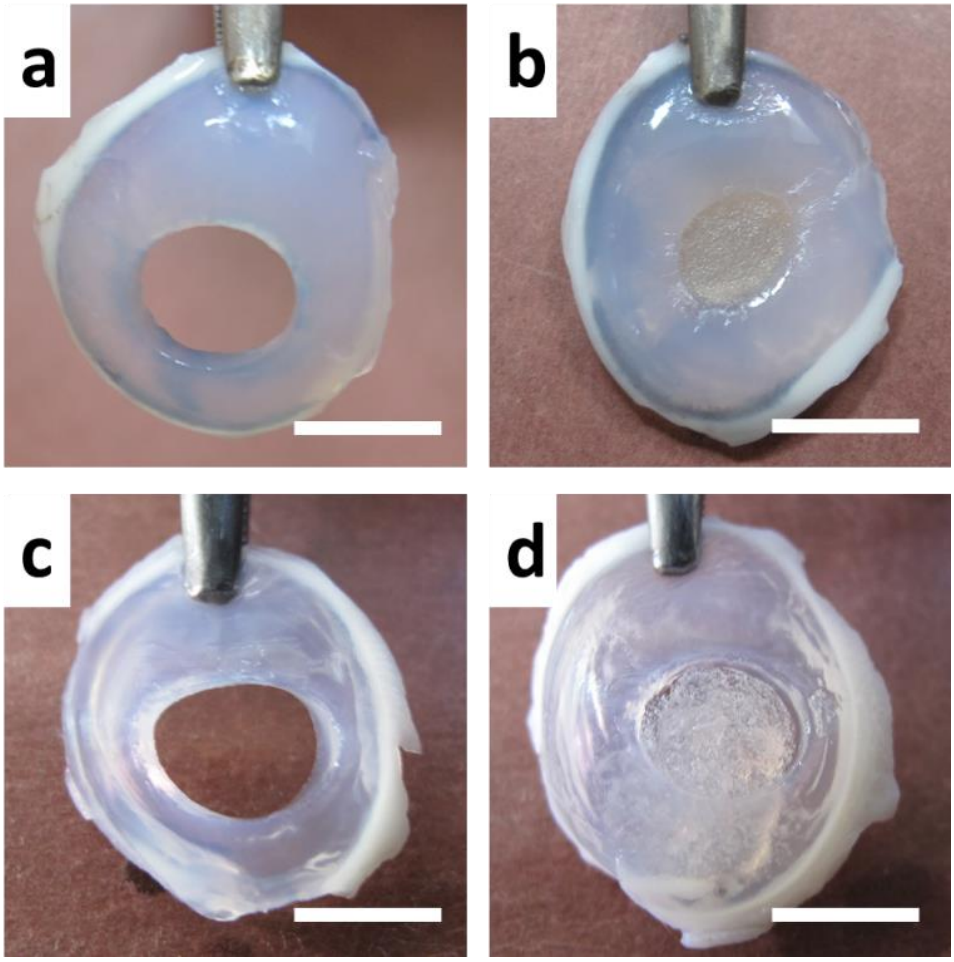

Figure 5.5: Tissue adhesion test of the microgel-based hydrogels. The composite microgels were added to a small hole (8 mm in diameter) in a porcine cornea and cured by a) UV irradiation (0.5% photoinitiator) b) UV irradiation (0.5% photoinitiator) + mTG c) UV irradiation (0.05% photoinitator) d) UV irradiation (0.05% photoinitiator) + mTG. After curing, the tissue-hydrogel constructs were immersed in a warm water bath (45 °C) and shaken. In all cases, the curing time was 2.5 min. The scale bar = 5 mm.

In addition to rapid curing, adhesion of the hydrogel upon application to tissue is another important feature to make this injectable formulation clinically relevant. Previously, macroporous hydrogel made by assembly of gelatin microgels adhered to porcine corneal tissue within 1 hour by the action of mTG were demonstrated [13]. The usage of mTG was considered safe, since it is known as meat glue [25]. Porcine corneas were used as a model tissue due to ready availability. Whether mTG-catalyzed tissue adhesion could be achieved more rapidly if it is used

in conjunction with UV photopolymerization was tested. The composite microgels were injected into an 8 mm hole in a porcine cornea and allowed to crosslink by UV irradiation (for 2.5 minutes) alone or by UV irradiation along with mTG crosslinking. Tissue adhesion of the bulk hydrogel was tested by immersing and shaking the construct in a warm water bath (45 °C). For both photoinitiator concentrations (0.5 and 0.05%), UV photopolymerization alone did not result in stable adhesion of the hydrogel to the tissue (Fig 5.5a, c). Either the microgel assembly fully dissociated (at 0.05% photoinitiator) or the bulk hydrogel readily detached from the tissue (at 0.5% photoinitiator). However, when mTG was added in addition to UV photopolymerization, the bulk hydrogels stably remained on the corneal tissue at both photoinitiator concentrations (Fig 5.5b, d), This result clearly shows that UV photopolymerization alone does not allow the hydrogel to adhere to the tissue. The enzymatic crosslinking by mTG not only stabilizes the microgel assembly to form a bulk macroporous hydrogel but also enables the bulk hydrogel to adhere to the tissue.

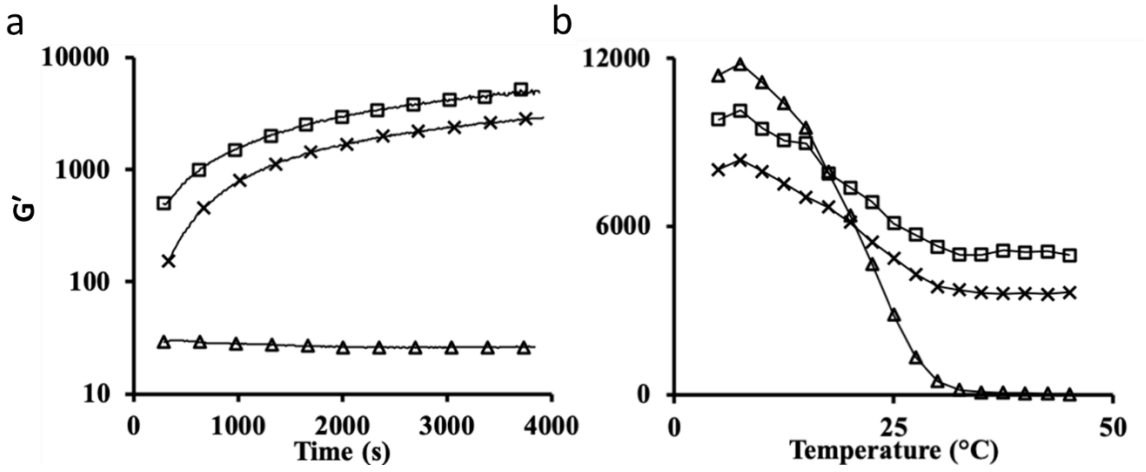

Figure 5.6: Rheology for a) time sweep and b) temperature sweep for samples of interest. □ denotes macroporous hydrogel crosslinked by both UV irradiation and mTG, × denotes macroporous hydrogel crosslinked by mTG only, and Δ denotes macroporous hydrogel crosslinked only by UV irradiation. The Y axis indicates G' in units of Pa.

Gelation kinetics and viscoelastic properties of the hydrogels were quantified by rheology. Photoinitiator concentration was 0.05%. The macroporous hydrogel crosslinked by both UV irradiation and mTG showed the highest storage modulus (G') at all times (Fig 5.6a). When microgels were cured by mTG (without UV irradiation), the gelation process was slower. For example, the time for G' to reach 1000 Pa was delayed by approximately 10.5 minutes of gelation time and G' at 1 hour was lower compared to the case of dual crosslinking. This result shows that utilization of both UV photopolymerization and enzymatic crosslinking more rapidly produces a stable gel than crosslinking by enzymatic action alone. When the microgels were cured only with UV irradiation (without mTG), G' did not increase with time. This indicates the photoinitiator concentration was too low to produce a stable hydrogel. This result is consistent with the results shown in Fig 5.3.

In the temperature sweep, as the temperature decreased, G' increased in all groups tested (Fig 5.6b). This is due to the formation of physical crosslinks by hydrogen bonds within the gelatin strands [24]. The porous hydrogel crosslinked by both UV irradiation and mTG had higher values of G' than the hydrogel crosslinked by mTG alone throughout the tested temperature range. In both cases, the hydrogels did not melt completely at high temperatures (> 30 °C) with their storage moduli settling at ~ 4500Pa, which further verifies the presence of covalent crosslinks in these hydrogels. When the microgels were cured by UV irradiation only (without mTG), a solid hydrogel was formed at low temperatures due to the formation of physical crosslinks, but the viscoelastic solid dissociated when heated above 30 °C. This again shows that UV photopolymerization alone did not produce enough covalent crosslinks at 0.05% photoinitiator to form a stable hydrogel.

5.3.3. Degradation of hydrogels

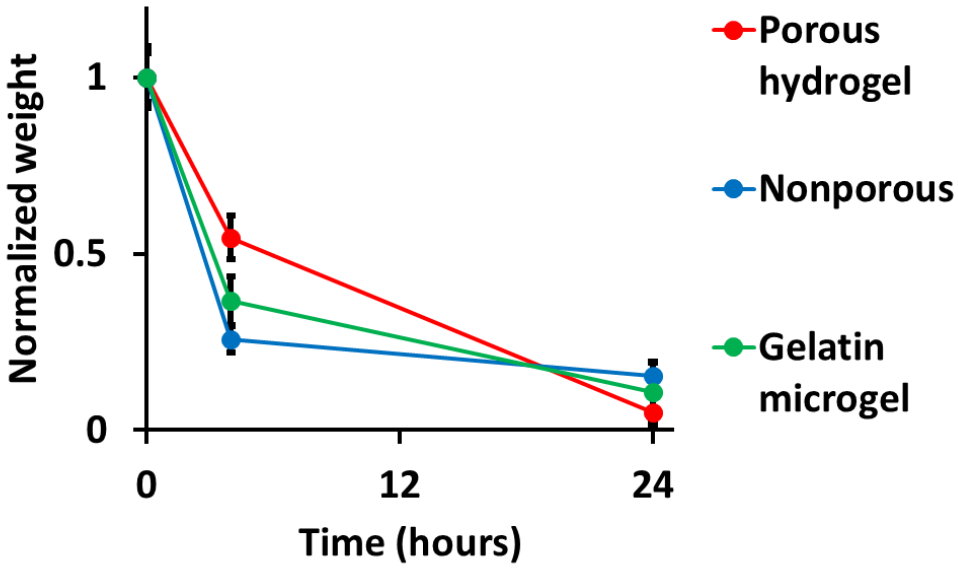

Figure 5.7: Degradation of the hydrogels.

Since the hydrogels were produced from gelatin and a gelatin derivative (GelMA) which have been shown to be degraded both *in vitro* and *in vivo* by various enzymes [26-28], it is expected that these hydrogels will be biodegradable [29-30]. We tested *in vitro* enzymatic degradation using collagenase type II. Although there were slight differences in the degradation kinetics, the macroporous hydrogels made of Gelatin/GelMA mixture degraded within 24 hours at a similar rate to their nonporous counterparts (Fig 5.7).

5.3.4. hDFs encapsulation and characterization

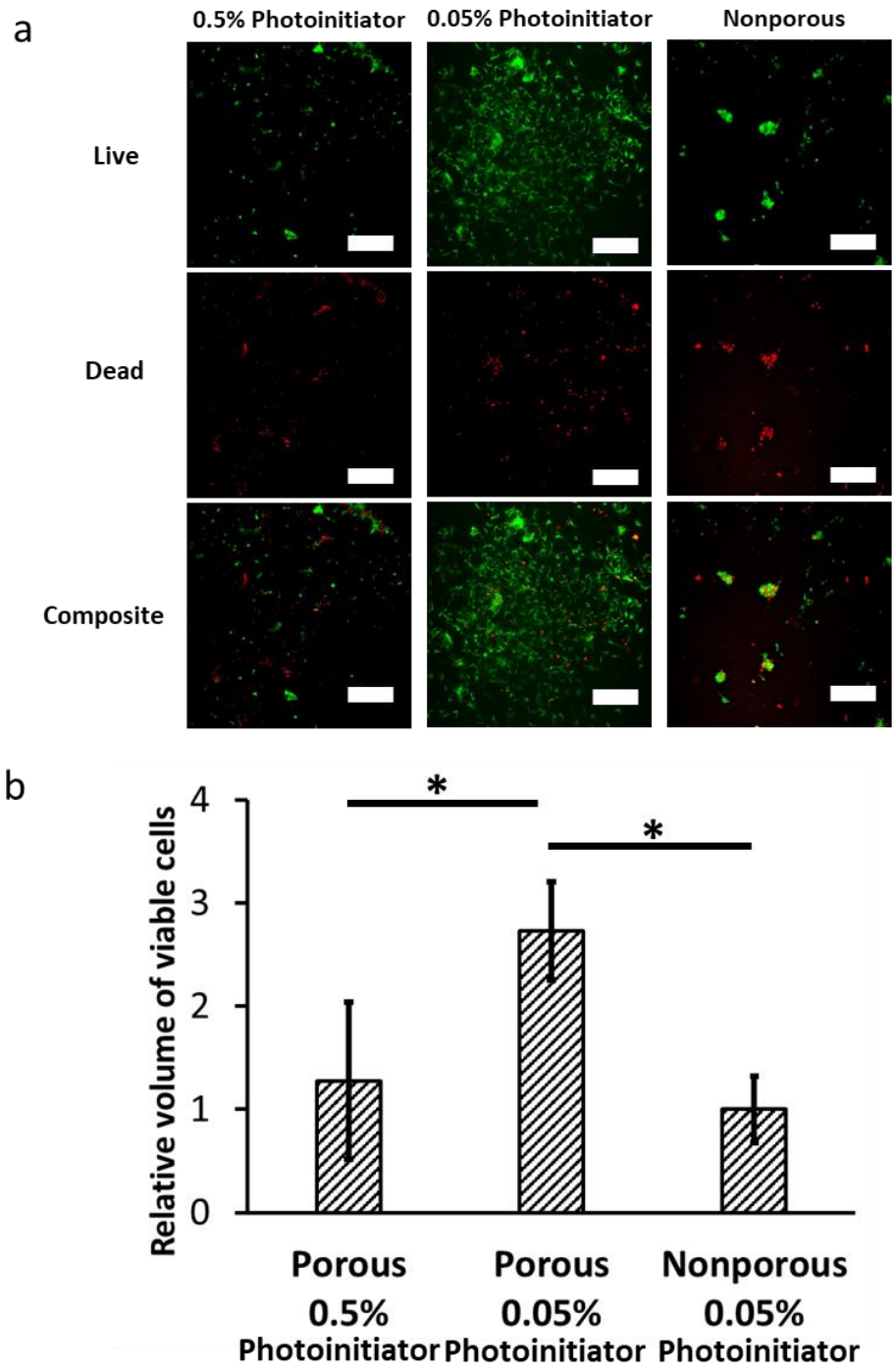

Figure 5.8: a) Flourescence image, and b) quantitative analysis of day 1 cell viability for macroporous hydrogel with 0.5% or 0.05% w/v photoinitiator concentration and for nonporous hydrogel with 0.05% w/v photoinitiator concentration. Green: live cells. Red: dead cells. Scale bar: 200 µm. * indicated $p < 0.05$

In situ cell encapsulation in a hydrogel is an important technology for the delivery of viable cells for wound healing and tissue regeneration [31-33]. The feasibility of using our microgel-based injectable hydrogel for cell delivery was tested using hDFs. Unlike most nonporous hydrogels in which encapsulated cells are trapped in the polymer mesh, cells were seeded in the interstitial space between microgels. Fig 5.8a shows 2D average intensity projections of confocal Z-stacked images from the live/dead assay one day post-encapsulation and Fig 5.8b indicates the quantitative analysis of the fluorescence image. Total volume of the viable cells was chosen to represent the number of live cells. Cell encapsulation was performed using two different photoinitiator concentrations (0.5% and 0.05%). For a comparison, cells were also encapsulated in a nonporous gelatin/GelMA composite hydrogel, which was produced by mixing the cells in a gelatin/GelMA solution and curing it by UV photopolymerization and the addition of mTG. Two results were noteworthy: (1) There were noticeably more viable cells in the macroporous hydrogel crosslinked with 0.05% photoinitiator than in the macroporous hydrogel crosslinked with 0.5% photoinitiator. Cytotoxicity of photoinitator and radical polymerization in cell encapsulation is well known [34]. When the cells were encapsulated in the hydrogel at 0.5% photoinitiator, the viability of the cell was a lot lower (Fig A1.1). To reduce the cytotoxicity of the photopolymerization process, anti-oxidants (specifically, ascorbic acid) were added during the polymerization [35-36]. As demonstrated above, lowering the photoinitiator concentration to 0.05% significantly altered the integrity of the hydrogel when curing was done by UV photopolymerization alone. The use of mTG in conjunction with UV photopolymerization at low photoinitiator concentration enabled the formation of a stable hydrogel and at the same time resulted in high cell viability of the encapsulated hDFs. (2) The hDFs encapsulated in the microgel-based hydrogels adhered and spread on the microgel surfaces within the interstitial

space within 1 day. This greatly contrasted with the cells encapsulated in a nonporous hydrogel which were trapped in the polymer mesh in spherical morphologies. In general, polymer concentration should be lowered in order to enhance cell spreading in nonporous hydrogels [37], but this can significantly affect the mechanical strength of the hydrogel. Our results provide clear evidence that cells encapsulated in the microgel-based hydrogels can adhere and spread much more quickly (as early as in 1 day) than in the traditional nonporous hydrogels.

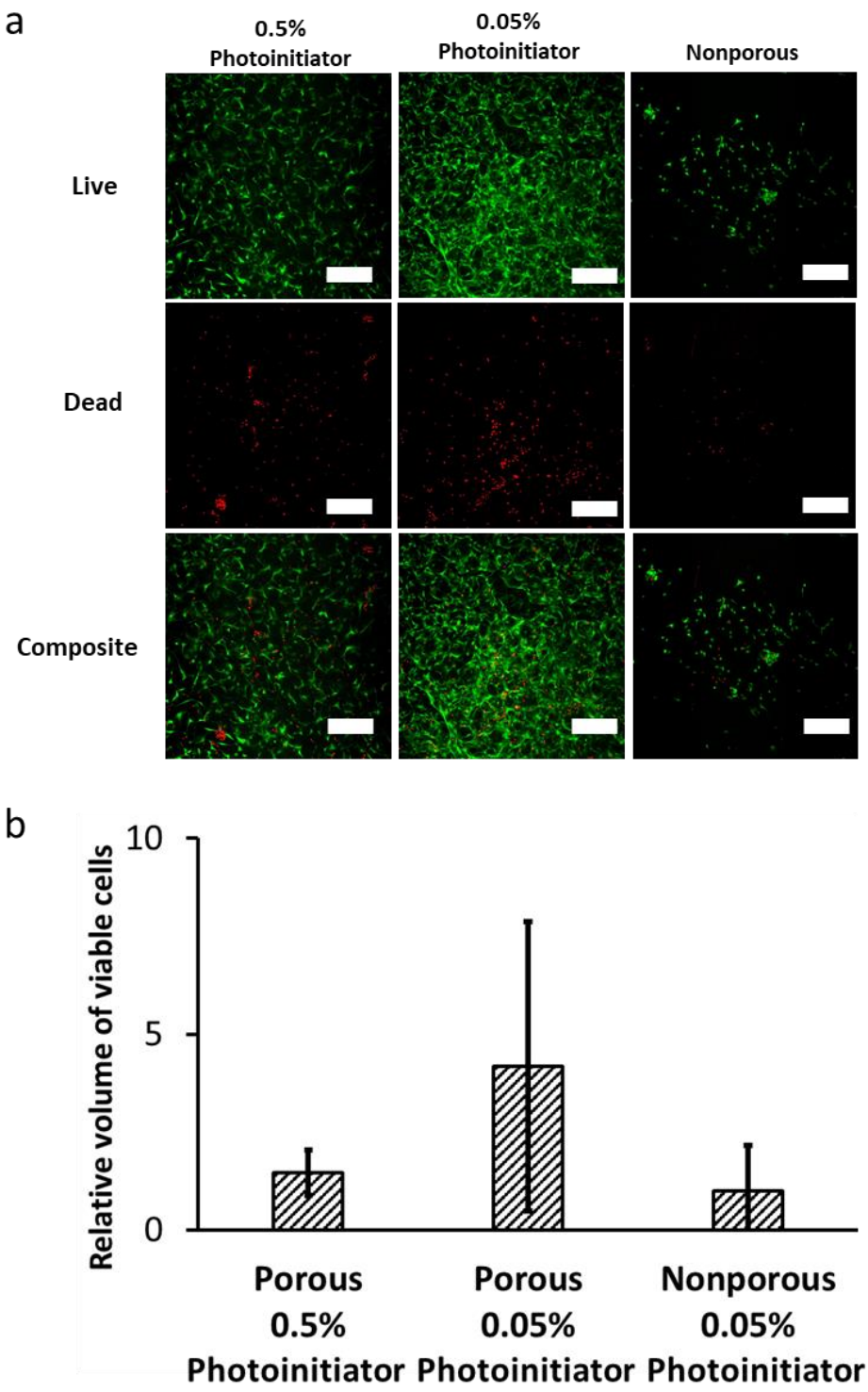

Figure 5.9: a) Flourescence image, and b) quantitative analysis of day 7 cell viability for macroporous hydrogel with 0.5% or 0.05% w/v photoinitiator concentration and for nonporous hydrogel with 0.05% w/v photoinitiator concentration. Green: live cells. Red: dead cells. Scale bar: 200 µm.

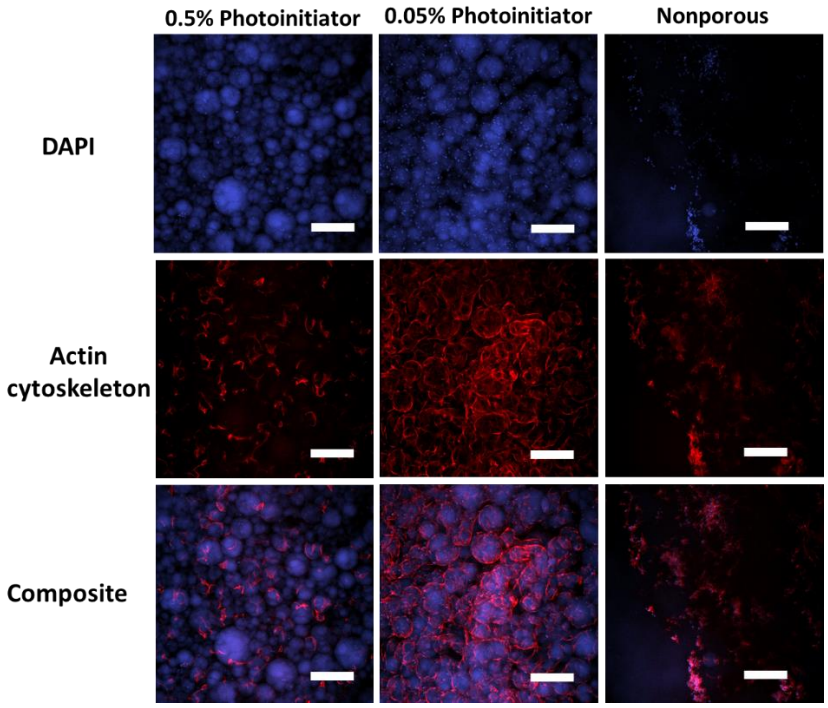

Figure 5.10: Day 7 cell fluorescence image for macroporous hydrogel with 0.5% or 0.05% photoinitiator concentration and for nonporous hydrogel with 0.05% w/v photoinitiator concentration. Red: actin cytoskeleton. Blue: cell nuclei. Scale bar: 200 μm.

The advantage of encapsulating cells in the macroporous hydrogels made of microgels was further demonstrated by the live/dead assay performed 7 days post-encapsulation (Fig 5.9a) and quantified confirmed in Fig 5.9b. With both photoinitiator concentrations, there was a significant increase of viable cell number in the macroporous hydrogels. More robust cell proliferation was observed for the hydrogel cured with 0.05% photoinitiator, presumably as a result of the minimal cytotoxicity caused by the photoinitiator and free radicals. As on day 1, the cells were well-spread around the microgels within the interstitial space. Most cells encapsulated in the nonporous hydrogel still exhibited round morphologies, and there was minimal spreading, likely because the cells were still trapped in the polymer mesh. The detailed structures of actin cytoskeleton presented in Fig 5.10 confirmed the result from the live/dead assay.

Overall, the injectable hydrogel formulation we describe in this dissertation has 4 major advantages compared to previously reported injectable hydrogels. (1) It gels quickly (2.5 min) under UV irradiation even at a low photoinitiator concentration (0.05%) due to the synergistic actions of UV photopolymerization and mTG-based enzymatic crosslinking. (2) The use of low photoinitiator concentration results in high viability and proliferation during the cell encapsulation process. (3) Due to the action of mTG in conjunction with UV photopolymerization, the hydrogel adheres to the target tissue stably within 2.5 min. (4) The presence of macropores allows enhanced interactions among cells as evidenced by the rapid adhesion, spreading, and proliferation of the encapsulated cells. We anticipate that this novel formulation will find many applications related to accelerated wound healing and cell delivery-based therapeutics [38].

5.4. Conclusion

Gelatin/GelMA composite microgels were successfully synthesized and crosslinked into macroporous hydrogel via duel crosslinking by photocrosslinking with 0.05% photoinitiator in the presence of 0.005% ascorbic acid, and by enzymatic crosslinking using mTG. The use of low photoinitiator concentration minimized associated cytotoxic effects, while enabling the hydrogel to stably form in 2.5 minutes, when simultaneously combined with enzymatic crosslinking by mTG. Use of mTG also facilitated binding between the hydrogel and the tissue. In summary, the hydrogel system reported here shows promise for use in wound healing and tissue engineering applications due to its injectable, fast curing, macroporous nature that minimizes cytotoxic effects of the photoinitiator.

5.5. Reference

1. Li, Y.; Rodrigues, J.; Tomas, H., Injectable and Biodegradable Hydrogels: Gelation, Biodegradation and Biomedical Applications. *Chem. Soc. Rev.* **2012,** *41* (6), 2193-2221.

2. Popa, E. G.; Caridade, S. G.; Mano, J. F.; Reis, R. L.; Gomes, M. E., Chondrogenic Potential of Injectable κ-Carrageenan Hydrogel with Encapsulated Adipose Stem Cells for Cartilage Tissue-Engineering Applications. *J. Tissue Eng. Regener. Med.* **2015,** *9* (5), 550-563.

3. Jooybar, E.; Abdekhodaie, M. J.; Alvi, M.; Mousavi, A.; Karperien, M.; Dijkstra, P. J., An Injectable Platelet Lysate-Hyaluronic Acid Hydrogel Supports Cellular Activities and Induces Chondrogenesis of Encapsulated Mesenchymal Stem Cells. *Acta Biomater.* **2019,** *83*, 233-244.

4. Cai, L.; Dewi, R. E.; Heilshorn, S. C., Injectable Hydrogels with *in Situ* Double Network Formation Enhance Retention of Transplanted Stem Cells. *Adv. Funct. Mater.* **2015,** *25* (9), 1344-1351.

5. Truong, V. X.; Ablett, M. P.; Richardson, S. M.; Hoyland, J. A.; Dove, A. P., Simultaneous Orthogonal Dual-Click Approach to Tough, in-Situ-Forming Hydrogels for Cell Encapsulation. *J. Am. Chem. Soc.* **2015,** *137* (4), 1618-1622.

6. Jeon, O.; Wolfson, D. W.; Alsberg, E., In-Situ Formation of Growth-Factor-Loaded Coacervate Microparticle-Embedded Hydrogels for Directing Encapsulated Stem Cell Fate. *Adv Mater.* **2015,** *27* (13), 2216-2223.

7. Liu, H.; Liu, J.; Qi, C.; Fang, Y.; Zhang, L.; Zhuo, R.; Jiang, X., Thermosensitive Injectable in-Situ Forming Carboxymethyl Chitin Hydrogel for Three-Dimensional Cell Culture. *Acta Biomater.* **2016,** *35*, 228-237.

8. DeQuach, J. A.; Lin, J. E.; Cam, C.; Hu, D.; Salvatore, M. A.; Sheikh, F.; Christman, K. L., Injectable Skeletal Muscle Matrix Hydrogel Promotes Neovascularization and Muscle Cell Infiltration in a Hindlimb Ischemia Model. *Eur. Cells Mater.* **2012,** *23*, 400.

9. Zustiak, S. P.; Leach, J. B., Hydrolytically Degradable Poly (Ethylene Glycol) Hydrogel Scaffolds with Tunable Degradation and Mechanical Properties. *Biomacromolecules* **2010,** *11* (5), 1348-1357.

10. Phelps, E. A.; Enemchukwu, N. O.; Fiore, V. F.; Sy, J. C.; Murthy, N.; Sulchek, T. A.; Barker, T. H.; García, A. J., Maleimide Cross-Linked Bioactive Peg Hydrogel Exhibits Improved Reaction Kinetics and Cross-Linking for Cell Encapsulation and *in Situ* Delivery. *Adv Mater.* **2012,** *24* (1), 64-70.

11. Li, L.; Lu, C.; Wang, L.; Chen, M.; White, J.; Hao, X.; McLean, K. M.; Chen, H.; Hughes, T. C., Gelatin-Based Photocurable Hydrogels for Corneal Wound Repair. *ACS Appl. Mater. Interfaces* **2018,** *10* (16), 13283-13292.

12. Scott, E. A.; Nichols, M. D.; Kuntz-Willits, R.; Elbert, D. L., Modular Scaffolds Assembled around Living Cells Using Poly (Ethylene Glycol) Microspheres with Macroporation Via a Non-Cytotoxic Porogen. *Acta Biomater.* **2010,** *6* (1), 29-38.

13. Griffin, D. R.; Weaver, W. M.; Scumpia, P. O.; Di Carlo, D.; Segura, T., Accelerated Wound Healing by Injectable Microporous Gel Scaffolds Assembled from Annealed Building Blocks. *Nat. Mater.* **2015,** *14* (7), 737.

14. Caldwell, A. S.; Campbell, G. T.; Shekiro, K. M.; Anseth, K. S., Clickable Microgel Scaffolds as Platforms for 3D Cell Encapsulation. *Adv. Healthcare Mater.* **2017,** *6* (15), 1700254.

15. Sideris, E.; Griffin, D. R.; Ding, Y.; Li, S.; Weaver, W. M.; Di Carlo, D.; Hsiai, T.; Segura, T., Particle Hydrogels Based on Hyaluronic Acid Building Blocks. *ACS Biomater. Sci. Eng.* **2016,** *2* (11), 2034-2041.

16. Nih, L. R.; Sideris, E.; Carmichael, S. T.; Segura, T., Injection of Microporous Annealing Particle (MAP) Hydrogels in the Stroke Cavity Reduces Gliosis and Inflammation and Promotes Npc Migration to the Lesion. *Adv Mater.* **2017,** *29* (32), 1606471.

17. Darling, N. J.; Sideris, E.; Hamada, N.; Carmichael, S. T.; Segura, T., Injectable and Spatially Patterned Microporous Annealed Particle (MAP) Hydrogels for Tissue Repair Applications. *Adv. Sci.* **2018,** *5* (11), 1801046.

18. Hou, S.; Lake, R.; Park, S.; Edwards, S.; Jones, C.; Jeong, K. J., Injectable Macroporous Hydrogel Formed by Enzymatic Cross-Linking of Gelatin Microgels. *ACS Appl. Bio Mater.* **2018,** *1* (5), 1430-1439.

19. Yamamoto, S.; Hirata, A.; Ishikawa, S.; Ohta, K.; Nakamura, K.-i.; Okinami, S., Feasibility of Using Gelatin-Microbial Transglutaminase Complex to Repair Experimental Retinal Detachment in Rabbit Eyes. *Graefe's Arch. Clin. Exp. Ophthalmol.* **2013,** *251* (4), 1109-1114.

20. Nichol, J. W.; Koshy, S. T.; Bae, H.; Hwang, C. M.; Yamanlar, S.; Khademhosseini, A., Cell-Laden Microengineered Gelatin Methacrylate Hydrogels. *Biomaterials* **2010,** *31* (21), 5536-5544.

21. Chen, Y. C.; Lin, R. Z.; Qi, H.; Yang, Y.; Bae, H.; Melero-Martin, J. M.; Khademhosseini, A., Functional Human Vascular Network Generated in Photocrosslinkable Gelatin Methacrylate Hydrogels. *Adv. Funct. Mater.* **2012,** *22* (10), 2027-2039.

22. Nikkhah, M.; Eshak, N.; Zorlutuna, P.; Annabi, N.; Castello, M.; Kim, K.; Dolatshahi-Pirouz, A.; Edalat, F.; Bae, H.; Yang, Y., Directed Endothelial Cell Morphogenesis in Micropatterned Gelatin Methacrylate Hydrogels. *Biomaterials* **2012,** *33* (35), 9009-9018.

23. Dinh, T. N.; Hou, S.; Park, S.; Shalek, B. A.; Jeong, K. J., Gelatin Hydrogel Combined with Polydopamine Coating to Enhance Tissue Integration of Medical Implants. *ACS Biomater. Sci. Eng.* **2018,** *4* (10), 3471-3477.

24. Hellio, D.; Djabourov, M. In Physically and Chemically Crosslinked Gelatin Gels, *Macromolecular Symposia*, Wiley Online Library: 2006; pp 23-27.

25. Yung, C.; Wu, L.; Tullman, J.; Payne, G.; Bentley, W.; Barbari, T., Transglutaminase Crosslinked Gelatin as a Tissue Engineering Scaffold. *J Biomed. Mater. Res. A* **2007,** *83* (4), 1039-1046.

26. Xiao, W.; Li, J.; Qu, X.; Wang, L.; Tan, Y.; Li, K.; Li, H.; Yue, X.; Li, B.; Liao, X., Cell-Laden Interpenetrating Network Hydrogels Formed from Methacrylated Gelatin and Silk Fibroin Via a Combination of Sonication and Photocrosslinking Approaches. *Mater. Sci. Eng. C Biomimetic Supramol. Syst.* **2019,** *99*, 57-67.

27. Koshy, S. T.; Desai, R. M.; Joly, P.; Li, J.; Bagrodia, R. K.; Lewin, S. A.; Joshi, N. S.; Mooney, D. J., Click‐Crosslinked Injectable Gelatin Hydrogels. *Adv. Healthcare Mater.* **2016,** *5* (5), 541-547.

28. Gattazzo, F.; De Maria, C.; Rimessi, A.; Donà, S.; Braghetta, P.; Pinton, P.; Vozzi, G.; Bonaldo, P., Gelatin–Genipin‐Based Biomaterials for Skeletal Muscle Tissue Engineering. *J. Biomed. Mater. Res., Part B* **2018,** *106* (8), 2763-2777.

29. Park, S.; Edwards, S.; Hou, S.; Boudreau, R.; Yee, R.; Jeong, K. J., A Multi-Interpenetrating Network (Ipn) Hydrogel with Gelatin and Silk Fibroin. *Biomater. Sci.* **2019**.

30. Zhao, X.; Lang, Q.; Yildirimer, L.; Lin, Z. Y.; Cui, W.; Annabi, N.; Ng, K. W.; Dokmeci, M. R.; Ghaemmaghami, A. M.; Khademhosseini, A., Photocrosslinkable Gelatin Hydrogel for Epidermal Tissue Engineering. *Adv. Healthcare Mater.* **2016,** *5* (1), 108-118.

31. Dong, Y.; Rodrigues, M.; Li, X.; Kwon, S. H.; Kosaric, N.; Khong, S.; Gao, Y.; Wang, W.; Gurtner, G. C., Injectable and Tunable Gelatin Hydrogels Enhance Stem Cell Retention and Improve Cutaneous Wound Healing. *Adv. Funct. Mater.* **2017,** *27* (24), 1606619.

32. Wei, Z.; Zhao, J.; Chen, Y. M.; Zhang, P.; Zhang, Q., Self-Healing Polysaccharide-Based Hydrogels as Injectable Carriers for Neural Stem Cells. *Sci. Rep.* **2016,** *6*, 37841.

33. Almeida, H.; Eswaramoorthy, R.; Cunniffe, G.; Buckley, C.; O'Brien, F.; Kelly, D., Fibrin Hydrogels Functionalized with Cartilage Extracellular Matrix and Incorporating Freshly Isolated Stromal Cells as an Injectable for Cartilage Regeneration. *Acta Biomater.* **2016,** *36*, 55-62.

34. Greene, T.; Lin, T. Y.; Andrisani, O. M.; Lin, C. C., Comparative Study of Visible Light Polymerized Gelatin Hydrogels for 3D Culture of Hepatic Progenitor Cells. *J. Appl. Polym. Sci.* **2017,** *134* (11).

35. Sabnis, A.; Rahimi, M.; Chapman, C.; Nguyen, K. T., Cytocompatibility Studies of an *in Situ* Photopolymerized Thermoresponsive Hydrogel Nanoparticle System Using Human Aortic Smooth Muscle Cells. *J. Biomed. Mater. Res., Part A* **2009,** *91* (1), 52-59.

36. Drzewiecki, K. E.; Malavade, J. N.; Ahmed, I.; Lowe, C. J.; Shreiber, D. I., A Thermoreversible, Photocrosslinkable Collagen Bio-Ink for Free-Form Fabrication of Scaffolds for Regenerative Medicine. *Technology* **2017,** *5* (04), 185-195.

37. Di Giuseppe, M.; Law, N.; Webb, B.; Macrae, R. A.; Liew, L. J.; Sercombe, T. B.; Dilley, R. J.; Doyle, B. J., Mechanical Behaviour of Alginate-Gelatin Hydrogels for 3D Bioprinting. *J. Mech. Behav. Biomed. Mater.* **2018,** *79*, 150-157.

38. Cheng, N.-C.; Lin, W.-J.; Ling, T.-Y.; Young, T.-H., Sustained Release of Adipose-Derived Stem Cells by Thermosensitive Chitosan/Gelatin Hydrogel for Therapeutic Angiogenesis. *Acta Biomater.* **2017,** *51*, 258-267.

Chapter 6:

Future Work

In chapters 3 and 4, the microgels were polydisperse in size. Using monodisperse microgels will enable us to control the size of the macropores and study the effects of pore size on cellular responses. For this purpose, the microfluidic channels can be used to create monodisperse microgels [1-3]. A gelatin solution gels at room temperature due to the intermolecular hydrogen bonds, which makes it difficult to apply microfluidics to produce monodisperse microgels. This challenge can be addressed by dissolving gelatin in acetic acid to produce a gelatin solution at room temperature [4]. Our preliminary results have shown that gelatin microgels can be produced at room temperature using this method, and acetic acid can be removed by washing the microgels with acetone and ethanol mixture.

In chapter 4, we demonstrated that the encapsulation of HL-1 cells in the macroporous hydrogel increased cell-cell contacts and facilitated gap junction formation. However, the staining for sarcomeric α-actinin in HL-1 was not obvious and the spontaneous beating rate was very low. As next step towards developing a cardiac patch, one can use the primary cardiomyocytes or the cardiomyocytes derived from the induced pluripotent stem cells (iPSCs). iPSCs are cells that have been reprogrammed back into an embryonic-like stem cells which are proliferative and capable of differentiating into cardiomyocytes [5]. We anticipate that using iPSC-derived cardiomyocytes will result in more efficient gap junction formation, better assembly of sarcomeric structures, regular spontaneous beating, and synchronized beating under external stimuli.

For ADSCs encapsulation, the results have shown the potential of enhancing osteogenic differentiation. However, whether this is the result of more viable cells in the hydrogel or from more efficient osteogenic differentiation is unclear. To test the mechanism behind this result, quantitative real-time polymerase chain reaction (qRT-PCR) can be used to reveal the

mechanisms at the gene level. Our preliminary results have shown that one of the relative quantity of the early and late stage osteogenic differentiation genes runt-related transcription factor 2 (RUNX2) [6] is similar for porous hydrogel and nonporous hydrogel (Fig A1.2). This may mean that the differences of the alizarin red and osteocalcin fluorescence are coming from the differences in cell proliferation. This result needs to be confirmed by additional experiments of late stage markers, for example osteocalcin [6].

This hydrogel system can also be applied to other cell related applications. For example, this hydrogel can be used as a delivery vehicle for mesenchymal stem cells (MSCs) to reduce inflammation [7], such as atopic dermatitis [8] and inflammatory bowel disease [9]. Our preliminary results have shown that the cells in the nonoporous hydrogel secreted more interleukin-10 (IL-10), an anti-inflammatory cytokine, than the porous hydrogel (Fig A1.3). Similar to other types of cell encapsulation, the macroporous hydrogel resulted in better spreading of the encapsulated MSCs compared with the nonporous hydrogel (Fig A1.4). It was recently found that cell morphologies affected the cytokine secretome of MSCs [10]. However, the difference of anti-inflammatory cytokines secretion of the MSCs in 3D environment has not been tested. We are hoping to understand if there is a correlation between the MSCs morphology and the anti-inflammatory cytokines secretion of the MSCs in the macroporous hydrogel. More experiments should be performed to verify our preliminary result by measuring other anti-inflammatory cytokines and pro-inflammatory cytokines, for instance IL-4 and interferon-γ (IFN-γ), respectively. The cell spreading can be characterized via analyzing the confocal image to calculate the spread area and cell shape index (CSI) of the cell [11]. CSI value is between 0 and 1, which refer to a line and a sphere, respectively. With the spread area and the CSI value, whether the cytokines secretion is affected by the cell spreading can be studied.

For chapter 5, the gelatin/GelMA macroporous hydrogel system shortened the curing time dramatically as well as minimized the cytotoxicity on hDFs. However, the use of photoinitiator can still have some cytotoxic effects on the cells. Encapsulation of other cell types (e.g. ADSCs, HUVECs and MSCs) should be tested on this hydrogel for tissue engineering applications.

Reference

1. Griffin, D. R.; Weaver, W. M.; Scumpia, P. O.; Di Carlo, D.; Segura, T., Accelerated Wound Healing by Injectable Microporous Gel Scaffolds Assembled from Annealed Building Blocks. *Nat. Mater.* 2015, *14* (7), 737.

2. Sideris, E.; Griffin, D. R.; Ding, Y.; Li, S.; Weaver, W. M.; Di Carlo, D.; Hsiai, T.; Segura, T., Particle Hydrogels Based on Hyaluronic Acid Building Blocks. *ACS Biomater. Sci. Eng.* 2016, *2* (11), 2034-2041.

3. Weidenbacher, L.; Abrishamkar, A.; Rottmar, M.; Guex, A. G.; Maniura-Weber, K.; deMello, A.; Ferguson, S. J.; Rossi, R. M.; Fortunato, G., Electrospraying of Microfluidic Encapsulated Cells for the Fabrication of Cell-Laden Electrospun Hybrid Tissue Constructs. *Acta Biomater.* 2017, *64*, 137-147.

4. Panzavolta, S.; Gioffrè, M.; Focarete, M. L.; Gualandi, C.; Foroni, L.; Bigi, A., Electrospun Gelatin Nanofibers: Optimization of Genipin Cross-Linking to Preserve Fiber Morphology after Exposure to Water. *Acta Biomater.* 2011, *7* (4), 1702-1709.

5. Kaiser, N. J.; Kant, R. J.; Minor, A. J.; Coulombe, K. L., Optimizing Blended Collagen-Fibrin Hydrogels for Cardiac Tissue Engineering with Human iPSC-Derived Cardiomyocytes. *ACS Biomater. Sci. Eng.* 2018, *5* (2), 887-899.

6. Huang, W.; Yang, S.; Shao, J.; Li, Y.-P., Signaling and Transcriptional Regulation in Osteoblast Commitment and Differentiation. *Front. Biosci.* 2007, *12*, 3068.

7. Sánchez-Sánchez, R.; Martínez-Arredondo, E.; Martínez-López, V.; Melgarejo-Ramírez, Y.; Brena-Molina, A.; Lugo-Martínez, H.; Gómez-García, R.; Garciadiego-Cázares, D.; Silva-Bermúdez, P.; Márquez-Gutiérrez, E., Development of Hydrogel with Anti-Inflammatory Properties Permissive for the Growth of Human Adipose Mesenchymal Stem Cells. *J. Nanomater.* 2016, *2016*, 72.

8. Villatoro, A. J.; Hermida-Prieto, M.; Fernandez, V.; Farinas, F.; Alcoholado, C.; Rodriguez-Garcia, M. I.; Marinas-Pardo, L.; Becerra, J., Allogeneic Adipose-Derived Mesenchymal Stem Cell Therapy in Dogs with Refractory Atopic Dermatitis: Clinical Efficacy and Safety. *Vet. Rec.* 2018, *183* (21), 654.

9. Ko, I. K.; Kim, B.-G.; Awadallah, A.; Mikulan, J.; Lin, P.; Letterio, J. J.; Dennis, J. E., Targeting Improves MSC Treatment of Inflammatory Bowel Disease. *Mol. Ther.* 2010, *18* (7), 1365-1372.

10. Leuning, D. G.; Beijer, N. R.; Fossé, N. A.; Vermeulen, S.; Lievers, E.; Kooten, C.; Rabelink, T. J.; de Boer, J., The Cytokine Secretion Profile of Mesenchymal Stromal Cells Is Determined by Surface Structure of the Microenvironment. *Sci. Rep.* 2018, *8* (1), 7716.

11. Caliari, S. R.; Vega, S. L.; Kwon, M.; Soulas, E. M.; Burdick, J. A., Dimensionality and Spreading Influence MSC YAP/TAZ Signaling in Hydrogel Environments. *Biomaterials* **2016,** *103*, 314-323.

APPENDICES

A1. Other Results

A2. Multi-functional Surface Chemistry that Enhances Cell Adhesion and Suppresses Bacterial Growth

A1. Other results

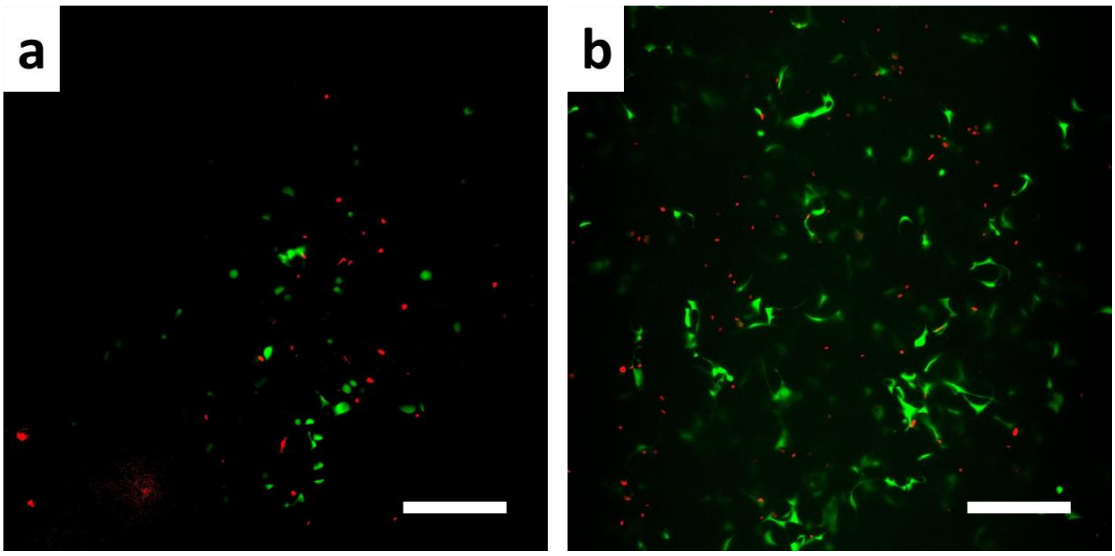

Figure A1.1: Cell viability for macroporous hydrogel with no ascorbic acid. a) 0.5% photoinitiator concentration, b) 0.05% photoinitiator concentration. Green: live cells. Red: dead cells. Scale bar: 200 µm.

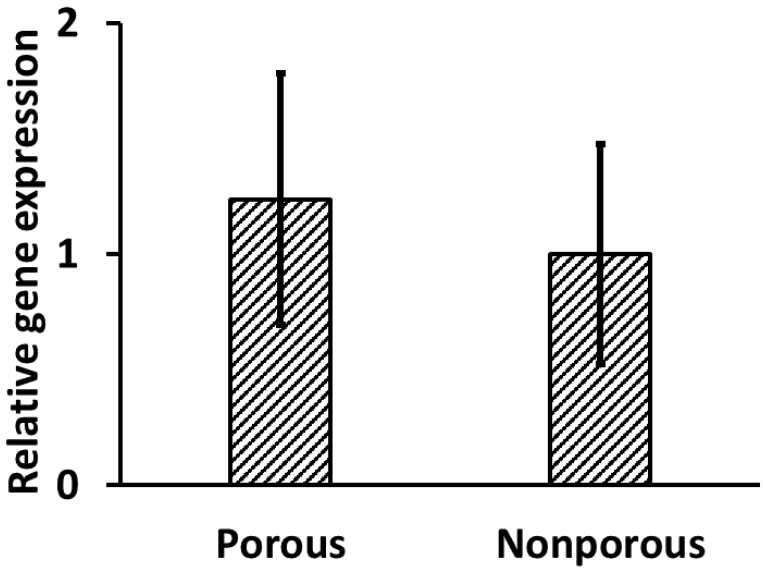

Figure A1.2: qRT-PCR result for relative expression of RUNX2 gene.

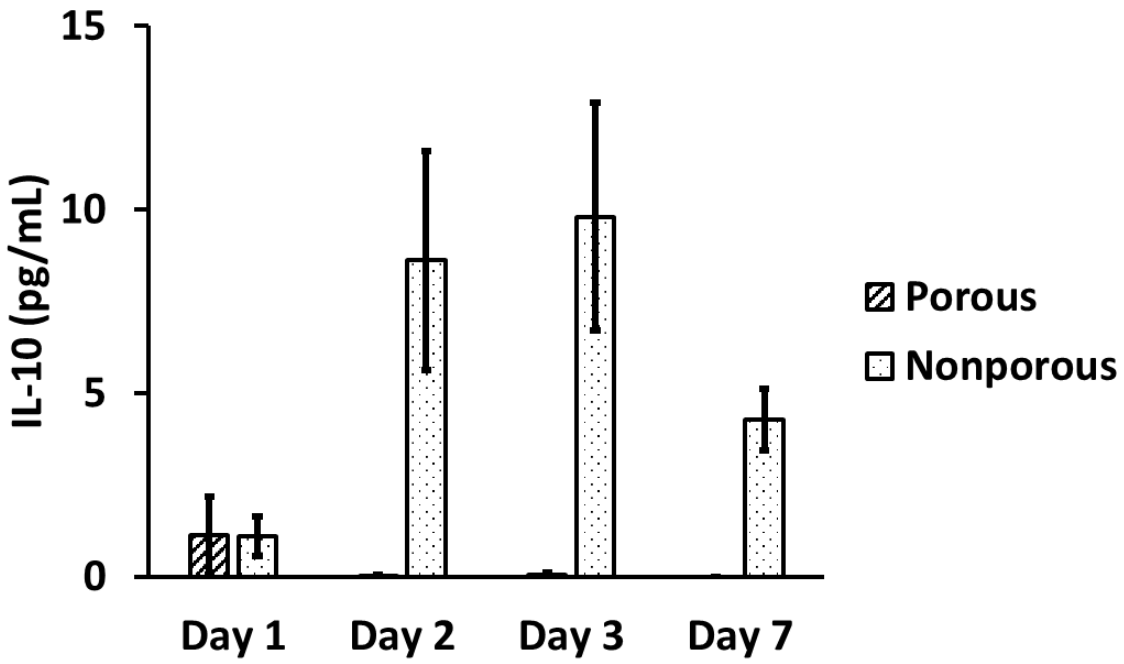

Figure A1.3: IL-10 release of the MSCs.

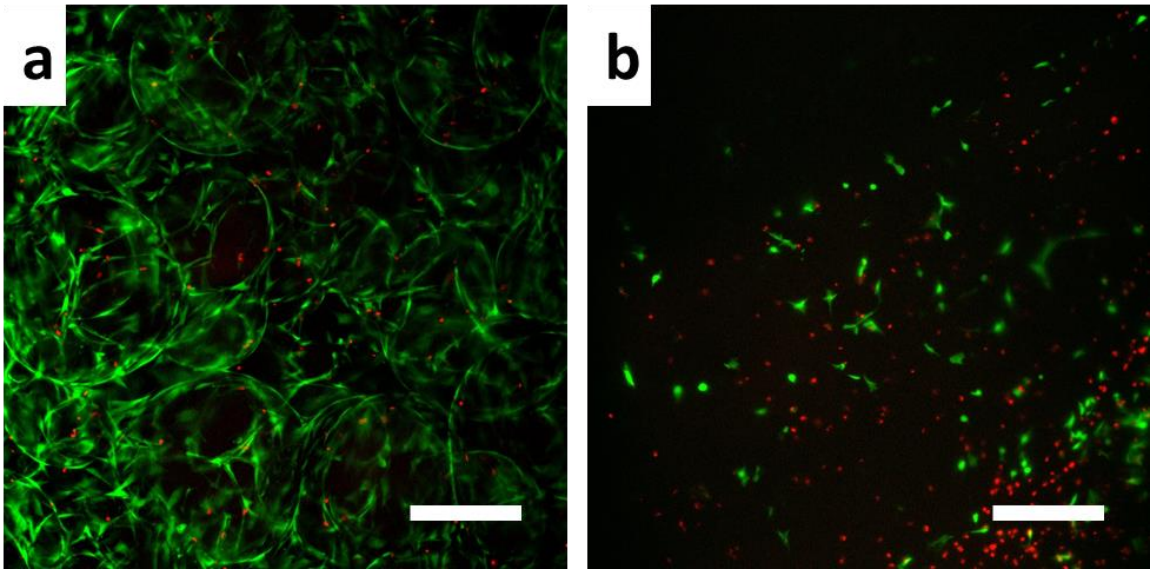

Figure A1.4: Cell viability of day 7 MSCs encapsulated in the a) macroporous hydrogel b) nonporous hydrogel. Green: live cells. Red: dead cells. scale bar: 200 μm.

A2. Multi-functional surface chemistry that enhances cell adhesion and suppresses bacterial growth

Shujie Hou[1a], Alison Deyett[1a], Seth Edwards[1], Shiwha Park[1], Jung-Jae Lee[2] and Kyung Jae Jeong[1*]

[1] Department of Chemical Engineering, University of New Hampshire, Durham, NH 03824

[2] Department of Chemistry, University of Colorado-Denver, Denver, CO 80204

[a] These authors contributed

*Corresponding author: Kyungjae.Jeong@unh.edu

Abstract

Two major causes of medical implant failure are (1) poor tissue-implant integration and (2) bacterial infection. To address this important medical issue, we introduce a multifunctional surface chemistry that enhances human cell adhesion and suppresses bacterial growth. The main feature of this surface chemistry is the presence of nanopatterns of cell adhesive ligands (RGD peptide) on the bactericidal coating. Quaternary ammonium-based bactericidal molecules were immobilized on the glass substrate through silane chemistry. Nanopatterns of cell adhesive ligands were added on the bactericidal coating by the adsorption of gold nanoparticles through electrostatic attraction and the subsequent surface immobilization of RGD peptides through gold-thiol bonds. The surface chemistry was confirmed by X-ray photoelectron spectroscopy (XPS) and scanning electron microscopy (SEM). The presence of RGD peptides on the gold nanoparticles significantly increased cell adhesion and enhanced osteogenic differentiation of human mesenchymal stem cells (hMSCs) confirmed by alkaline phosphatase (ALP) and osteocalcin staining. The same surface achieved ~20% reduction of bacterial growth. This novel surface chemistry has the potential to be applied to various medical implant surfaces by reducing the risk of biofilm formation and increasing cell adhesion.

1. Introduction

Biointegration of medical implants – a seamless interconnection between the implant surface and the recipient tissue – is of paramount importance in medicine [1-2]. Numerous surface chemistries have been developed to improve biointegration, mainly through enhancing cell adhesion, such as the modification of the implant surface with extracellular matrix (ECM) proteins [3-5] or with short synthetic peptides that can promote cell adhesion [6-9]. Physical parameters of the implant surface, such as surface roughness and micro/nano-patterns have been found to affect implant biointegration [10-14]. However, the efforts to enhance tissue growth on the implant surface may also increase the risk of bacteria growth as evidenced by the fibronectin binding proteins expressed by a wide spectrum of bacteria [15]. Once formed, biofilm is quite difficult to remove, and often, the only solution is to remove the implant completely, which is painful and costly [16].

Bacterial infection and biointegration are often not independent phenomena. Bacterial infection can be caused by poor tissue-implant integration, as seen in dental implants, transdermal and ophthalmic prostheses, because these devices span across both sterile and non-sterile environments. For example, dental implants interface both soft (gingiva) and hard (bone) tissues, and even if the integration with the bone tissue (osseointegration) is achieved, poor integration with the gum tissue can lead to bacterial infection around the implant surface, called peri-implantitis, resulting in the bone loss near the implant and the eventual implant failure [17]. Poor integration of the ophthalmic prostheses such as Boston Keratoprosthesis (Boston KPro), the most commonly used artificial cornea in the US [18], can lead to devastating bacterial infection called endopthalmitis [19].

Strategies to kill bacteria or suppress the implant-associated bacterial proliferation include the controlled release of antibiotics [20-22], silver coating [23-25], and the immobilization of bactericidal molecules on the implant surface [26-29]. However, efforts to suppress bacterial growth do not necessarily achieve tissue-material integration, prompting the need for a strategy that addresses both bacterial infection and poor biointegration at the same time [30-31].

Here, we introduce a novel multi-functional surface chemistry that shows potential for both biointegration and suppression of bacterial growth (Fig 1a). The central feature of the surface chemistry is the nano-patterns of cell adhesive ligands on top of the bactericidal coating. Since the size of bacteria is larger than that of the pattern, the bacteria will make contacts with the bactericidal coating anywhere they land on the surface, suppressing their growth. Mammalian cells, however, can make multiple contacts with the cell adhesive ligands presented on the nanopatterns, adhere, and proliferate. Covering the entire surface with bactericidal coating alone would most effectively kill bacteria. However, this would come at the cost of reduced human cell adhesion. By adjusting the ratio of the two factors, we can find the optimal surface composition that promotes the best of human cell adhesion and bactericidal properties.

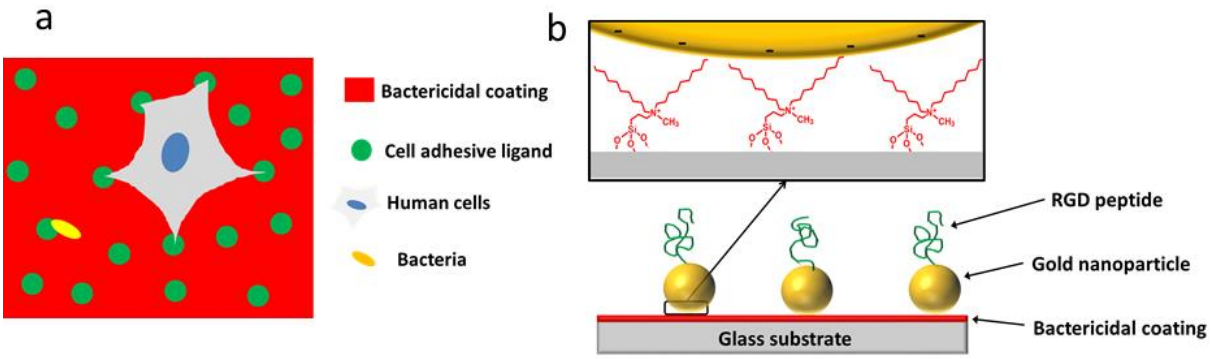

Figure 1. (a) Overview of the multifunctional surface chemistry. Cell adhesive ligands are presented as nanopatterns on top of the bactericidal coating. Bacteria make contact with the bactericidal coating anywhere they land on the surface. Human cells can make multiple contacts with the cell adhesive ligands and adhere and spread. (b) Schematic of the surface chemistry. Bactericidal coating, containing quaternary ammonium and C10 alkyl chains, is added on the glass substrates through silane chemistry. Negatively charged gold nanoparticles are added on the positively charged bactericidal coating. RGD peptides are added on gold nanoparticles through gold-thiol bond.

Fig 1b is the schematic of the surface chemistry. The bactericidal coating, based on a permanent charge of quaternary ammonium and an alkyl chain (C10), was added onto the glass surface by silane chemistry. The combination of quaternary ammonium and long hydrophobic carbon chains have been shown to effectively kill both Gram positive and Gram negative bacteria by disrupting the cell membrane upon contact [26]. Gold nanoparticles (20 nm) were immobilized on this coating through the charge interaction to create a nanopattern. The surface density of gold nanoparticles was controlled by changing the gold nanoparticle concentrations during the incubation of the surface in the gold nanoparticle solution. Subsequently, a cysteine-containing RGD peptide was added to form a nanopattern of cell adhesive ligand through gold-thiol bonds.

As a model implant surface, glass coverslip was chosen due to the ease of microscopic visualization. However, the same concept of surface chemistry can be easily transferred to a wide variety of implant materials.

2. Materials and Methods

2.1. Materials

All chemicals were purchased from Sigma Aldrich (St. Louis, MO) unless stated otherwise.

2.2. Surface modification

12 mm circular glass coverslips were cleaned with Alconox®, washed with deionized water and ethanol and immersed in piranha solution (7:3 sulfuric acid: hydrogen peroxide mixture) for 30 minutes at 80°C. (**Warning**: *piranha is a strong oxidant and must be handled according to documented safety procedures*.) The coverslips were then rinsed with deionized water three times, and blown dried with nitrogen gas.

To add the bactericidal molecules, the piranha-cleaned coverslips were submerged into 5% N,N-didecyl-N-methyl-N-(3-tri-methoxysilylpropyl) ammonium chloride (Gelest, Morrisville, PA) in anhydrous toluene for two hours. The coverslips were rinsed with toluene, with 50% toluene 50 % ethanol, and three times with ethanol, followed by drying with nitrogen gas.

Gold nanoparticles (diameter = 20nm) (BBI solutions, Madison, WI) were added to the bactericidal coating, by submerging the modified glass coverslips in gold nanoparticle solutions of various nanoparticle concentrations overnight. The coverslips were rinsed with deionized water and dried under nitrogen. RGD peptide was immobilized on the gold nanoparticles by submerging the coverslips in a phosphate buffered saline (PBS, pH = 7.4) containing cysteine labeled-RGD peptide (GCGYGRGDSPG, Genscript, Piscataway, NJ) for 4 hours at room temperature. The concentration of the peptide was 10 μM. The coverslips were then washed with DI water and dried.

2.3. Surface characterization

The modified surfaces were sputter-coated with gold and palladium (10 nm) and imaged with Tescan Lyra 3 GMU FE SEM (Tescan, Kohoutovice, Czech Republic). X-ray photoelectron spectroscopy (XPS) was used to obtain elemental compositions of the surface by Kratos Axis Supra XPS (Kratos Analytical, Manchester, United Kingdom) equipped with a monochromatized Al Kα source.

2.4. Bacteria study

E. coli was used as model bacteria to test the bactericidal property of the modified surfaces. *E.coli* was taken by sterile toothpick from the cultured plate before, put into liquid LB, and incubated overnight in a 37 °C shaking incubator. After the incubation, the bacteria concentration was adjusted to OD600 = 0.00125 (~ 1.0 x 10^6 CFU/mL) using PBS. 200 µL of the bacteria solution was added to each modified glass coverslip. After 4 hours of incubation, the bacteria solution was collected, and the number of bacteria was determined by BacTiter assay (Promega, Madison, WI), which measures the concentration of bacteria by measuring the metabolic activity. For quantitative analyses, a standard curve was generated using the bacteria solutions of known concentrations.

2.5. Cell culture

The human mesenchymal stem cells (hMSC) were purchased from Lonza Biologics (Portsmouth, NH) and were cultured in a humidified chamber at 37°C and 5% CO_2 environment. Cells from less than 4 passages were used for all experiments with the media provided by the vendor. hMSCs at 5 x 10^3 cells at 1 x 10^4 cells/mL was added to each surface contained in a well of 24-well plate. For the initial cell adhesion study, the cells were fixed 24 hours after the initial seeding with 4% formaldehyde in PBS. For the fluorescence analysis, the fixed cells were labeled with TRITC-modified phalloidin to stain actin cytoskeleton and with DAPI to stain the cell nuclei. The fluorescence microscope images were taken by EVOS FL Cell Imaging System (Thermo Fisher Scientific, Waltham, MA). Three images were taken from each surface (four surfaces for each test group). The number of adhered cells were quantified using ImageJ.

2.6. Osteogenic differentiation of hMSCs

For the osteogenic differentiation study, the cells were cultured on the surface in a growth media for the first week after which the media was switched to the osteogenic media provided by the vendor, and cultured for another two weeks. The media was changed every other day. The alkaline phosphatase (ALP) assay was performed using SensoLyte® pNPP Alkaline Phosphatase Assay Kit from Anaspec (Fremont, CA). This colorimetric assay utilizes p-nitrophenyphosphate (pNPP) as a substrate for ALP. The absorbance at 405nm from each sample was measured by a plate reader (Model number here, Biotek, Winooski, VT) to estimate the concentration of ALP. The ALP assay results were normalized to the total amount of proteins using the BCA assay from the Pierce Biotechnology (Waltham, MA).

Staining of the osteocalcin within the differentiated hMSCs was achieved by first fixing the cells with 4% formaldehyde and incubating them with anti-osteocalcin derived from mouse (Abcam, Cambridge, MA). Fluorescence labeling of this antibody was done by FITC-labeled anti-IgG derived from goat. DAPI was stained for cell nuclei.

2.7. Statistics

The data are presented as means ± standard deviation unless stated otherwise. The statistical significance of two sample groups was assessed by student-t test. For the statistical significance among multiple sample groups, ANOVA was performed followed by Tukey's *post hoc* test using Origin 8.1.

3. Results

High resolution X-ray photoelectron spectroscopy (XPS) was used to characterize the surface chemistry. The successful coating of glass surface with bactericidal molecules was confirmed by the quaternary ammonium peak at ~ 403 eV in the high resolution spectra of N 1s (Fig 2a). As expected no gold signal (Au 4f) was detected (Fig 2b).

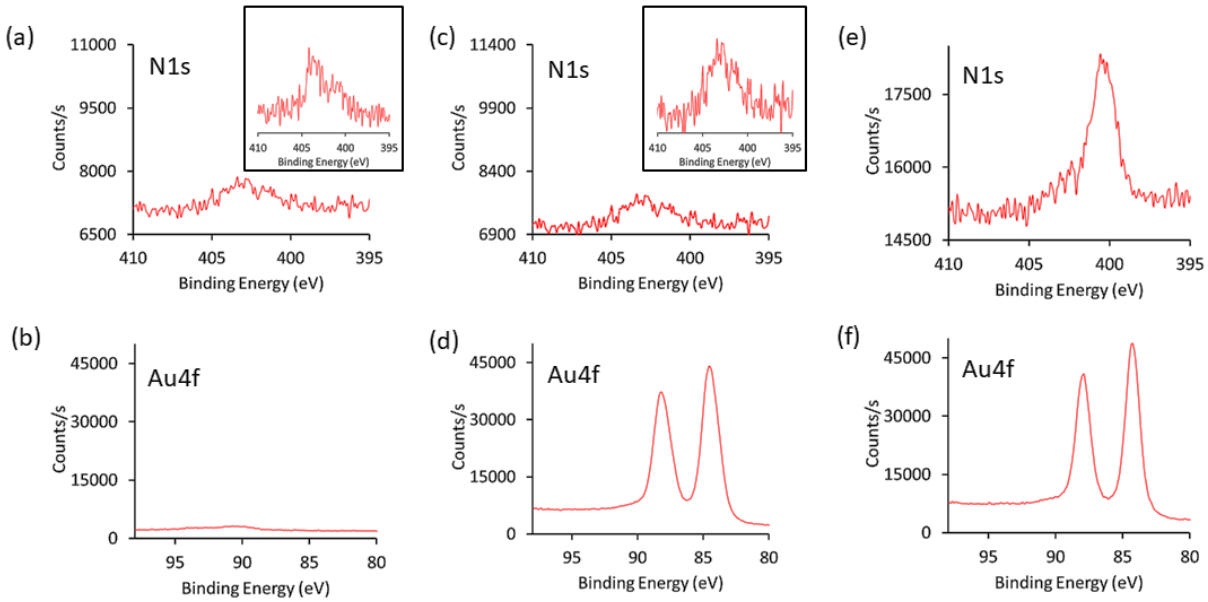

Figure 2. N1s and Au4f XPS high resolution spectra with the progression of surface chemistry. (a), (b) Bactericidal coating, (c), (d) Addition of gold nanoparticles (e), (f) Addition of RGD peptide. The insets in (a) and (c) are the N1s peaks that were rescaled.

When the surfaces were incubated in a gold nanoparticle solution, N 1s peak decreased slightly (Fig 2c) as clear Au 4f peaks appeared in the XPS (Fig 2d). The area of Au 4f peak increased as the concentration of gold nanoparticles increased during the incubation (Fig S1a). This was consistent with the thicker pink color of the glass coverslips (Fig S1b). It is suspected that the negatively charged, citric acid-stabilized gold colloids adhered to the positively charged bactericidal coating through electrostatic attraction. In another study, binding between quaternary ammonium and citric acid-stabilized gold nanoparticles was strong enough to cause aggregation of gold nanoparticles, and was used for sensing quaternary ammonium [32]. The surface binding of the gold nanoparticles was stable and we did not observe any loss of nanoparticles from the surface in all of experiments.

Addition of RGD to the gold nanoparticle-modified surfaces increased the nitrogen signal (N1s in Fig 2e), but the gold signal was unaffected (Fig 2f). The RGD peptide used in this study contained a cysteine residue for the immobilization on the gold nanoparticles through gold-thiol bonds [33-35]. The high resolution spectrum of N1s confirms the presence of primary amines from the peptides with a peak at ~400 eV.

Figure 3 is the scanning electron microscope (SEM) images of the modified glass surfaces. As the concentration of gold nanoparticles was increased from 4.4 x 10^{10} particles/mL to 7.0 x 10^{11} particles/mL, the fraction of surface coverage by the particles increased from 0.05 to 0.27. This result is consistent with the Au4f signals from XPS (Fig S1a).

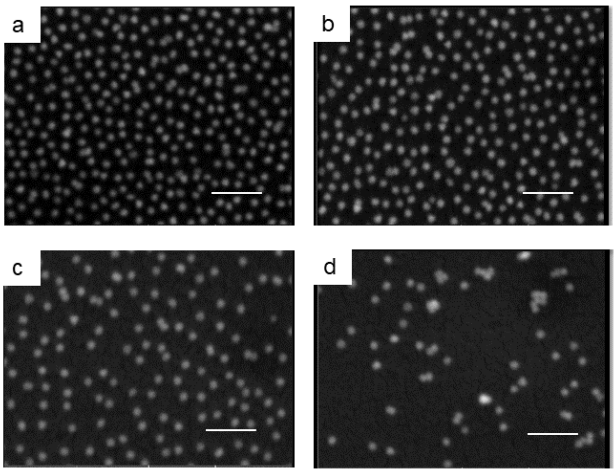

Figure 3. SEM images of gold nanoparticles immobilized on the bactericidal coating. The concentration of gold nanoparticles during the immobilization was (a) 7.0 x 10^{11}/mL (b) 2.8 x 10^{11}/mL (c) 1.1 x 10^{11}/mL (d) 4.4 x 10^{10}/mL. Scale bar = 100 nm.

Since high densities of gold nanoparticles on the surface will hinder the effective physical contact between bacteria and the bactericidal coating, we chose to use two lower gold nanoparticle density surfaces for the rest of the experiments (corresponding to Fig 3c and Fig 3d). We did not use the surfaces with lower gold nanoparticle density than Fig 3d because at such low gold nanoparticle densities, the addition of RGD did not enhance cell adhesion (data not shown). This observation is consistent with the previously reported findings that the spacing between RGD peptides presented on gold nanoparticles should be less than ~70 nm for the efficient focal adhesion formation by the cells [36].

For the simplicity of the further experimental descriptions, the surfaces that were modified with the bactericidal coating are designated as **Bac.** The surfaces with a higher gold nanoparticle density are designated as **Bac-HG** (Fig 3c), and the ones with a lower gold nanoparticle density as **Bac-LG** (Fig 3d). **Bac-HG-RGD** and **Bac-LG-RGD** refer to **Bac-HG** and **Bac-LG** that were further treated with RGD peptide, respectively.

The gold nanoparticles on the bactericidal surface were used to provide anchorage for RGD peptides and to promote better cell adhesion. hMSCs were added on the surfaces, and their initial adhesion after 24 hours was observed by fluorescence microscopy. The addition of RGD peptides to the gold nanoparticles significantly increased the number of adherent cells (Fig 4, Fig S2). Addition of RGD peptides directly to **Bac** also increased cell adhesion slightly, but there was no statistical significance ($p > 0.05$).

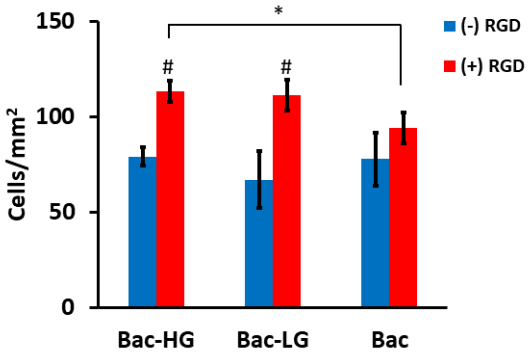

Figure 4. Average number of adherent cells per area. * $p < 0.05$. # stands for $p < 0.05$ compared to the (-) RGD group (n = 4). (+) RGD groups of **Bac-HG** and **Bac-LG** are the same as **Bac-HG-RGD** and **Bac-LG-RGD**, respectively.

Next, long-term effects of the different surface chemistries on the osteogenic differentiation of hMSCs were tested for the potential applications in orthopedic implants. hMSCs were cultured on the surfaces for two weeks in osteogenic media and the concentration of ALP – a well-known osteogenic marker -was measured (Fig 5a). Both **Bac-HG-RGD** and **Bac-LG-RGD** resulted in significantly higher ALP activities than **Bac**. The same samples without RGD (**Bac-HG** and **Bac-LG**) did not show such enhanced ALP activities by hMSCs. This result is consistent with the fact that the stable cell adhesion and the formation of focal adhesion of hMSCs is critical for the osteogenic differentiation [37].

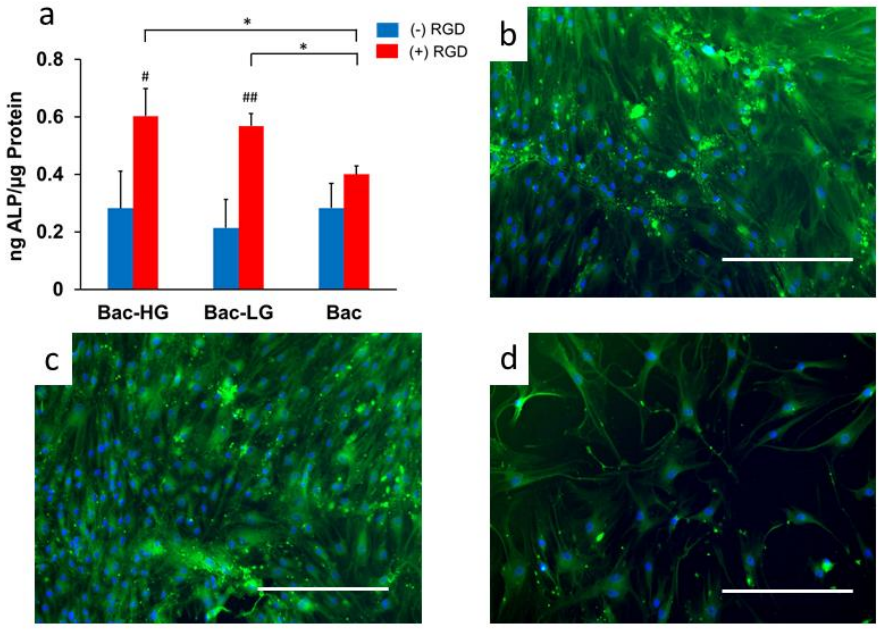

Figure 5. Osteogenic differentiation of hMSCs on different surfaces. (a) ALP assay. * $p < 0.05$. # and ## indicate the (+) RGD groups that had statistical significance compared to the (-) RGD groups (# $p < 0.05$, ## $p < 0.01$) (n = 4) (b-d) Fluorescence microscope images of hMSCs cultured on (b) **Bac-HG-RGD** (c) **Bac-LG-RGD** and (d) **Bac**. Green fluorescence is for osteocalcin and blue fluorescence for nuclei. Scale bar = 400 µm.

When the hMSCs were fluorescently stained for osteocalcin (green fluorescence), another marker for osteogenic differentiation, in all surfaces, most of the adherent cells exhibited green fluorescence, suggesting that most of the adhered hMSCs differentiated into osteoblasts. Both **Bac-HG-RGD** and **Bac-LG-RGD** showed much stronger fluorescence signals than **Bac**, consistent with the results from the ALP assay (Fig 5b-d). These results suggest that the presence of the RGD peptides on the gold nanoparticles enhanced the initial cell adhesion and supported more robust osteogenic differentiation of hMSCs long-term.

Next, bactericidal property of the surfaces was tested by adding an *E.coli* solution on the different surfaces and by measuring the viable bacterial concentrations. The luminescence-based assay we used allowed us to measure the bacteria concentration as low as 1000 CFU/mL (Fig S3). Although *E. coli*, Gram-negative bacteria, were chosen in this study, the bactericidal efficiency against both Gram-negative and Gram-positive bacteria by the combination of quaternary ammonium and alkyl chains is well documented in the literature [38].

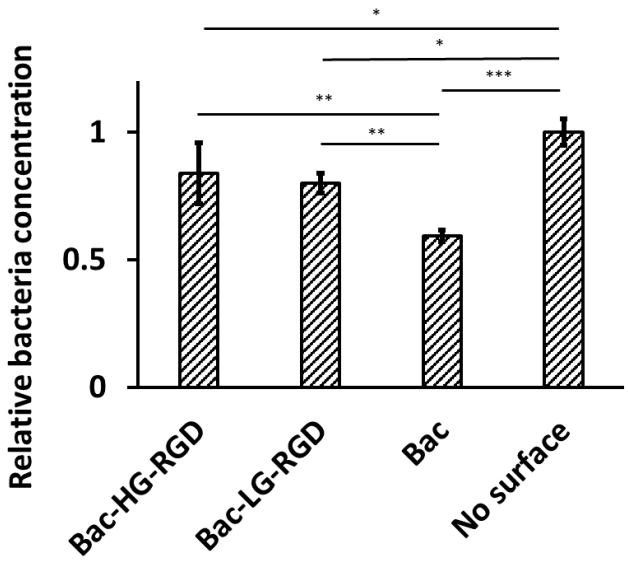

Figure 6. Viable *E. coli* concentration after incubation with surfaces. 200 µL of *E. coli* (concentration = 1.0 x 10^6 CFU/mL) was added to each surface (diameter = 12 mm) and incubated for 4 hours, after which the concentration of the viable *E. coli* was measured. The results were normalized to the "No surface" group, in which the bacteria was not exposed to the glass coverslips. * $p < 0.05$, ** $p < 0.01$, *** $p < 0.001$ ($n = 4$).

Fig 6 shows the fraction of viable bacteria after 4 hours of incubation on different surfaces compared to the bacteria solution that was not exposed to any glass coverslips. **Bac** reduced the number of bacteria by 40% under the conditions we used. The addition of gold nanoparticles and RGD peptide reduced the bactericidal property, but was still effective in suppressing the bacterial growth. For example, **Bac-HG-RGD** and **Bac-LG-RGD** reduced the number of bacteria by 16% and 21% compared to the no treatment group ($p < 0.05$), despite the reduced available area of bactericidal coating by the gold nanoparticles.

In the current approach, decreasing the surface density of gold nanoparticles would enhance bactericidal property. However, further decrease in the surface density of gold nanoparticles than

Bac-LG increases the average distance between RGD peptides beyond a critical value (~ 70 nm), which would nullify the actions of RGD peptides on gold nanoparticles to enhance cell adhesion. One potential approach would be to increase the surface density of bactericidal molecules. In our experiments, we used a silane molecule that already had alkyl chains and a quaternary ammonium for the simplicity of the chemistry. The surface density of bactericidal moieties can be increased significantly by a series of surface chemistry that involves the coating the surface with polyethyleneimine (PEI), followed by the addition of alkyl chains to produce quaternary ammonium, which resulted in more efficient bacteria-killing effects [38].

Conclusion

The novel surface chemistry introduced here enhanced the initial adhesion and the long-term osteogenic differentiation of hMSCs on the glass coverslips. The same surface chemistry also suppressed the bacterial growth by 21%. Further optimization of this multifunctional surface chemistry will find applications in various medical implants where enhanced biointegration and antibacterial property are required.

Acknowledgement

This work was supported in part by an NIH COBRE Center of Integrated Biomedical and Bioengineering Research (CIBBR, P20 GM113131) through an Institutional Development Award (IDeA) from the National Institute of General Medical Sciences. The authors thank Erin Drufva and Professor Kang Wu for providing the *E. coli*.

Supporting information

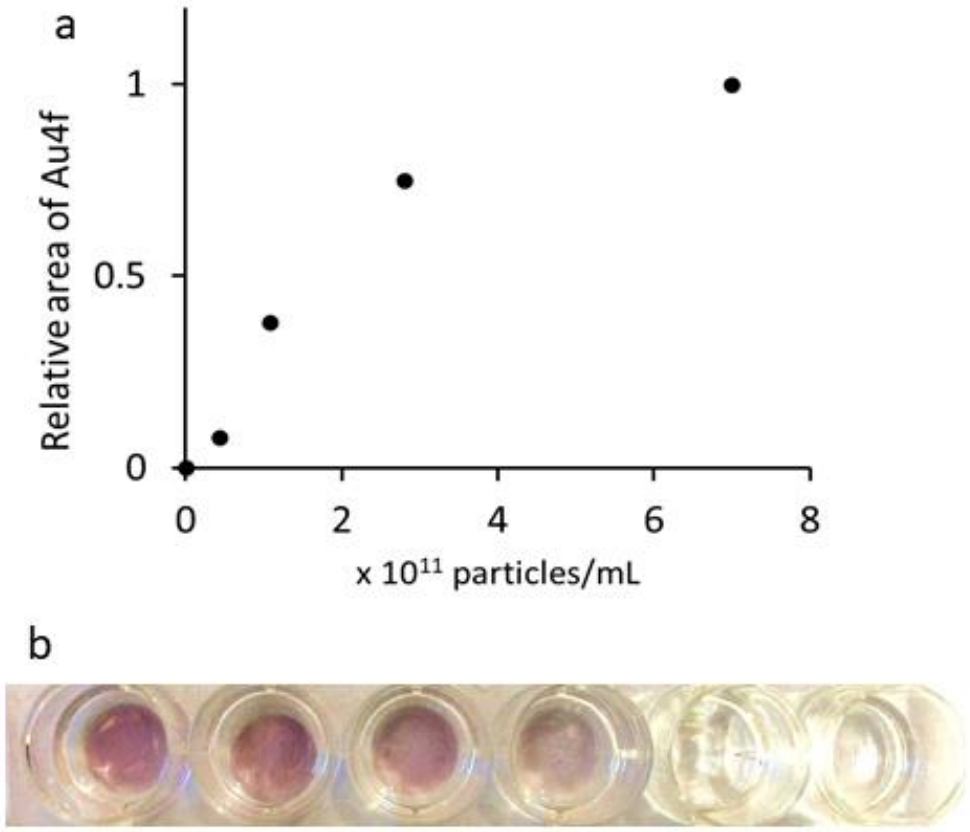

Figure S1. (a) Area of Au4f peaks as a function of the concentration of gold nanoparticle solution. The glass coverslips with bactericidal coating were immersed in gold nanoparticle solutions of varying concentrations (x-axis) for 4 hours. The area under the curve of each Au 4f peak was normalized to the case of highest gold nanoparticle concentration (7 x 10^{11} particles/mL) (b) Glass coverslips after the immobilization of gold nanoparticles. The concentration of gold nanoparticles during the surface immobilization was decreased from 7 x 10^{11}/mL to 0/mL from left to right.

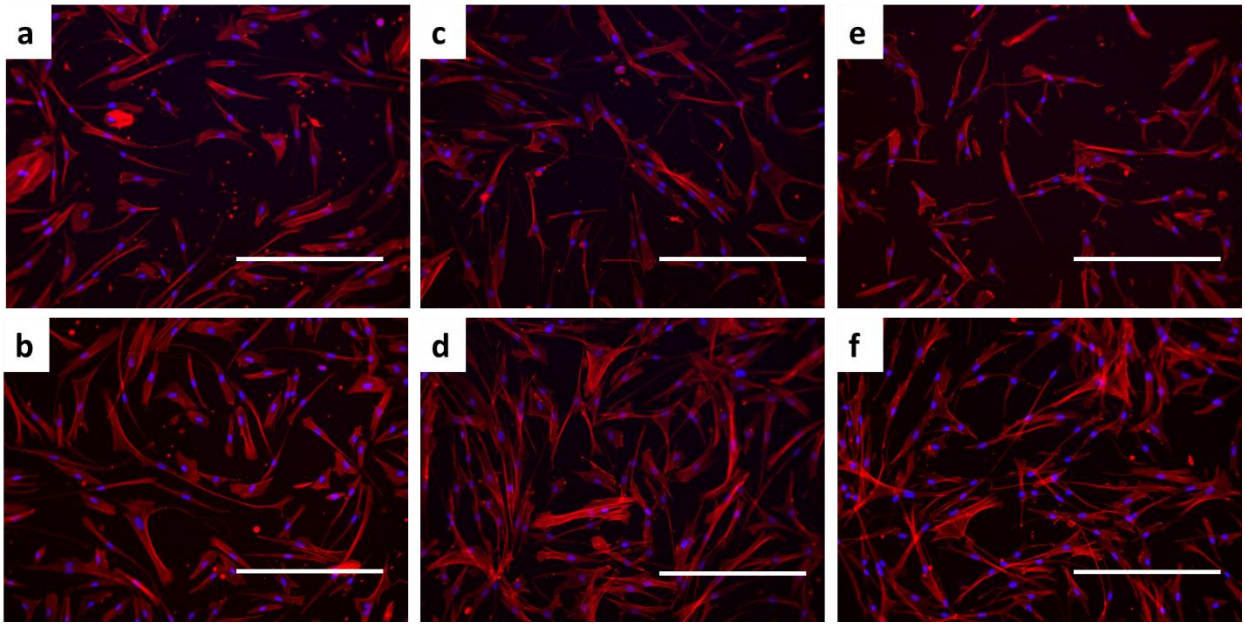

Figure S2. Initial cell adhesion (a) **Bac** (b) **Bac-RGD** (c) **Bac-HG** (d) **Bac-HG-RGD** (e) **Bac-LG** (f) **Bac-LG-RGD**. hMSCs were stained for actin cytoskeleton (red) and nuclei (blue). Scale bar = 400 μm.

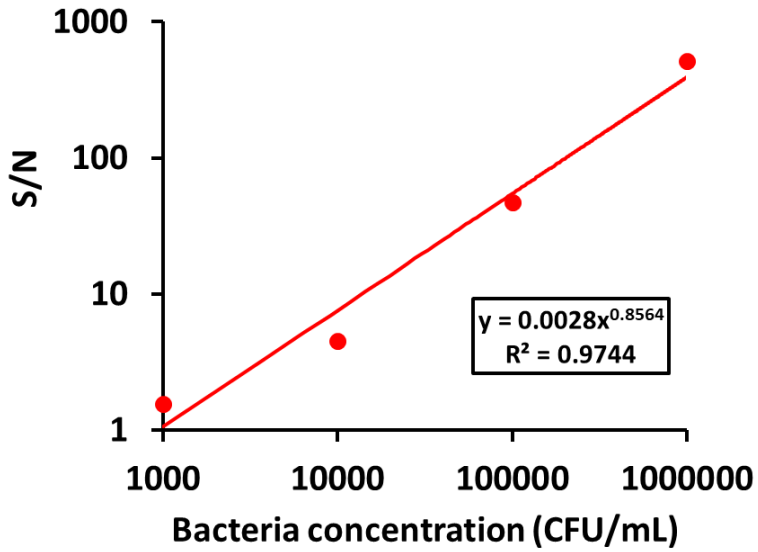

Figure S3. Signal to noise ratio (S/N) of luminescence as a function of bacteria concentration. S/N = [mean luminescence of standard samples – mean luminescence of the background (buffer only sample)]/standard deviation of the background.

References

1. Jeong, K. J.; Kohane, D. S., Surface Modification and Drug Delivery for Biointegration. *Therapeutic delivery* **2011,** *2* (6), 737-752.

2. Peramo, A.; Marcelo, C. L., Bioengineering the Skin–Implant Interface: The Use of Regenerative Therapies in Implanted Devices. *Annals of biomedical engineering* **2010,** *38* (6), 2013-2031.

3. He, W.; Ma, Z.; Yong, T.; Teo, W. E.; Ramakrishna, S., Fabrication of Collagen-Coated Biodegradable Polymer Nanofiber Mesh and Its Potential for Endothelial Cells Growth. *Biomaterials* **2005,** *26* (36), 7606-7615.

4. Yang, J.; Bei, J.; Wang, S., Enhanced Cell Affinity of Poly (D, L-Lactide) by Combining Plasma Treatment with Collagen Anchorage. *Biomaterials* **2002,** *23* (12), 2607-2614.

5. Woo, K. M.; Jun, J.-H.; Chen, V. J.; Seo, J.; Baek, J.-H.; Ryoo, H.-M.; Kim, G.-S.; Somerman, M. J.; Ma, P. X., Nano-Fibrous Scaffolding Promotes Osteoblast Differentiation and Biomineralization. *Biomaterials* **2007,** *28* (2), 335-343.

6. Santiago, L. Y.; Nowak, R. W.; Rubin, J. P.; Marra, K. G., Peptide-Surface Modification of Poly (Caprolactone) with Laminin-Derived Sequences for Adipose-Derived Stem Cell Applications. *Biomaterials* **2006,** *27* (15), 2962-2969.

7. Widhe, M.; Johansson, U.; Hillerdahl, C.-O.; Hedhammar, M., Recombinant Spider Silk with Cell Binding Motifs for Specific Adherence of Cells. *Biomaterials* **2013,** *34* (33), 8223-8234.

8. Zustiak, S. P.; Durbal, R.; Leach, J. B., Influence of Cell-Adhesive Peptide Ligands on Poly (Ethylene Glycol) Hydrogel Physical, Mechanical and Transport Properties. *Acta biomaterialia* **2010,** *6* (9), 3404-3414.

9. Povimonsky, A. G.; Rapaport, H., Peptide Coating Applied on the Spot Improves Osseointegration of Titanium Implants. *Journal of Materials Chemistry B* **2017,** *5* (11), 2096-2105.

10. Salvador-Culla, B.; Jeong, K. J.; Kolovou, P. E.; Chiang, H. H.; Chodosh, J.; Dohlman, C. H.; Kohane, D. S., Titanium Coating of the Boston Keratoprosthesis. *Translational vision science & technology* **2016,** *5* (2), 17-17.

11. Buser, D.; Schenk, R.; Steinemann, S.; Fiorellini, J.; Fox, C.; Stich, H., Influence of Surface Characteristics on Bone Integration of Titanium Implants. A Histomorphometric Study in Miniature Pigs. *Journal of biomedical materials research* **1991,** *25* (7), 889-902.

12. Cochran, D.; Schenk, R.; Lussi, A.; Higginbottom, F.; Buser, D., Bone Response to Unloaded and Loaded Titanium Implants with a Sandblasted and Acid-Etched Surface: A

Histometric Study in the Canine Mandible. *Journal of Biomedical Materials Research: An Official Journal of The Society for Biomaterials, The Japanese Society for Biomaterials, and the Australian Society for Biomaterials* **1998,** *40* (1), 1-11.

13. Karazisis, D.; Petronis, S.; Agheli, H.; Emanuelsson, L.; Norlindh, B.; Johansson, A.; Rasmusson, L.; Thomsen, P.; Omar, O., The Influence of Controlled Surface Nanotopography on the Early Biological Events of Osseointegration. *Acta biomaterialia* **2017,** *53*, 559-571.

14. Li, S.; Chow, T.; Chu, J., Engineering Microdent Structures of Bone Implant Surfaces to Enhance Osteogenic Activity in Mscs. *Biochemistry and biophysics reports* **2017,** *9*, 100-105.

15. Hymes, J. P.; Klaenhammer, T. R., Stuck in the Middle: Fibronectin-Binding Proteins in Gram-Positive Bacteria. *Frontiers in microbiology* **2016,** *7*, 1504.

16. Carmen, J. C.; Roeder, B. L.; Nelson, J. L.; Ogilvie, R. L. R.; Robison, R. A.; Schaalje, G. B.; Pitt, W. G., Treatment of Biofilm Infections on Implants with Low-Frequency Ultrasound and Antibiotics. *American journal of infection control* **2005,** *33* (2), 78-82.

17. Zhao, B.; Van Der Mei, H. C.; Rustema-Abbing, M.; Busscher, H. J.; Ren, Y., Osteoblast Integration of Dental Implant Materials after Challenge by Sub-Gingival Pathogens: A Co-Culture Study *in Vitro*. *International journal of oral science* **2015,** *7* (4), 250.

18. Akpek, E. K.; Alkharashi, M.; Hwang, F. S.; Ng, S. M.; Lindsley, K., Artificial Corneas Versus Donor Corneas for Repeat Corneal Transplants. *The Cochrane database of systematic reviews* **2014,** *11*, CD009561.

19. Behlau, I.; Martin, K. V.; Martin, J. N.; Naumova, E. N.; Cadorette, J. J.; Sforza, J. T.; Pineda, R.; Dohlman, C. H., Infectious Endophthalmitis in Boston Keratoprosthesis: Incidence and Prevention. *Acta ophthalmologica* **2014,** *92* (7), e546-e555.

20. Kazemzadeh-Narbat, M.; Lai, B. F.; Ding, C.; Kizhakkedathu, J. N.; Hancock, R. E.; Wang, R., Multilayered Coating on Titanium for Controlled Release of Antimicrobial Peptides for the Prevention of Implant-Associated Infections. *Biomaterials* **2013,** *34* (24), 5969-5977.

21. Min, J.; Braatz, R. D.; Hammond, P. T., Tunable Staged Release of Therapeutics from Layer-by-Layer Coatings with Clay Interlayer Barrier. *Biomaterials* **2014,** *35* (8), 2507-2517.

22. Wei, T.; Zhan, W.; Cao, L.; Hu, C.; Qu, Y.; Yu, Q.; Chen, H., Multifunctional and Regenerable Antibacterial Surfaces Fabricated by a Universal Strategy. *ACS applied materials & interfaces* **2016,** *8* (44), 30048-30057.

23. Masse, A.; Bruno, A.; Bosetti, M.; Biasibetti, A.; Cannas, M.; Gallinaro, P., Prevention of Pin Track Infection in External Fixation with Silver Coated Pins: Clinical and Microbiological Results. *Journal of Biomedical Materials Research: An Official Journal of The Society for Biomaterials, The Japanese Society for Biomaterials, and The Australian Society for Biomaterials and the Korean Society for Biomaterials* **2000,** *53* (5), 600-604.

24. Hardes, J.; Von Eiff, C.; Streitbuerger, A.; Balke, M.; Budny, T.; Henrichs, M. P.; Hauschild, G.; Ahrens, H., Reduction of Periprosthetic Infection with Silver-Coated Megaprostheses in Patients with Bone Sarcoma. *Journal of surgical oncology* **2010,** *101* (5), 389-395.

25. Kuehl, R.; Brunetto, P. S.; Woischnig, A.-K.; Varisco, M.; Rajacic, Z.; Vosbeck, J.; Terracciano, L.; Fromm, K. M.; Khanna, N., Preventing Implant-Associated Infections by Silver Coating. *Antimicrobial agents and chemotherapy* **2016**, AAC. 02934-02915.

26. Tiller, J. C.; Liao, C.-J.; Lewis, K.; Klibanov, A. M., Designing Surfaces That Kill Bacteria on Contact. *Proceedings of the National Academy of Sciences* **2001,** *98* (11), 5981-5985.

27. Tan, X. W.; Goh, T. W.; Saraswathi, P.; Nyein, C. L.; Setiawan, M.; Riau, A.; Lakshminarayanan, R.; Liu, S.; Tan, D.; Beuerman, R. W., Effectiveness of Antimicrobial Peptide Immobilization for Preventing Perioperative Cornea Implants Associated Bacteria Infection. *Antimicrobial agents and chemotherapy* **2014**, AAC. 02859-02814.

28. Shi, Z.; Neoh, K.; Kang, E.; Poh, C.; Wang, W., Bacterial Adhesion and Osteoblast Function on Titanium with Surface-Grafted Chitosan and Immobilized Rgd Peptide. *Journal of Biomedical Materials Research Part A: An Official Journal of The Society for Biomaterials, The Japanese Society for Biomaterials, and The Australian Society for Biomaterials and the Korean Society for Biomaterials* **2008,** *86* (4), 865-872.

29. Zhao, L.; Hu, Y.; Xu, D.; Cai, K., Surface Functionalization of Titanium Substrates with Chitosan–Lauric Acid Conjugate to Enhance Osteoblasts Functions and Inhibit Bacteria Adhesion. *Colloids and Surfaces B: Biointerfaces* **2014,** *119*, 115-125.

30. Kulkarni Aranya, A.; Pushalkar, S.; Zhao, M.; LeGeros, R. Z.; Zhang, Y.; Saxena, D., Antibacterial and Bioactive Coatings on Titanium Implant Surfaces. *Journal of Biomedical Materials Research Part A* **2017,** *105* (8), 2218-2227.

31. Raphel, J.; Holodniy, M.; Goodman, S. B.; Heilshorn, S. C., Multifunctional Coatings to Simultaneously Promote Osseointegration and Prevent Infection of Orthopaedic Implants. *Biomaterials* **2016,** *84*, 301-314.

32. Zheng, L.-Q.; Yu, X.-D.; Xu, J.-J.; Chen, H.-Y., Colorimetric Detection of Quaternary Ammonium Surfactants Using Citrate-Stabilized Gold Nanoparticles (Au Nps). *Analytical Methods* **2014,** *6* (7), 2031-2033.

33. Cohen-Karni, T.; Jeong, K. J.; Tsui, J. H.; Reznor, G.; Mustata, M.; Wanunu, M.; Graham, A.; Marks, C.; Bell, D. C.; Langer, R., Nanocomposite Gold-Silk Nanofibers. *Nano letters* **2012,** *12* (10), 5403-5406.

34. Huang, J.; Grater, S. V.; Corbellini, F.; Rinck, S.; Bock, E.; Kemkemer, R.; Kessler, H.; Ding, J.; Spatz, J. P., Impact of Order and Disorder in Rgd Nanopatterns on Cell Adhesion. *Nano letters* **2009,** *9* (3), 1111-1116.

35. Soylemez, S.; Demir, B.; Eyrilmez, G. O.; Kesici, S.; Saylam, A.; Demirkol, D. O.; Özçubukçu, S.; Timur, S.; Toppare, L., Comparative Cell Adhesion Properties of Cysteine Extended Peptide Architectures. *RSC Advances* **2016,** *6* (4), 2695-2702.

36. Arnold, M.; Cavalcanti-Adam, E. A.; Glass, R.; Blümmel, J.; Eck, W.; Kantlehner, M.; Kessler, H.; Spatz, J. P., Activation of Integrin Function by Nanopatterned Adhesive Interfaces. *ChemPhysChem* **2004,** *5* (3), 383-388.

37. Mathieu, P. S.; Loboa, E. G., Cytoskeletal and Focal Adhesion Influences on Mesenchymal Stem Cell Shape, Mechanical Properties, and Differentiation Down Osteogenic, Adipogenic, and Chondrogenic Pathways. *Tissue Engineering Part B: Reviews* **2012,** *18* (6), 436-444.

38. Milović, N. M.; Wang, J.; Lewis, K.; Klibanov, A. M., Immobilized N-Alkylated Polyethylenimine Avidly Kills Bacteria by Rupturing Cell Membranes with No Resistance Developed. *Biotechnology and bioengineering* **2005,** *90* (6), 715-722.